UNIVERSIDADE FEDERAL DE SANTA CATARINA
CENTRO TÉCNOLÓGICO
PROGRAMA DE PÓS-GRADUAÇÃO EM ENGENHARIA MECÂNICA

Theodor Rucker van Caspel

WORKPIECE TEMPERATURE MEASUREMENT IN RADIAL TURNING FOR THE PURPOSE OF MODELING AND SIMULATION

Florianópolis
2022

Theodor Rucker van Caspel

WORKPIECE TEMPERATURE MEASUREMENT IN RADIAL TURNING FOR THE PURPOSE OF MODELING AND SIMULATION

Dissertação/Tese submetida ao Programa de Programa de Pós-Graduação em Engenharia Mecânica da Universidade Federal de Santa Catarina para a obtenção do título de Mestre em Engenharia Mecânica
Orientador: Prof. Rolf Bertrand Schroeter, Dr. Eng.
Coorientador: Prof. Claudio Abilio da Silveira, Dr. Eng.

Florianópolis
2022

Ficha de identificação da obra elaborada pelo autor,
através do Programa de Geração Automática da Biblioteca Universitária da UFSC.

van Caspel, Theodor Rucker
Worpiece temperature measurement in radial turning for the purpose of modeling and simulation / Theodor Rucker van Caspel ; orientador, Rolf Bertrand Schroeter, coorientador, Claudio Abilio da Silveira, 2022.
129 p.

Tese (doutorado) - Universidade Federal de Santa Catarina, Centro Tecnológico, Programa de Pós-Graduação em Engenharia Mecânica, Florianópolis, 2022.

Inclui referências.

1. Engenharia Mecânica. 2. usinagem. 3. torneamento radial. 4. medição de temperatura. 5. camada branca. I. Schroeter, Rolf Bertrand. II. da Silveira, Claudio Abilio. III. Universidade Federal de Santa Catarina. Programa de Pós-Graduação em Engenharia Mecânica. IV. Título.

Theodor Rucker van Caspel

WORKPIECE TEMPERATURE MEASUREMENT IN RADIAL TURNING FOR THE PURPOSE OF MODELING AND SIMULATION

O presente trabalho em nível de mestrado foi avaliado e aprovado por banca examinadora composta pelos seguintes membros:

Prof. Rolf Bertrand Schroeter, Dr. Eng.
Universidade Federal de Santa Catarina

Prof. Milton Pereira, Dr. Eng.
Universidade Federal de Santa Catarina

Prof. André Roberto de Souza, Dr. Eng.
Instituto Federal de Santa Catarina

Dr. Eng. Felipe Gustavo Ebersbach,
Universidade Federal de Santa Catarina

Certificamos que esta é a **versão original e final** do trabalho de conclusão que foi julgado adequado para obtenção do título de mestre em Engenharia Mecânica.

ICP-Edu
Documento assinado digitalmente
Henrique Simas
Data: 30/11/2022 09:48:54-0300
CPF: ***.194.639-**
Verifique as assinaturas em https://v.ufsc.br

Coordenação do Programa de Pós-Graduação

ICP-Edu
Documento assinado digitalmente
Rolf Bertrand Schroeter
Data: 29/11/2022 21:52:25-0300
CPF: ***.631.589-**
Verifique as assinaturas em https://v.ufsc.br

Prof. Rolf Bertrand Schroeter, Dr. Eng.
Orientador

Florianópolis, 2022.

This work is dedicated to all those who helped me through the years.

ACKNOWLEDGES

I would like to thank my parents for all the support that they gave me over the years. I would like to thank my girlfriend, Alana, for being my partner and helping me stay sane during the time we have been together. Also, I would like to tank my brothers for their support.

I would like to thank my advisor, Professor Rolf, for teaching me many things and supporting my work. I'd like to thank my co-advisor, Doctor Claudio for helping me learn what I needed about electronics. I'd also like to thank the professors from UFSC that taught me many things, not only in the field of engineering.

I would also like to thank my colleagues in LMP. Michel Tavares helped me in all areas of my project, that did not directly involve electronics. I'd also like to thank all other members of LMP for their help, discussions, and camaraderie.

I would like to thank LMP, LEPTEN, Instituto SENAI de Inovação em Sistemas de Manufatura e Processamento a Laser and IFSC Florianópolis for providing access and use of equipment and infra-structure. I'd like to thank CAPES for the stipend provided and UFSC and POSMEC for the opportunity to do this work.

“Accurate and minute measurement seems to the non-scientific imagination, a less lofty and dignified work than looking for something new. But nearly all the grandest discoveries of science have been but the rewards of accurate measurement and patient long continued labor in the minute sifting of numerical results.”

-Baron William Thomson Kelvin

RESUMO

Muitas peças que requerem resistência à fadiga e são submetidas a elevados esforços mecânicos são fabricadas em aços endurecidos. O processo de acabamento tradicionalmente utilizado para aços endurecidos é a retificação, entretanto, o torneamento se tornou uma alternativa à retificação no início dos anos 80. Desde então, há a necessidade do melhor entendimento do processo de torneamento de materiais endurecidos. Estudos recentes de torneamento de aços endurecidos reportaram uma diminuição nas forças e um aumento na formação de camada branca conforme a ferramenta se aproxima do centro da peça durante o torneamento radial, indicando um aumento de temperatura ao longo do processo. Com o movimento da ferramenta em direção ao centro de rotação da peça, o raio do arco que descreve o movimento entre ferramenta e peça diminui, necessitando um aumento da velocidade angular para manter a velocidade escalar. Este aumento de velocidade, na forma de aumento de rotação, diminui o intervalo de tempo entre a passagem da ferramenta por uma região da peça. Devido a isso a medição da temperatura e pontos específicos da peça pode trazer mais informações sobre o fenômeno. Portanto, o objetivo desta pesquisa foi medir a temperatura na peça durante o torneamento radial de modo a verificar se o suposto aumento de temperatura ocorre e investigar possíveis causas para este aumento. Para isso, um dispositivo para medição de temperatura foi desenvolvido utilizando uma plataforma de prototipagem como base. Termopares tipo K embutidos próximos à superfície em diferentes distâncias do centro da peça foram usados para verificar se há diferença de temperatura entre as regiões. Devido ao dispositivo de medição de temperatura estar em fase de protótipo, os experimentos nesta pesquisa foram feitos usando o aço AISI 1040 ao invés de aço endurecido, e ferramentas novas e desgastadas foram utilizadas. Além da medição de temperatura durante o torneamento utilizando o dispositivo desenvolvido, as forças do processo foram medidas utilizando um dinamômetro piezelétrico. Análises no domínio do tempo e da frequência foram feitas após os experimentos. O dispositivo desenvolvido indicou um aumento de temperatura durante o processo nas áreas mais próximas ao centro da peça. O dispositivo também foi capaz de medir pulsos de temperatura nestas regiões com frequências próximas da frequência instantâneas de rotação da peça, o que significa que provavelmente existe uma relação entre o aumento da rotação e o aumento da temperatura. Vibrações foram detectadas em regiões próximas aos termopares causados por seus furos de inserção. Foi feita uma análise das falhas do dispositivo. Soluções para as falhas e possíveis melhorias para o dispositivo foram propostas. Algumas das soluções e melhorias não foram aplicadas neste momento pois as mesmas requerem a o reprojeto e a fabricação e teste de um novo protótipo e, portanto, devem ser aplicadas em trabalhos futuros.

Palavras-chave: usinagem; torneamento radial; medição de temperatura; camada branca.

RESUMO EXPANDIDO

Introdução

Muitas peças que requerem resistência à fadiga e são submetidas a elevados esforços mecânicos são fabricadas em aços endurecidos. Devido a elevada dureza, o processo de acabamento tradicionalmente empregado para aços endurecido é a retificação. Porém, a partir da década de 80 o torneamento de materiais endurecidos tornou-se uma alternativa à retificação. Devido a isso, existe a necessidade de entender melhor este processo. Análise dos esforços, desgaste de ferramentas e a formação de camada branca durante o torneamento do aço endurecido AISI 52100 usando ferramentas de PCBN mostraram que no torneamento radial há um decréscimo nos esforços e um aumento na formação de camada branca conforme a ferramenta se aproxima do centro da peça, comportamento que indica um aumento da temperatura na região de corte conforme a ferramenta se aproxima do centro da peça. Tal aumento pode estar relacionado à variação da rotação do torno durante o processo, logo o fenômeno poderia ser melhor observado medindo a temperatura em pontos fixos da peça ao longo do seu raio.

Objetivos

O objetivo deste trabalho foi realizar medições na peça durante o torneamento radial. Para isso um dispositivo capaz de medir a temperatura na peça durante o torneamento radial foi desenvolvido. Este dispositivo tem o objetivo de verificar se as suspeitas levantadas em trabalhos anteriores estavam corretas, de que ocorre um aumento de temperatura conforme a ferramenta de corte se aproxima do centro da peça no torneamento radial e identificar a possível causa deste aumento.

Metodologia

O dispositivo foi desenvolvido a partir de uma plataforma de prototipagem, mais especificamente um Arduino nano, utilizando termopares tipo K para medir a temperatura. O dispositivo foi projetado sendo composto por três sistemas distintos: aquisição, amplificação e fixação.

O sistema de aquisição é composto pelo Arduino, um módulo de cartão de memória microSD, botões e LEDs e resistores. Este sistema é responsável pelo controle do dispositivo e aquisição e armazenamento de dados. Este sistema foi primeiramente testado isoladamente em placas de testes e posteriormente montado em um circuito impresso.

O sistema de amplificação é composto por amplificadores INA333, capacitores e resistores. Este sistema é responsável por amplificar os sinais dos termopares para um nível em que o Arduino possa adquirir e gerar o sinal do termistor que é responsável pela compensação da junção fria dos termopares. Este sistema foi simulado, testado em placas de teste junto ao sistema de aquisição e posteriormente montado em um circuito impresso.

O sistema de fixação é composto por um cilindro de alumínio e uma seção de tubo de PVC recoberto por borracha. Este sistema tem a função de alojar os outros sistemas e fixar o dispositivo na placa do torno. Este sistema foi testado no torno com rotações de até 4500 rpm antes das cavidades para o alojamento dos outros sistemas fossem feitas.

Foram realizados testes em corpos de prova compostos de aço AISI 1040 submetidos a torneamento radial. Em cada teste foram realizados múltiplos passes. Durante os testes a temperatura e os esforços foram medidos. Os esforços foram medidos utilizando um dinamômetro piezelétrico.

A temperatura foi medida utilizando o protótipo do dispositivo desenvolvido. Cada corpo de prova continha três termopares tipo K embutidos próximos à superfície usinada e espaçados ao longo do raio. Para embutir os termopares, furos foram feitos nos corpos de prova usando eletroerosão do lado oposto ao lado a ser usinado. Os termopares foram fixados nos furos usando cola acrílica.

Resultados e discussão

O sistema apresentou falhas e quatro dos seis ensaios não obtiveram os dados de temperatura planejados. As falhas foram analisadas de modo a propor soluções e métodos de identificá-los em testes futuros. As que causaram maior perda de testes foram falhas nos conectores, na junção com os termopares, e desgaste do sistema de fixação. Uma solução para as falhas nos conectores foi definida e testada, porém mais testes serão necessários em trabalhos futuros. Para corrigir o sistema de fixação são necessárias alterações no projeto.

Foram analisadas possíveis interações entre os resultados apresentados pelo dinamômetro e a presença do dispositivo de medição de temperatura. A única interação causada

pela utilização do dispositivo foi a interação física devido à presença dos furos que alojam os termopares.

Os testes bem sucedidos mostraram que existe um aumento de temperatura da peça em regiões mais próximas ao centro. Além disto, nos passes finais de cada teste foram identificados sinais de temperatura na forma de pulsos com frequência semelhante à frequência de rotação instantânea da peça naquela posição. Isto indica uma relação entre a rotação da peça e o aumento de temperatura.

Foram apresentadas possíveis melhorias para o desenvolvimento do sistema. Entre elas a modularização do sistema e adição de uma maneira de obter os dados do dispositivo sem a necessidade de removê-lo da máquina.

Considerações finais

Um sistema para a medição de temperatura em torneamento radial foi desenvolvido e um protótipo foi montado. Apesar de haver problemas e uma parcela considerável de testes não terem obtidos os dados de temperatura planejados, estes testes foram utilizados para identificar problemas no dispositivo. Os testes bem sucedidos foram capazes de confirmar as suspeitas levantadas em trabalhos anteriores e mostraram uma causa para este aumento.

Em trabalhos futuros o desenvolvimento do dispositivo poderá ser continuado de modo a eliminar ou mitigar as falhas e tornar o dispositivo mais confiável. Após o dispositivo apresentar confiabilidade e características adequadas, ele poderá ser utilizado para a medição de temperatura em torneamento radial de AISI 52100. Os dados coletados serão então utilizados para criar e validar modelos de temperatura para este processo.

Foram inclusas neste trabalho as informações necessárias para replicar e alterar o dispositivo. É esperado que estas informações possam ser utilizadas para o desenvolvimento de dispositivos semelhantes para outras aplicações.

Palavras-chave: usinagem; torneamento radial; medição de temperatura; camada branca.

ABSTRACT

Many parts that require fatigue resistance and are submitted to high mechanical loads are fabricated in hardened steels. The traditional finishing process used for hardened steels is grinding, however, hard turning has become an alternative to grinding in the early 80s. Since then, there is a need to better understand the hard turning process. Recent hard turning studies reported a decrease in forces and an increase in white layer formation as the tool approached the workpiece center during radial turning, which indicates a temperature increase along the process. With the movement of the tool toward the workpiece rotation center, the radius of the arch that describes the movement between tool and workpiece diminishes, requiring an increase of angular speed to maintain the scalar speed. This speed increase, in the form of rotation increase, decreases the time interval between tool passage by a region of the workpiece. Because of that, measuring the temperature in specific points of the workpiece can bring more information about the phenomena. Therefore, the objective of this research was to measure the temperature in the workpiece during radial turning to verify if the supposed temperature increase occurs and to investigate possible causes for this increase. For this, a temperature measurement device was developed using a prototyping platform as a basis. Type K thermocouples embedded close to the surface at different distances from the workpiece center were used to verify if there is a difference in temperature between the regions. Due to the temperature measurement device being in a prototyping phase, the machining experiments in this research were made using the AISI 1040 steel instead of hardened steel, and new and worn tools were used. In addition to temperature measurement during turning using the developed device, the process forces were measured using a piezoelectric dynamometer. Analyzes in the domain of time and frequency were made after the experiments. The developed device indicated a temperature increase during the process in regions closer to the workpiece center. The device was also capable of measuring temperature pulses in these regions with frequency close to the instant rotation frequency of the workpiece, meaning that there probably is a relation between the rotation increase and temperature increase. Vibration was detected in the regions close to the thermocouples caused by their insertion holes. A failure analysis was done for the device. Solutions for the failures and possible enhancements for the device were proposed. Some of the solutions and enhancements were not applied in this moment because they require redesign and fabrication and testing of a new prototype and, therefore, must be applied in a future work.

Keywords: machining; radial turning; temperature measurement; white layer.

ABBREVIATION LIST

ADC	Analog digital converter
EDM	Electrical discharge machining
CD Welding	Capacitor discharge welding
FDM	Finite differences method
FEM	Finite elements method
FFT	Fast Fourier transform
IA	Instrumentation amplifier
IDE	Integrated development environment
LED	Light emitting diode
LEPTEN	Laboratory of Conversion Processes Engineering and Energy Technology
LMP	Precision Engineering Laboratory
PCB	Printed circuit board
PCBN	Polycrystalline boron nitrite
RAM	Random access memory
SEM	Scanning electron microscope
SMD	Surface mounted device
SPI	Serial peripheral interface
UFSC	Federal University of Santa Catarina
USB	Universal serial bus

SYMBOL LIST

F	N	Machining force
F_c	N	Cutting force
F_f	N	Feed force
F_p	N	Passive force
F_a	N	Active force
F_D	N	Thrust force
v_c	m/min	Cutting speed
v_f	mm	Feed velocity
v_e	m/min	Effective cutting speed
k_f	n/mm²	Flow stress
h	mm	Width of undeformed chip
γ_0	-	Tool orthogonal rake angle
F	Hz	Spindle rotation
R	mm	Tool radial position
V_A	mm²/s	Removed area
t_i	s	Time interval between positions
R_0	mm	Initial tool radial position

SUMMARY

1 INTRODUCTION

In many industries, there is a balance between costs, performance, and quality due to client demands and competition [1]. Therefore, there is a constant need for optimization and innovation. This can be made in the project stage, but also the manufacturing stage.

A great number of high-performance automotive parts (like bearings and gears), as well as tools and injection and conformation molds, are fabricated of materials with elevated hardness [2]. Many of those parts undergo grinding processes to attain tight dimension tolerances and low surface roughness. However, in recent years the grinding processes have been replaced by hard turning for many parts since the hard turning usually has a lower cost, lower preparation time, more flexibility to part geometry, greater removal rate, and can be done without cutting fluid [2]. Nevertheless, hard turning still has some drawbacks in relation to grinding, such as process reliability and surface quality [3].

In hard turning white layer formation is considered a high importance attribute in the fabrication of parts susceptible to fatigue [3]. The white layer is an indicator of alterations in the material structure that can result in residual stresses. If these residual stresses result in tensile stress, the fatigue life of the part can be reduced. The white layer can be formed by mechanical and/or thermal effects, where in turning the thermal effects usually produce tensile stresses and mechanical effects produce compression stress [4].

The white layer formation during the radial turning of the hardened steel AISI 52100 with a Polycrystalline Cubic Boron Nitrite (PCBN) tool at constant cutting speed were analyzed by Bortoli [5]. The results of this work show an increase in the thickness of the white layer in areas closer to the center of the workpiece. In the study developed by Camargo [6], the behavior of the cutting forces during this same process was evaluated (Figure 1). As the tool becomes more worn there is an increase of the forces at the start of each pass, but as the tool advances there in the direction of the center of the workpiece the forces decline, and this decline also increases as the tool becomes more worn.

An increase in the white layer thickness accompanied by the decline in the cutting forces points to an increase in temperature in the cutting area as the tool approaches the center of the workpiece [4, 7]. As temperature changes during cutting can affect the quality of parts [4], it is essential to confirm this phenomenon, as well as the development of models that predict temperature changes.

To be able to model this temperature, first, it is necessary to have data on its behavior. The quantity, quality as well as the type of data may determine type and quality of models that

can be developed. In this case, confirming the increase of temperature during the cutting process and quantifying this increase would be enough to create a simple predictive model, but having data that brings an understanding of what is the cause of this increase would enable the use of some more versatile types of models.

Figure 1 – Forces during the hard turning of AISI 52100 using PCBN tool along the tool life.

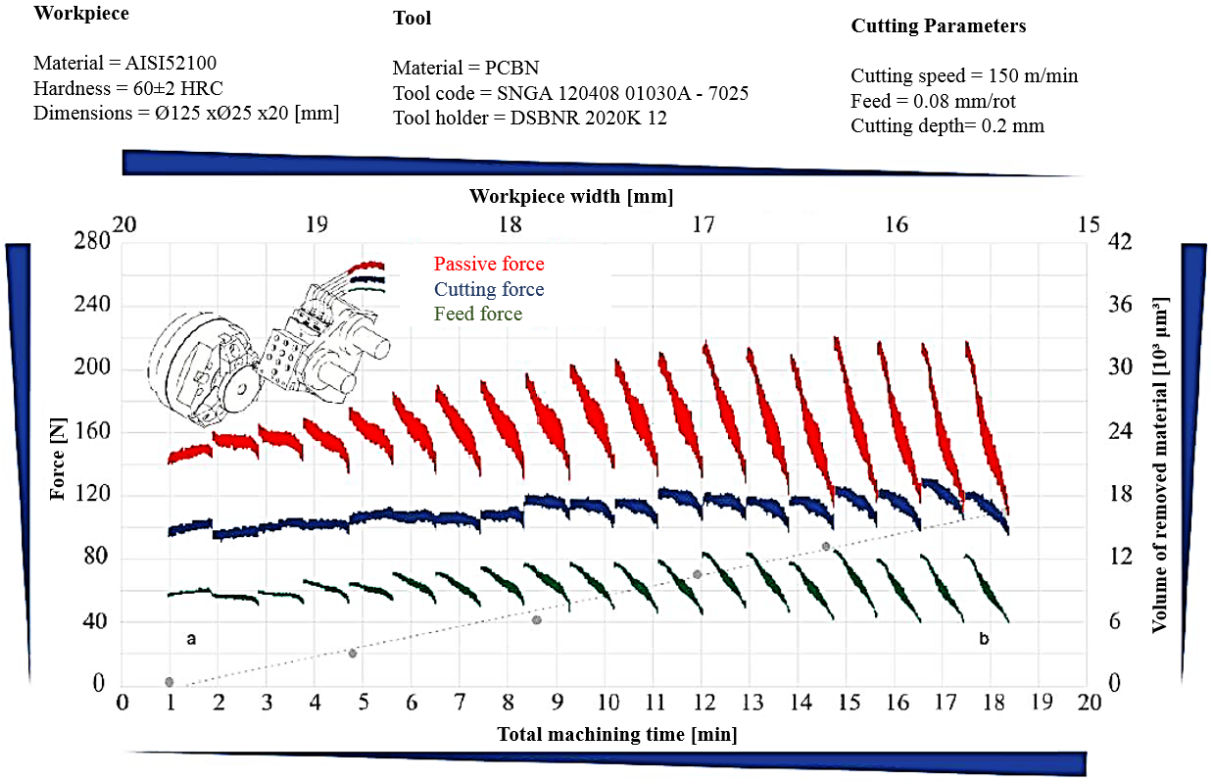

Source: Adapted from Camargo [6].

To understand what may cause this supposed increase in temperature during radial turning, the machining process must be analyzed to identify the parameters related to this increase. In Camargo's experiments [6] most of the cutting parameters were fixed. One of the parameters that changed over time and was clearly related to the temperature change was the radial position of the tool.

To maintain a constant cutting speed in radial turning, the rotation of the lathe spindle increases as the tool approaches the center of rotation. Therefore, in a certain time interval with a constant cutting speed, the tool will move a certain length in an arch. As the tool position approaches the center of the workpiece, this length is constant, but the radius from the arch decreases. In Figure 2 all the blue lines have the same length but different radii. The centermost line forms a complete circle while the most external one forms a third of a circle.

Figure 2 – Behavior of circumference arches with the same length but different radius.

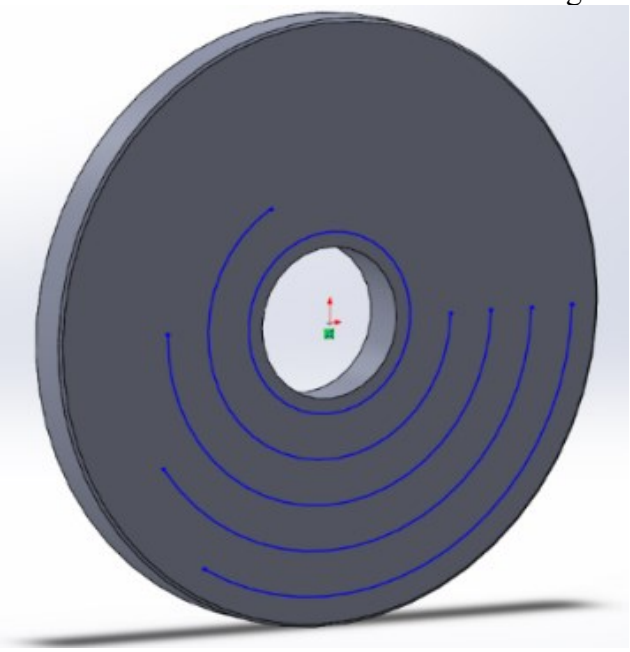

Source: Author.

As the tool needs to move a shorter length to complete a revolution and the speed is constant, there is an increase in rotation frequency. If this rotation increase is related to the increase in temperature, the temperature increase can be caused by the shortening of time between the passage of the tool on a region of the workpiece. As the tool can be considered a heat source, each workpiece region is heated as the tool passes and then cooled before the next tool pass in this same region [8]. Therefore, increasing the rotation frequency results in a shortening of this cooling period.

Another parameter that also change is the tool wear. In each subsequent pass there is an increase of the initial machining forces and there is an increase in the forces decrease during the pass. This indicates that tool wear probably exacerbates the phenomena of forces decrease but it does not cause it directly. Tool wear can cause an increase in generated heat [7], delivering a greater quantity of heat in a region would exacerbate the heat accumulation in a region of the workpiece due to a decrease of cooling time.

In machining, it is very common to try to measure the temperature on the tool cutting edge or in the tool/chip interface. However, measuring the temperature in a few regions of the workpiece would be better to obtain data to corroborate or negate the influence of the rotation frequency in the temperature during radial turning, as it allows for evaluating the cooling phenomenon during the process.

Researchers at the Precision Engineering Laboratory (LMP-UFSC) have been trying to measure the temperature during the previously discussed process (radial turning). Firstly, a thermometric camera was used, but no reliable data was acquired. A few other possibilities were considered, but they were considered expensive to be acquired to be used in exploratory research. Therefore, this research project aims to develop a temperature measuring device that allows the evaluation of temperature changes in radial turning, the first step in opening a new area of study in the LMP-UFSC.

This work is divided into 6 sections. The first, this section, describes the problem and set the objectives. The second section is the state of the art, describing recent developments and established knowledge about subjects related to this research. The third section it is presented the initial development and testing of the temperature measuring device. The fourth section describes the equipment, materials, and methodology used in the experiments. In the fifth section, the results and discussions from the experiments are presented. The sixth section concludes this work and makes suggestions for future works.

1.1 OBJECTIVES

This subsection has the goal to define the main objective of this research and enumerating the secondary objectives.

1.1.1 Main objective

The main objective of this research project is to obtain data to support or negate the assumption that there is an increase in temperature in radial turning as the tool approaches the rotation center of the workpiece. For this purpose, it is necessary to develop a device capable of measuring the temperature in fixed points of the workpiece during radial turning.

1.1.2 Secondary objectives

The secondary objectives of this research are:

a) Investigate possible causes for the temperature increase.
b) Analyze the errors and failures of the temperature measurement device.
c) Investigate possible interferences between the temperature measurement device and other sensors and equipment used.

d) Evaluate the temperature measured in the frequency domain.

e) The proposition of enhancements based on the prototype performance.

2 STATE OF THE ART

This section will make a brief bibliographic revision of the subjects that are pertinent to this research project with the objective of presenting the current state of the art on these topics.

2.1 DATA BASE ANALIZYS

To understand the state of art related to the topic of this research project a publication analysis using the Scopus [9] database was made. This database has a search engine that uses keywords to locate related publications. This search engine uses many logic operators and codes to determine the location of the documents to search for specific keywords and what combination of keywords is desired.

The first search made was to search for the keywords machining and temperature and containing at least one of the terms “face turning” or “radial turning”. The search for these keywords was limited to the title, abstract, and keywords of the publications. The code used for this search was: TITLE-ABS-KEY (machining AND temperature AND ("face turning" OR "radial turning")). This search resulted in 26 publications since 1970. Limiting the analysis to the last 5 years (2017 until 2022) results in only 7 publications. From these, 2 publications measured the temperature in the tool and 1 publication measured the temperature in the workpiece, but it was unrelated to the cutting process temperature as it measured the cooling of the workpiece after casting.

Repeating the search using the keywords machining, temperature, and turning and limiting to the title, abstract, and keywords, resulted in 1250 publications between 2017 and 2022. The code used for this search was: TITLE-ABS-KEY (machining AND temperature AND turning). From this search, limited from 2017 to 2022, the first 10 publications were read to determine if there was temperature measurement. Of these, 6 publications presented temperature measurements, and all of them focused on the tool temperature. Moreover, 5 studies used non-contact methods, 3 used thermography cameras, 1 used an infrared thermometer, 1 used a spectrometer, and 1 used thermocouples.

This brief database analysis illustrates the scarce literature focused on the measuring of temperature in radial turning. Furthermore, there are not many publications containing temperature measurements in the workpiece even in longitudinal turning.

2.2 RADIAL TURNING AND HARD TURNING

This subsection will cover the basics of radial turning and hard turning. Both are subdivisions of the turning process and the combination of both is called radial hard turning.

2.2.1 Radial turning

Turning is a machining process with defined tool geometry where the workpiece is rotated while the cutting tool moves in a longitudinal and/or a radial path in relation to the workpiece [10]. In the radial turning case, also known as face turning, the tool moves in a radial direction during the cut. The process variants for radial turning can be seen in Figure 3.

Figure 3- Process variants of radial turning, according to DIN 8589-1 [10].

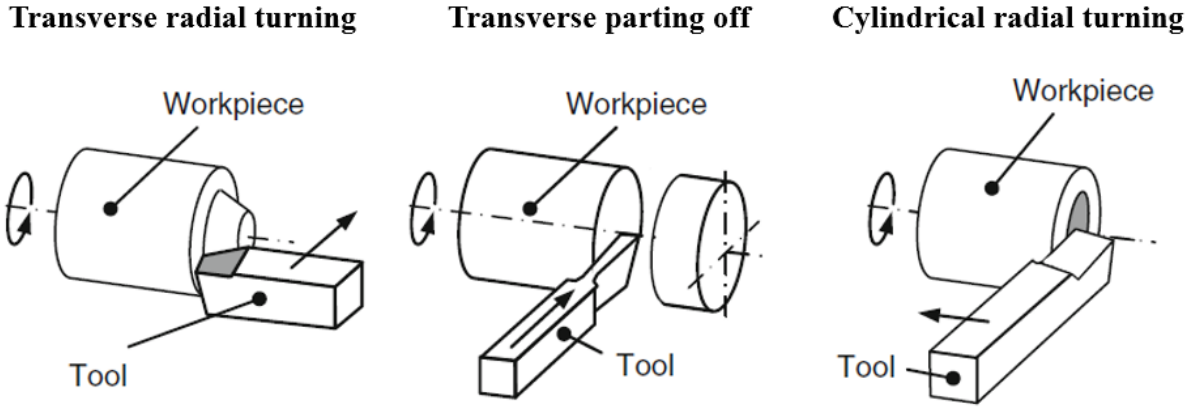

Source: dapted from Klocke [7].

One characteristic important in radial turning, when compared with longitudinal turning, is related to the lathe spindle. In a manual lathe is common that the operator will have control over the spindle rotation but not over the cutting speed. That is not a problem in longitudinal turning as the distance between the center of rotation and the tool is constant, enabling a constant cutting speed [7].

On the other hand, in radial turning is not possible to maintain a constant cutting speed with a constant spindle rotation since the cutting speed is reduced as the tool gets closer to the rotation center. To maintain a constant cutting speed in radial turning is necessary to increase the spindle rotation as the tool moves to the center of rotation, which can be achieved using a CNC lathe [7].

2.2.2 Hard turning

Although the exact definition can vary, when the machined material has a high surface hardness the process can be classified as hard turning. The hardness that is necessary for the processes to receive the classification varies from author to author. There are authors that consider the minimum hardness to be 45 HRC [11, 12] while others consider it to be 50 HRC [7] and other authors consider that this classification is applied only when the rupture strain of the material is above 1700 MPa [13].

Hard turning can be done with or without coolant, but when used it must be in small quantities. This is due to a need for the heat generated by the process to reduce the cutting forces, by softening the material, and making the process viable [11]. As most of the heat remains in the chips, they become a good source of diagnostic to see if the process is well-tuned. During continuous cutting, the chip should be blazing orange and flow off like a ribbon. The chip should also be brittle after it cools off [11].

Hard turning has become an alternative to grinding with the development of cutting tools with high hardness at the end of the 1980s [14]. The replacement of grinding for hard turning can result in a decrease in white layer formation [3]. In Figure 4, a general comparison between grinding and hard turning is presented. It can be noted that hard turning offers advantages in flexibility and process time and some drawbacks in the reliability and precision of the workpiece.

Figure 4 – Comparison between hard turning and grinding processes.

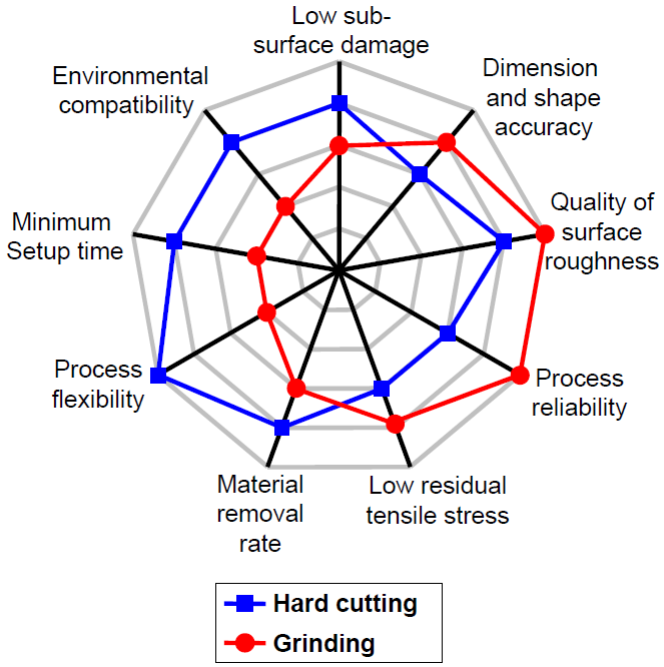

Source: Klocke *et al.* [3].

Hard turning and grinding are usually finishing processes, making the part aggregated value higher. One characteristic that needs to be better understood is the residual stress caused by hard turning since it can decrease the fatigue life of the machined component [3]. As the hard turning requires heat to diminish the cutting force, the formation of a white layer and residual stresses is a price paid to enable the process [11], but these problems can be controlled or reduced.

2.3 MACHINING FORCES

In the machining process where there is a cutting edge that will cause a removal of material, there will appear a resistive force applied in the tool. This force is usually decomposed into three perpendicular components. These three components are the cutting force in the direction of the cutting speed, the feed force in the direction of the feed, and the passive force perpendicular to the first two [7, 15]. This can be seen applied to axial turning in Figure 5.

Figure 5 – Machining force usual decompositions.

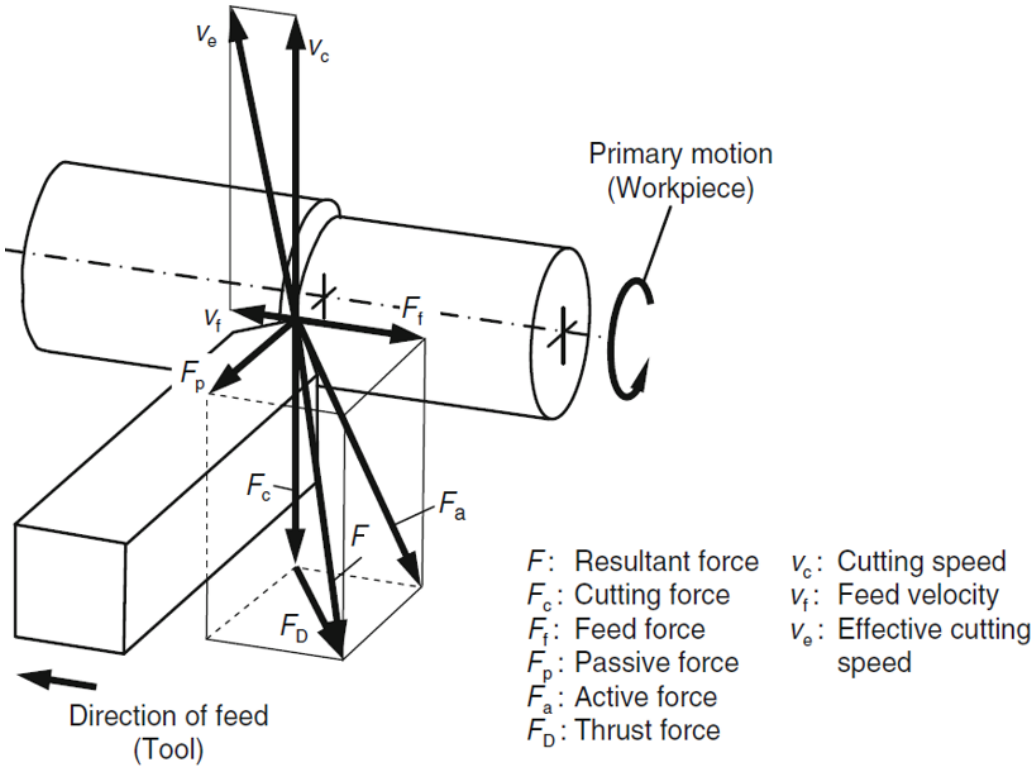

Source: Klocke [7].

As the cutting force and feed force are in the direction of the cutting speed and the feed, respectively, cutting power and feed power can be calculated. The total process power can be calculated using the active force, which is the combination of cutting and feed forces, and the effective cutting speed, which is a combination of cutting speed and feed [7, 15]. Knowing the power needed and forces applied in a machining process is very important for dimensioning machines and parts [7].

As the tool edge becomes more worn, the changes in its geometry can alter the machining forces [7]. These forces are influenced by the tool and workpiece materials, tool geometry and wear, process parameters, etc. [7, 15]. In Figure 6 the usual variation of forces with cutting parameters variations is shown.

Figure 6 – Qualitative variation of cutting forces components.

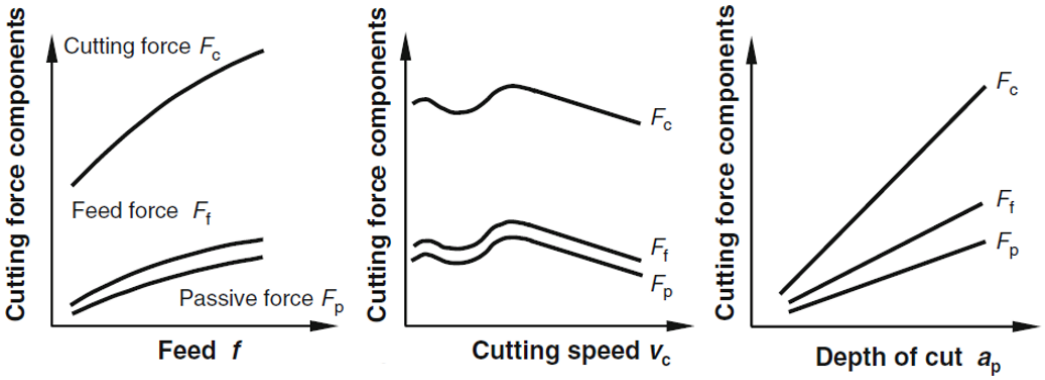

Source: Klocke [7].

The increase in cutting depth and feed causes an increase in all force components since the increase of these parameters increases the depth and thickness of the undeformed chip [7, 15]. With the increase in cutting speed there is an increase in power and, as most of the power is converted to heat, occurs an increase in temperature, leading to the softening of the material and a decrease in force. The exception of this is a certain temperature range where there is a formation of built-up edge, where there will be an increase of cutting force [7]. This temperature increase is used in hard machining to enable the cut [11].

As the tool becomes worn the forces will be affected. Depending on the predominant type of wear the forces can decrease or increase [7]. With a predominance of crater wear usually occurs a decrease in forces due to the alteration of tool geometry. The flank wear predominance usually causes an increase of the forces due to an increase in friction area between the workpiece and tool flank [7].

A characteristic of the forces involved in hard turning is that due to the cutting depth being smaller than the tool nozzle radius, contrary to regular processes, the passive force becomes dominant, this occurs because this will change the effective tool edge angle due to the curvature [16]. Therefore, there is a greater mechanical load applied to the workpiece surface and although the passive force does not generate work, it cannot be neglected [16].

2.4 HEAT GENERATION IN MACHINING

During the machining, most of the energy used is converted to heat. Most of the heat in regular processes is converted in the shear zone, meaning that a big portion of the heat stays in the chip. A smaller part of the heat is transferred to the tool and a very small part is conducted to the workpiece bulk. A small part of the heat is converted by friction, both between the chip

and tool face and the workpiece and tool flank [7]. Figure 7 shows the approximate heat distribution in steel cutting and a temperature diagram.

Figure 7 – Heat and temperature distribution in the process of steel cutting.

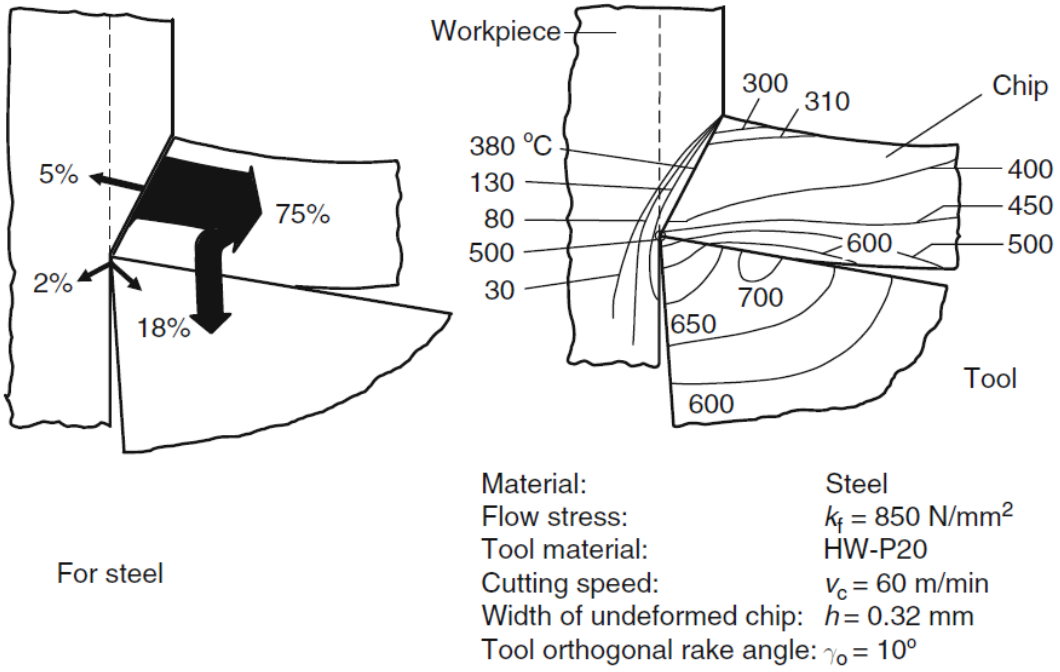

Source: Klocke [7].

The heat is generated mainly in two areas: i) the shear zone and ii) the interface between the cutting tool and chip [17–19]. In the shear zone, the heat is generated by the conformation of the machined material, while in the interface of the cutting tool and chip it is generated by friction [17–19]. Due to the movement of the material and heat sources, the region with the highest temperature is not the tip of the cutting tool, but a point on the rake face of the tool [7]. During machining processes, the temperature gradient can be extremely high and the process is very dynamic, therefore temperature measurement can be a challenge [7].

The level of the temperatures in a process depends on the tool material, workpiece material, cutting parameters, tool wear, and cooling medium [7]. As an example of how high the temperatures can reach, there are reports of temperature measurements of 1000 ºC on the tool rake face and 800ºC on the tool flank while cutting steel using cemented carbide tools [7].

Astakhov and Shvets [8] propose that in a turning process, with the right conditions, the heat generated in a position of the workpiece can affect the process temperature in the same angular position in the next revolution. For that to occur the heat propagation speed must be greater than the feed speed, but not so greater as to disperse the heat before the tool passes. This

proposition was validated only through force data to longitudinal turning due to a decrease in the forces. Experimentation with radial turning did not present similar results and was justified that the machine used was only capable of constant rotation and not constant cutting speed.

Even before Joule established the equivalence between heat and mechanical labor, Count Rumford [20] already investigated this concept by studying the heat generated during the boring of cannons [17]. Already in 1907 Taylor [21] recognized a relation between heat and tool wear. Besides tool wear, there is an interest to predict workpiece quality, subsurface integrity, part accuracy, and many other process characteristics that depend on the process temperature [22]. Among these, the prediction of white layer formation is very important for the fabrication of parts subjected to fatigue [4].

2.4.1 White layer formation

During the fabrication processes, the microstructure of the workpiece can be affected by a variety of process factors. One of the microstructural changes that can occur in turning, and especially in hard turning [11], is the formation of the white layers [4].

The white layer is usually identified as a white-colored layer in the subsurface of the material when an optic microscope is used [4]. An image by a Scanning Electron Microscope (SEM) can be seen in Figure 8. This layer can be composed of unquenched austenite, regions of refined grains or impurities, and can present compressive or tractive residual strains. Both the composition and residual strains depend on how the layer is formed [4].

Figure 8 – SEM image showing the white layer in an AISI 52100 steel radially turned with PCBN tool. Cutting speed: 150m/min, feed 0.08mm and cutting depth 0.20mm.

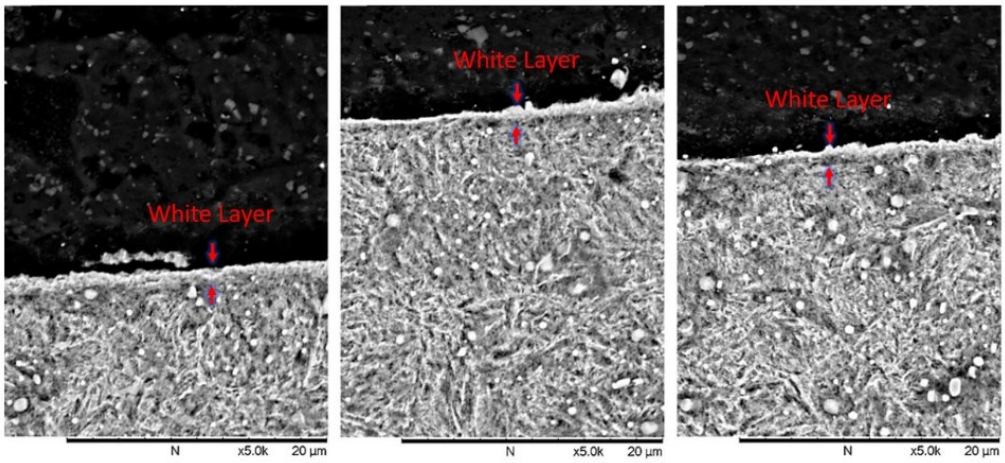

Source: Adapted from Bortoli [5].

Thermal effects usually generate tensile residual stresses as well as phase change, generating unquenched austenite and martensite because of the temperature increase followed by a rapid temperature decrease. Austenite having a smaller volume than ferrite tends to contract, but the bulk of the material will prevent this contraction, generating tensile stress [4]. On the other hand, mechanical effects can cause grain refining due to the temperature and compression of the material, usually generating compressive residual stresses. Furthermore, the presence of oxygen and other impurities on the surface can cause the appearance of oxides and impurities in the crystalline matrix on the surface and subsurface of the material [4].

During the turning process, the white layer formation occurs by a combination of the previously described effects. Because of fatigue life problems caused by tensile residual stresses the white layer formation by thermal effects is of great importance for components subjected to fatigue [4].

Bortoli [5] analyzed the relation of passive forces (the most significant forces in the analyzed process), tool state, and white layer formation with the radius of the workpiece in hard radial turning of AISI 52100 with PCBN tools (Figure 9).

Figure 9 – White layer thickness and passive force variation in function of distance to workpiece center.

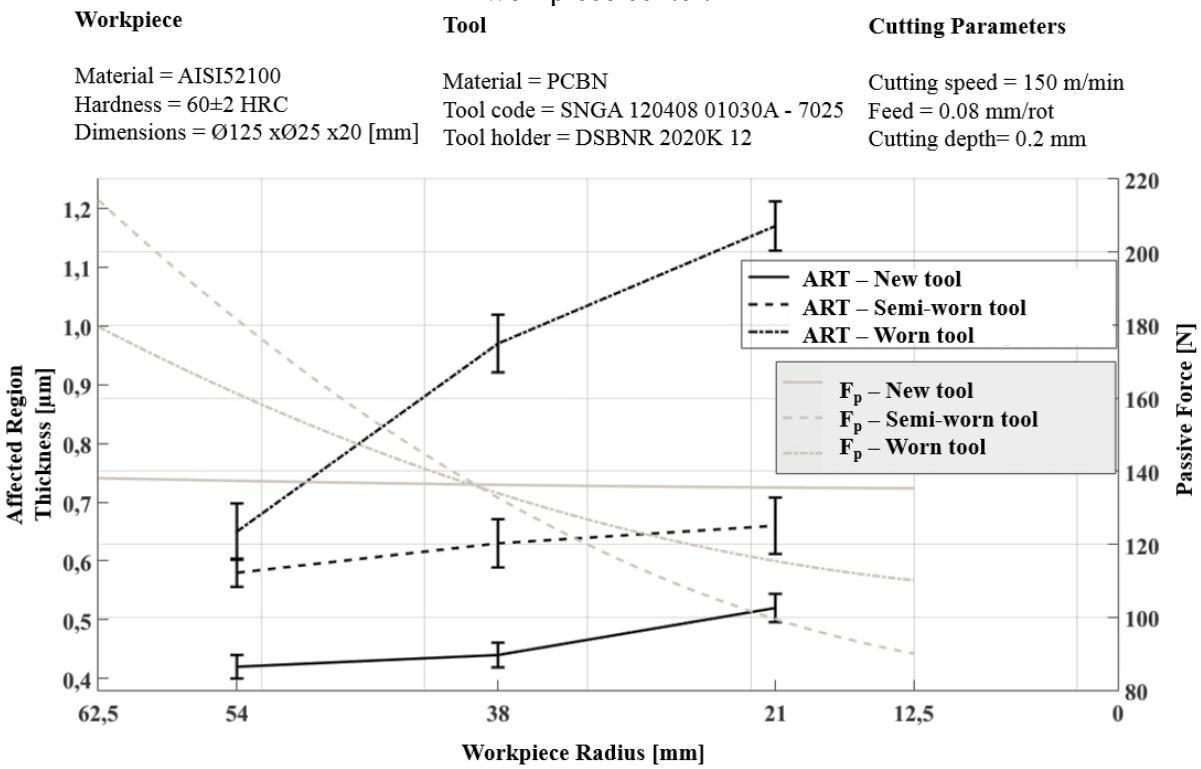

Source: Adapted from Bortoli [5].

In Figure 9 the horizontal axis represents the distance to the workpiece center, the left side being farther from the center. On the left vertical axis is the affected region thickness, representing the measured white layer thickness. On the right vertical axis, the passive forces are represented. It shows an increase in white layer thickness as the tool approaches the workpiece center, which is accompanied by a decrease in the forces. Both the increase of the white layer and the decrease of passive force indicate an increase in temperature in the process as the tool approaches the workpiece center [5].

2.5 MODELING AND SIMULATION IN MACHINING

Simulations can be defined as a simplified imitation of a system, used to better understand and improve the original system [23]. A simulation is a tool used to predict how a system will behave in certain conditions without exposing the system to those conditions or without having access to the system. Therefore, with the use of an appropriate model or a set of models is possible to simulate the system response to damaging conditions without risking the system, and reduce the expenditure of raw material in testing and identifying system problems before it is constructed, among other applications [23]. In machining, simulation is used, for example, to optimize parameters and machine sizing [22].

In the last decades, great progress was made in the modeling and simulation of machining processes [22]. The most used models for machining processes can be divided into five groups: analytical, numerical, empirical, artificial intelligence, and hybrids [22]. In Table 1 a comparison of the modeling and simulation methods can be seen while a brief description of each model type can be seen below:

a) The analytical models use equations of the phenomena involved in the processes and can be used to predict with detail the behavior of the system. The equations can vary greatly between applications and these equations can be hard to obtain [22, 24].
b) Numeric models reduce the system in many codependents, smaller and simpler systems, which simplifies the equations, but it may require a lot of computational power [22, 24].
c) Empiric models are obtained through regressions of empirical data, requiring a greater quantity of tests, and their applications are limited by the testing parameters [22, 24].
d) Artificial intelligence models use iterative methods to obtain regression without the need for previous knowledge of the form of the equations but require a large amount of data [22, 24].

e) Hybrid models combine two or more types of models with the intent to balance their shortcomings [22].

Table 1 - Capabilities and limitations of modeling approaches.

	Analytical	**Numerical**
Principle	Slip-line theory or minimum energy principle.	Continuum mechanics using FEM, FDM & meshless FEM.
Capabilities	Predicts cutting forces, chip geometry, tool-chip contact length, average stresses, strains, strain-rates and temperature.	Predicts forces, chip geometry, stresses, strain, strain-rates and temperatures.
Limitations	Usually limited to 2-D analysis with single and multiple cutting edge, but some 3-D models exist.	Material model, friction as input, computational limitations: e.g., meshing.
Advantages	Ability to develop fast practical tools	Opportunities to connect to industry-relevant parameters.
Disadvantages	Unique to each machining problem	Long computation time.

	Empirical	**Artificial intelligence**	**Hybrid**
Principle	Curve fitting of experimental data.	Fuzzy set theory, artificial neural network, etc..	Combines the strengths of other approaches.
Capabilities	Applicable to most machining operations for measurable process variable only.	Applicable to most machining operations. Some methods are applicable to qualitative data.	Provides meta-models for a family of models to be integrated.
Limitations	Valid only for the range of experimentation.	Requires enough data to define algorithm rules and/or training	Limited to the strength of the base model: i.e., analytical, numerical, empirical, etc.
Advantages	Practical, fast and direct estimation of industry-relevant parameters.	Can model qualitative parameters, linear and no-linear relations, and form equations using the data set used for training.	Improves the capabilities and accuracies of the base model.
Disadvantages	Extensive experimentation, time-consuming and costly.	Requires extensive data set for training and/or requires expert knowledge to define qualitative rules.	Need for extensive data from experiments and/or simulations.

Source: Adapted from Arrazola *et. al* [22] and Rao [25].

Usually, the inputs in a machining model are the characteristic of the workpiece, tool, and machine tool, besides the process parameters. The final outputs, usually called stage II output, are relative to part quality and production costs, and wastes. Intermediary outputs, usually called stage I output, are resulting information that has no direct economic relevance,

but are used to obtain stage II outputs [22]. In Figure 10 there is a representation of this two-stage modeling approach.

Figure 10 – Two-stage modeling approach in machining processes.

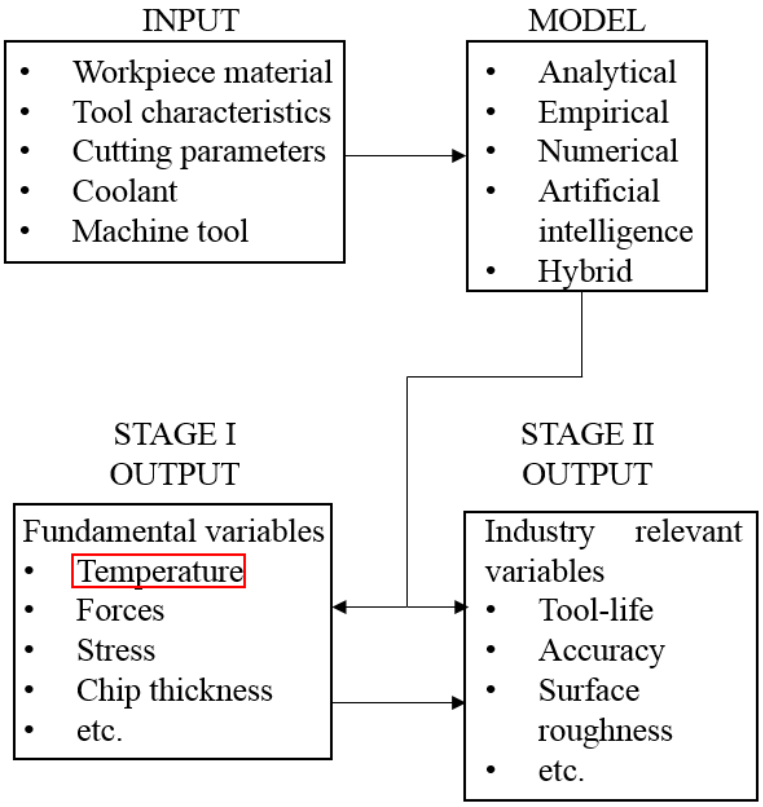

Source: Adapted from Arrazola *et al.* [22].

The main objective of modeling in machining processes is to predict stage II variables, but in many cases, it is difficult to predict them analytically. Thus, most models capable of outputting stage II variables directly from the inputs depend on expensive experimental testing. For this reason, there is a focus on researching models that output stage I variables and using these variables to reach the stage II variable [22]. For example, the temperature is a stage I variable that can be used to predict stage II variables such as tool life and surface integrity [22].

In modeling and simulation of temperature in machining processes, there are many models of many types that can be applied, but a great hindrance in their application is the need for validation. All models, independent of the type, need to be validated with empirical data to ascertain that their behavior is truly analog to the real system. Because of the difficulty in the measurement of temperature in machining processes, this validation can be a challenge [22].

2.5.1 Modeling and simulation of forces

There are many models used to predict machining forces during a turning process. A well-known model is an empirical model called the Kinzle model, which uses the cutting section area to determine the cutting forces [7, 15]. Kinzle's model requires extensive testing and is limited to the testing parameters. Although there are correction factors to variations of tool geometry, cutting speed, chip thickness, etc. [15].

Another well-known model is the analytical model called the Merchant model [26, 27], which uses shearing plane angles, material constants, friction, etc. to predict cutting forces [7]. The limitations of the Merchant model are that it can be very hard to obtain all required variables for its application. Although the original model was published in 1945 [26, 27], there is still research being done to refine it like the study developed by Molinari and Moufki [28].

Another type of model used to predict cutting forces is the Finite Element Method (FEM) [7]. This type of model can be used to simulate a 2D cutting [29], but there are many complex processes that require the use of 3D modeling [30]. It should be noted that some material properties are temperature dependent. For example, in the research of Tzotzis *et al.* [30], the material flow stress was temperature dependent. Material flow stress is used in damage criteria, which predicts when there is material rupture, and in material deformation. This means that it was necessary to simulate the temperature to be able to correctly simulate forces. This also means that the temperature model must also be validated with temperature data.

2.5.2 Modeling and simulation of temperature

Due to the dynamic nature of most machining processes, most analytical temperature models use a moving heat source model presented by Carslaw and Jaeger [31]. In the year 2000 Komanduri and Hou [17–19] revised many previously proposed models that considered the shear zone as a moving heat source and refined them into a new model. Their model considers the heat generated in the shear zone and the tool-chip interface separately and then made a superposition of both.

A recent example of numerical models application developed by García-Martínez *et al.* [32] proposes a method to estimate the temperature field in the turning process. The methodology used can be seen in Figure 11. They considered 3 main heat sources: the shear zone, the tool-chip interface, and the tool flank and workpiece interface that becomes relevant due to wear. The tool-workpiece thermocouple method was used to measure the heat generated

by the tool flank and workpiece interface. To do that temperature was measured with feed set to zero, meaning that no chip was formed. Then, an infrared camera was used to measure the tool rake face during the process with regular feed. Later a FEM model was used to estimate the temperature field and the result was compared with the measurements to validate it [32].

Figure 11 – García-Martínez *et al.* [32] methodology schematic.

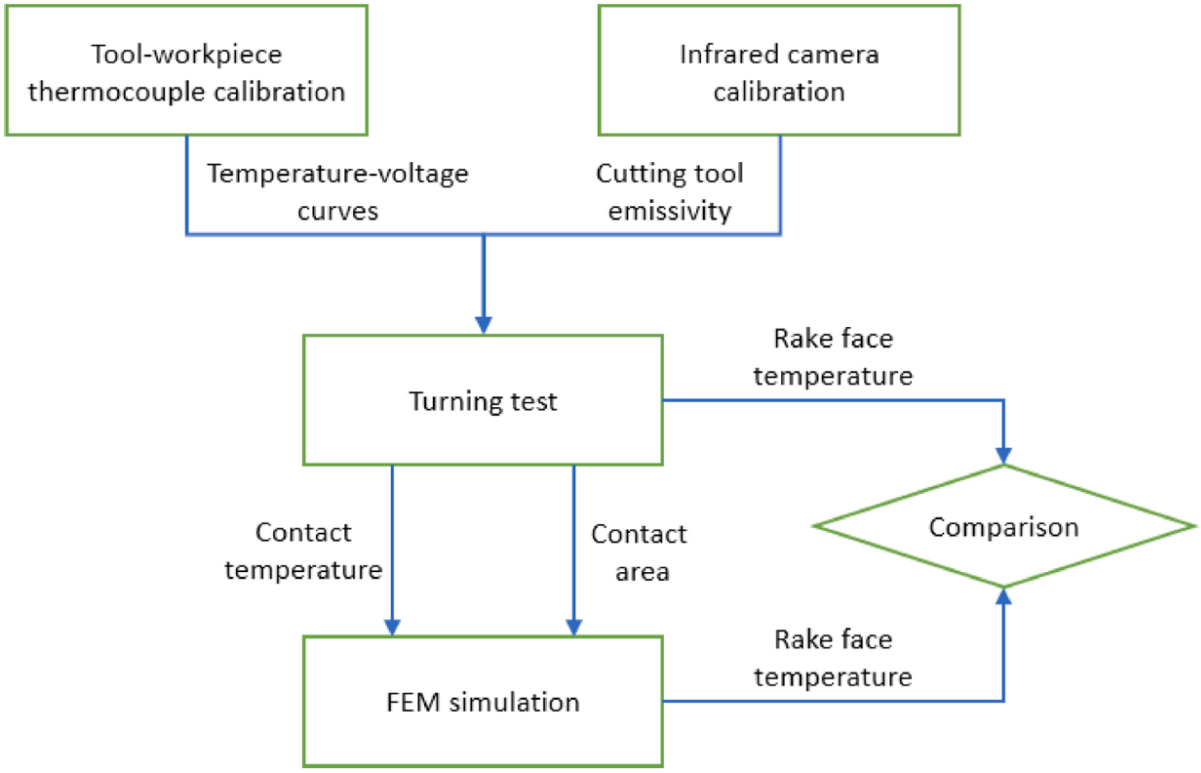

Source: García-Martínez *et al.* [32].

Zhou *et al.* [33] used a FEM model to generate data to train an artificial neural network. This was done because although it was possible to use the FEM model to calculate the temperature field reliably, it was time consuming, and developing a new faster method, even if less reliable, would be advantageous. Experimental data was not used to train the artificial neural network because would be too costly and hard to guarantee data consistency. After obtaining the new model, the results from both models were compared to experimental data for validation, as validation required a smaller volume of data than training the artificial neural network. The resulting artificial neural network model was able to predict tool-tip temperature using the process parameters and the measured temperature of 4 thermocouples in specific positions.

2.6 TEMPERATURE MEASUREMENT IN MACHINING

Figure 12 shows an outline of the history of the measuring methods used in machining. As previously stated, before Joule's experiment, to find the equivalence between mechanical labor and thermal energy, in 1798 Count Rumford [20] analyzed the generation of heat in the machining of cannons using calorimetry concepts. Since then, many other methods were used. The most common method is the use of thermocouples [7]. Spectral radiance thermometry methods are usually considered non-invasive and have the advantage of not adding significant distortions to the system [34].

Figure 12 – Historical outline of temperature measurement in machining.

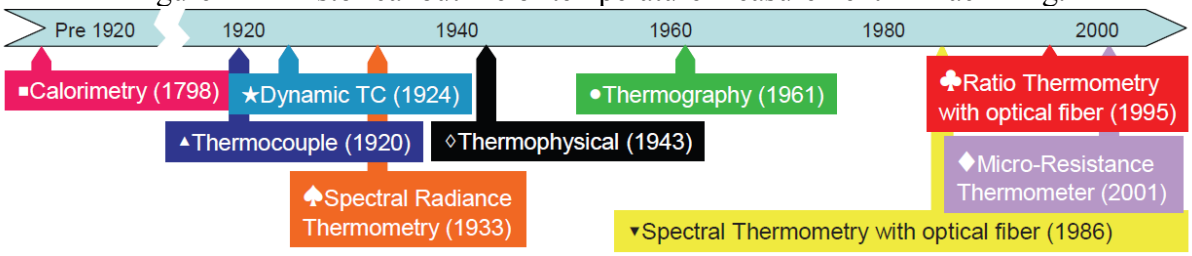

Source: Davies *et al.* [34].

Resistance methods, that rely on the resistance variation with the temperature, are relatively low cost and simple, but they can be relatively large and have a long time constant [34]. Some of its disadvantages can be overcome by the introduction of thin film elements [34], like the recent developments published by Plogmeyer *et al.* [35] (Figure 13).

Figure 13 – (a) Overview of sensors and contact pads. (b) & (c) Magnification of two possible sensor structures.

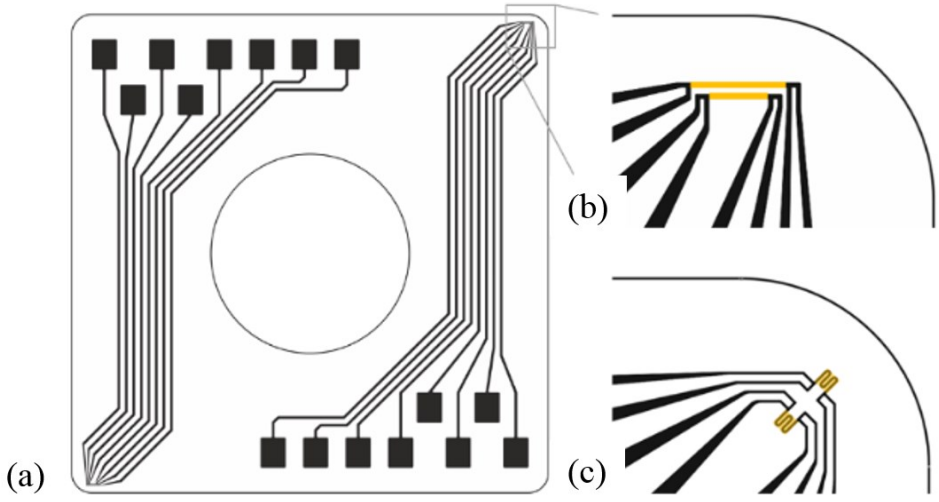

Source: Plogmeyer *et al.* [35].

One way to measure temperature is to quantify thermal emissions. One method of doing that is with the use of a thermographic camera, schematically represented in Figure 14. An advantage of this method is that it is non-invasive, but to use it the emissivity of the material where the temperature will be measured must be known [22].

Figure 14 – Schematic representation of a thermographic camera.

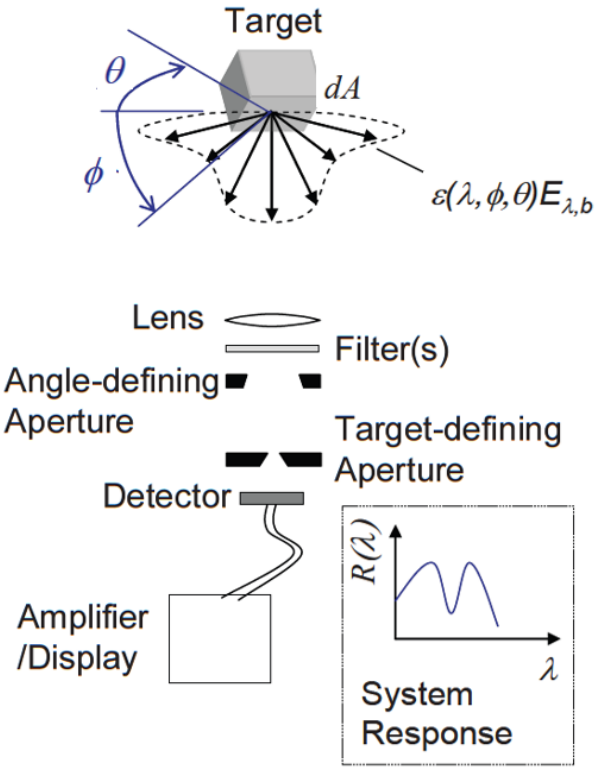

Source: Davies *et al.* [34].

As shown in Figure 14, the emissivity of a non-ideal body can vary according to the measured wavelength and the emission direction, among other factors. To prevent these sources of errors it is common to keep the camera and the analyzed object stationary between each other. In Figure 15 the arrangement used by Lee *et al.* [36] can be seen, where both the camera and tool are kept stationary between each other. In a recent work, García-Martinez *et al.* [32] used a thermographic camera to validate the FEM model used to predict the temperature fields.

Figure 15 – Representation of the measurement of temperature in turning using a thermographic camera to generate data to calibrate a neural network model.

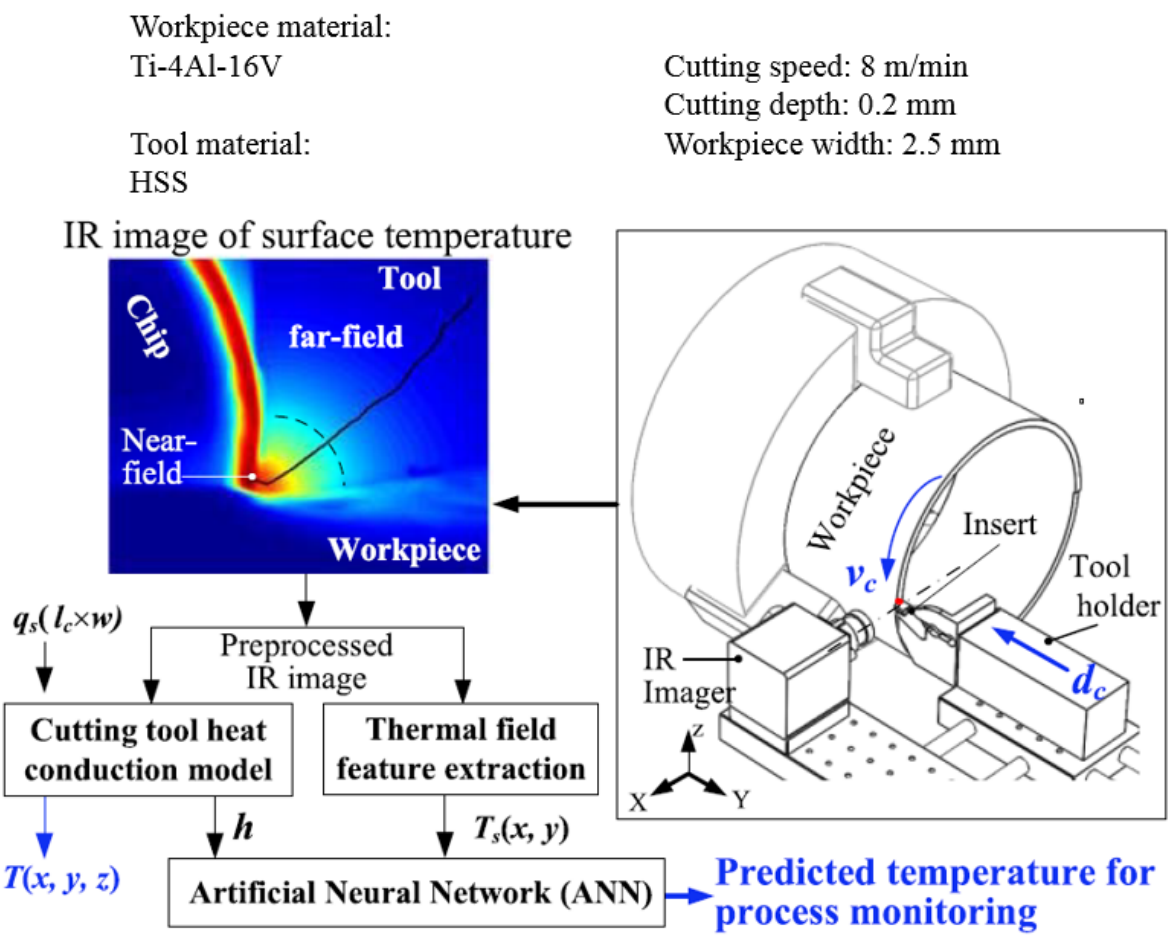

Source: Lee *et al.* [36].

Another method that relies upon the measurement of the thermal emissions, but in a more localized way, is the measurement using a pyrometer. As with the thermographic camera, the pyrometer requires the knowledge of emissivity in the specific frequency used by it. When this information is not known a two-color pyrometer can be used. This equipment measures the emission in two distinct frequencies to determine the temperature without the need to know the emissivity. One care must be taken when using a two-color pyrometer, as it assumes that the measured body can be classified as a grey body and have the same emissivity for all frequencies, or at least in the two frequencies used by the device. Figure 16 is a schematic representation of a two-color pyrometer [7, 34].

Figure 16 – Schematic representation of a two-color pyrometer

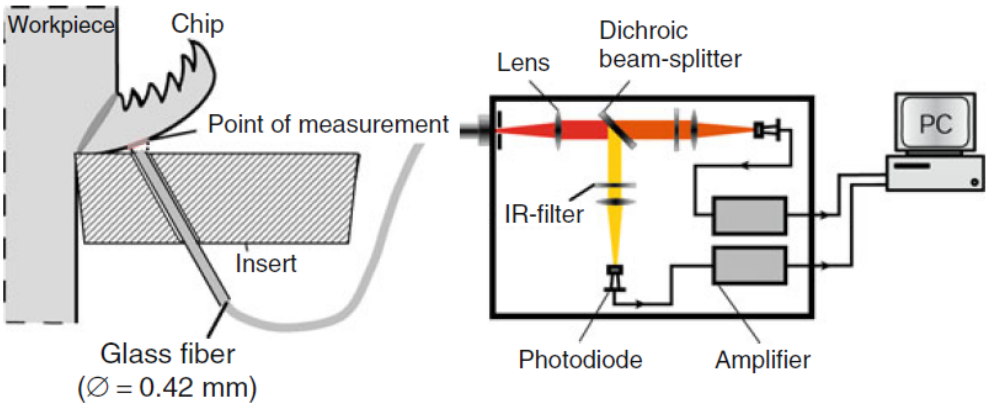

Source: Klocke [7].

In a recent study, Rezende *et al.* [37] used an infrared pyrometer to measure chip temperature to try to estimate the cutting temperature. In another study, Han *et al.* [38] used a two color pyrometer to obtain real time measurements that could be used as an early warning for a tool's end of life.

Among the techniques mentioned in Figure 12, the ones most commonly used in turning are the thermocouple, both embedded thermocouples and tool-chip pair, and one or two color pyrometers [34]. The thermocouples function is based on the Seebeck effect, where when you have two different materials joined in two points there will be a voltage in the joints that will vary with the difference in temperature between the two joints. This voltage depends on the pair of materials used [34].

The use of a thermocouple to measure temperature requires knowing the relation between voltage and temperature differences between the joints, besides the knowledge of the temperature of one of the joints. A couple of possible configurations for the use of thermocouples are presented in Figure 17. For the most common material pairs, there are tables relating voltage and temperature when one of the joints is kept at 0 °C, if the known joint is not at that temperature there needs to be compensation [39].

Figure 17 – Temperature measurement using thermocouples, T0 is the reference temperature, T1 is the measured temperature, Ta is the ambient temperature and V is the voltage. (a) Measuring system with thermocouple with two distinct materials. (b) Measuring system with thermocouple with three distinct materials.

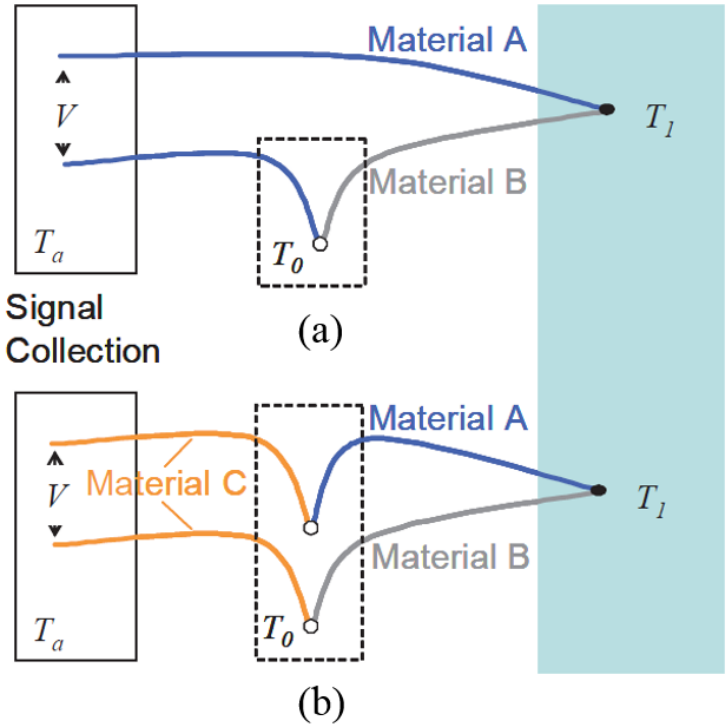

Source: Davies *et al.* [34].

One example of the embedded thermocouple used in turning experiments can be seen in Figure 18. In this method, the objective is to put the thermocouple's measuring joint as close as possible to the tool edge [40]. Unfortunately, it is usually necessary to remove material from the tool to insert the thermocouple, which can diminish the tool's rigidity, causing tool chipping [40].

Figure 18 – Embedded thermocouple. (a) Grinded slot for thermocouple insertion. (b) Tool with the embedded thermocouple.

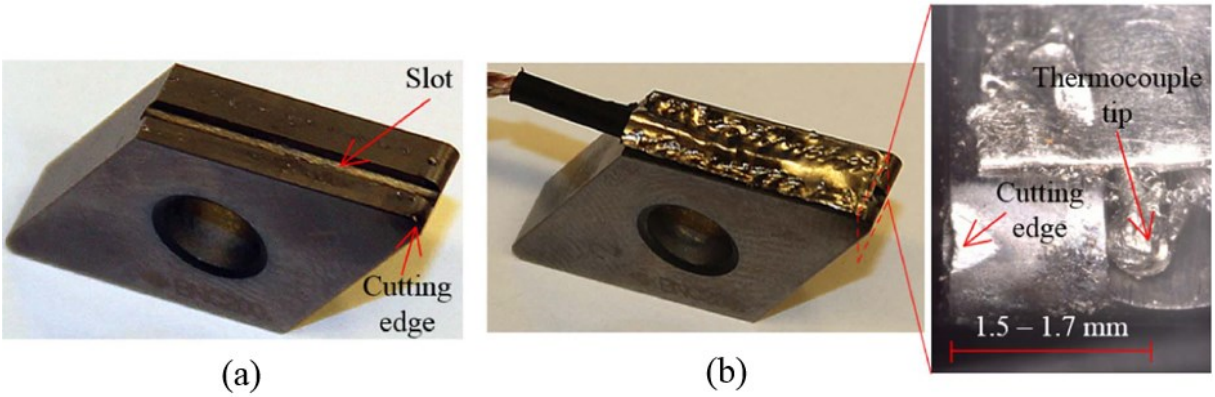

Source: Chen *et al.* [40].

Another method using thermocouples to measure temperature in turning is the tool-chip thermocouples, where the tool and the workpiece take the role of the two distinct materials that make the thermocouple (Figure 19). Although it is possible to measure the temperature in the tool-chip interface, there is no way to properly calibrate this system to compensate for the oxidation, material structure changes, and other phenomena that can influence the measured voltage [34].

Figure 19 – Tool-chip thermocouple.

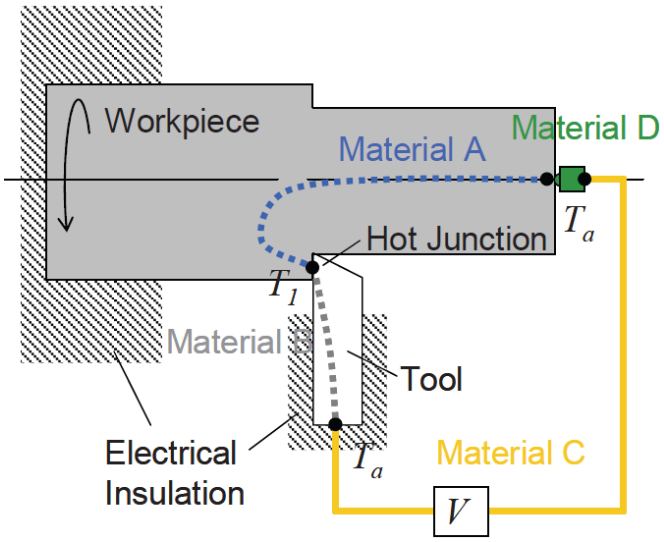

Source: Davies *et al.* [34].

In the study published by Zhou *et al.* [33] a total of five thermocouples (four on the top and one embedded near the tool tip through a hole on the bottom) were applied to validate the models used in the research. This assembly (Figure 20) was used to obtain data on specific points to compare the data with the temperature fields simulated by FEM and artificial intelligence models. Shallow holes in the rake face and the hole in the bottom were made by Electrical Discharge Machining (EDM).

Figure 20 – a) Global vision of the setup used. b) Rake face with thermocouples. c) Bottom of the tool. d) Thermocouples position on the tool.

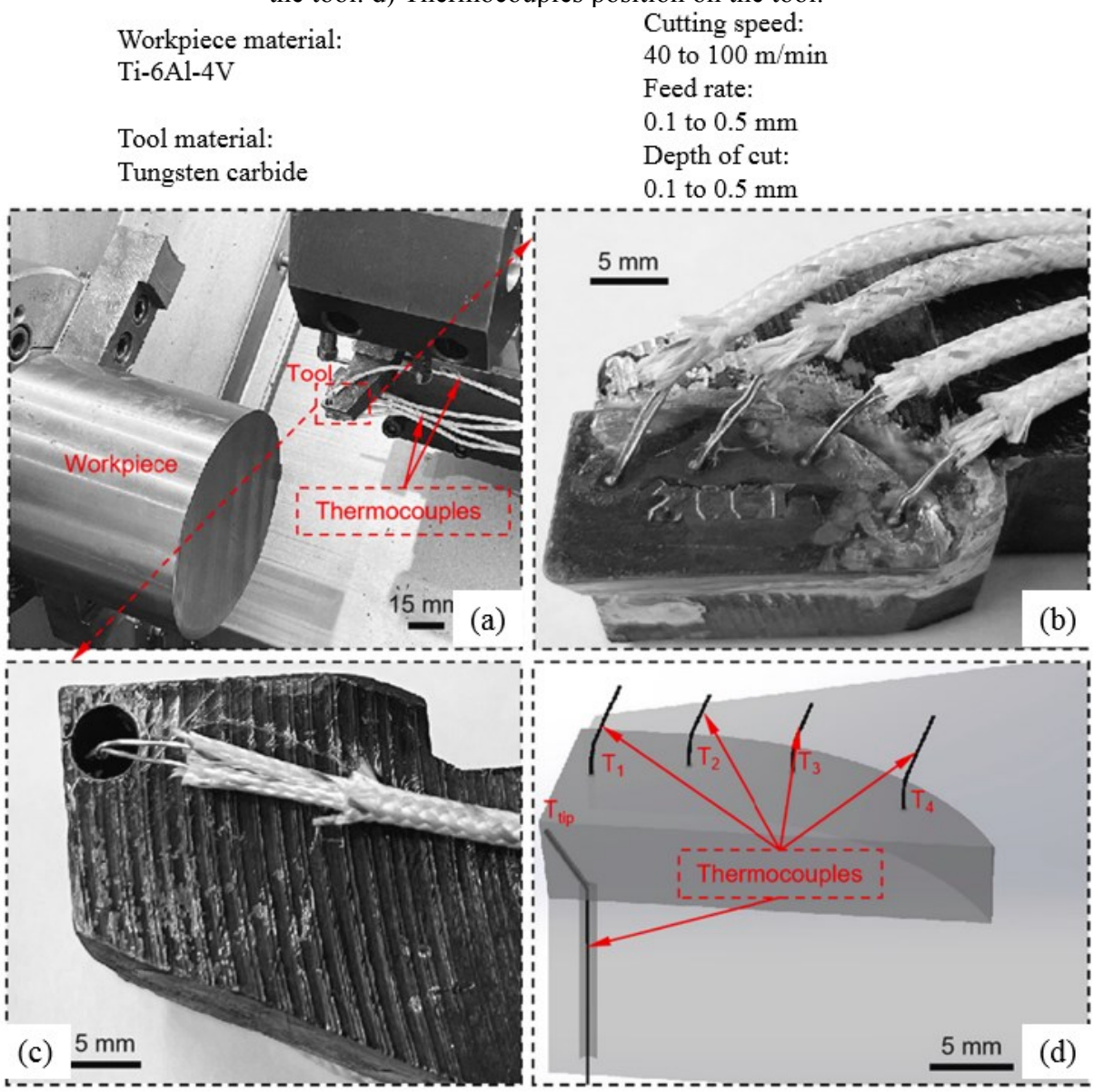

Source: Zhou *et al*. [33].

Chen *et al.* [40] used two methods to measure temperature in hard turning. The first was an embedded thermocouple on the tool as seen in Figure 18. The second was a thermocouple formed between the tool and a metal foil on the workpiece which can be seen in Figure 21.

Figure 21 – Exploded view of the of the tool-foil thermocouple assembly.

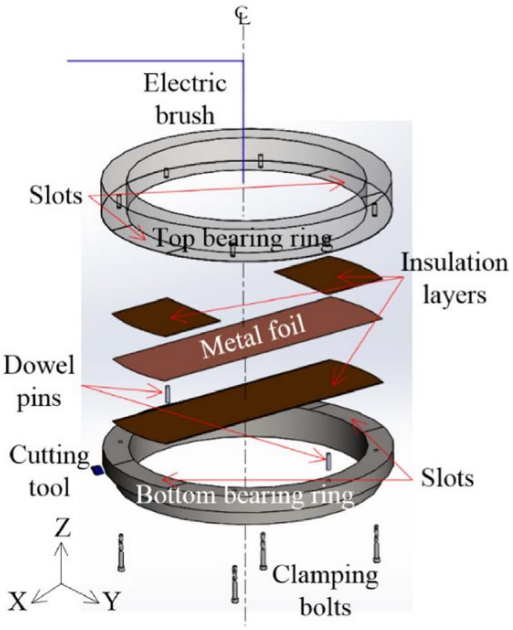

Source: Chen *et al.* [40].

In the tool-foil method, a metal foil was compressed between two parts of the workpiece with insulation between the foil and the workpiece parts [40]. The voltage between the foil and the cutting tool was measured with the help of an electric brush. This assembly means that the temperature would only be measured when there was contact between the tool and foil. In Figure 22 a sample measurement done by Chen *et al*. [40] can be seen. The assembly caused disturbances in the cutting process in the region where the tool-foil thermocouple was active, however, this disturbance was not addressed in the publication. The results show that the peak temperature measured with the embedded thermocouple was in agreement with the data from the tool-foil thermocouple, validating both methods.

Figure 22 – Sample of hard turning measurement with 0.05 mm feed.

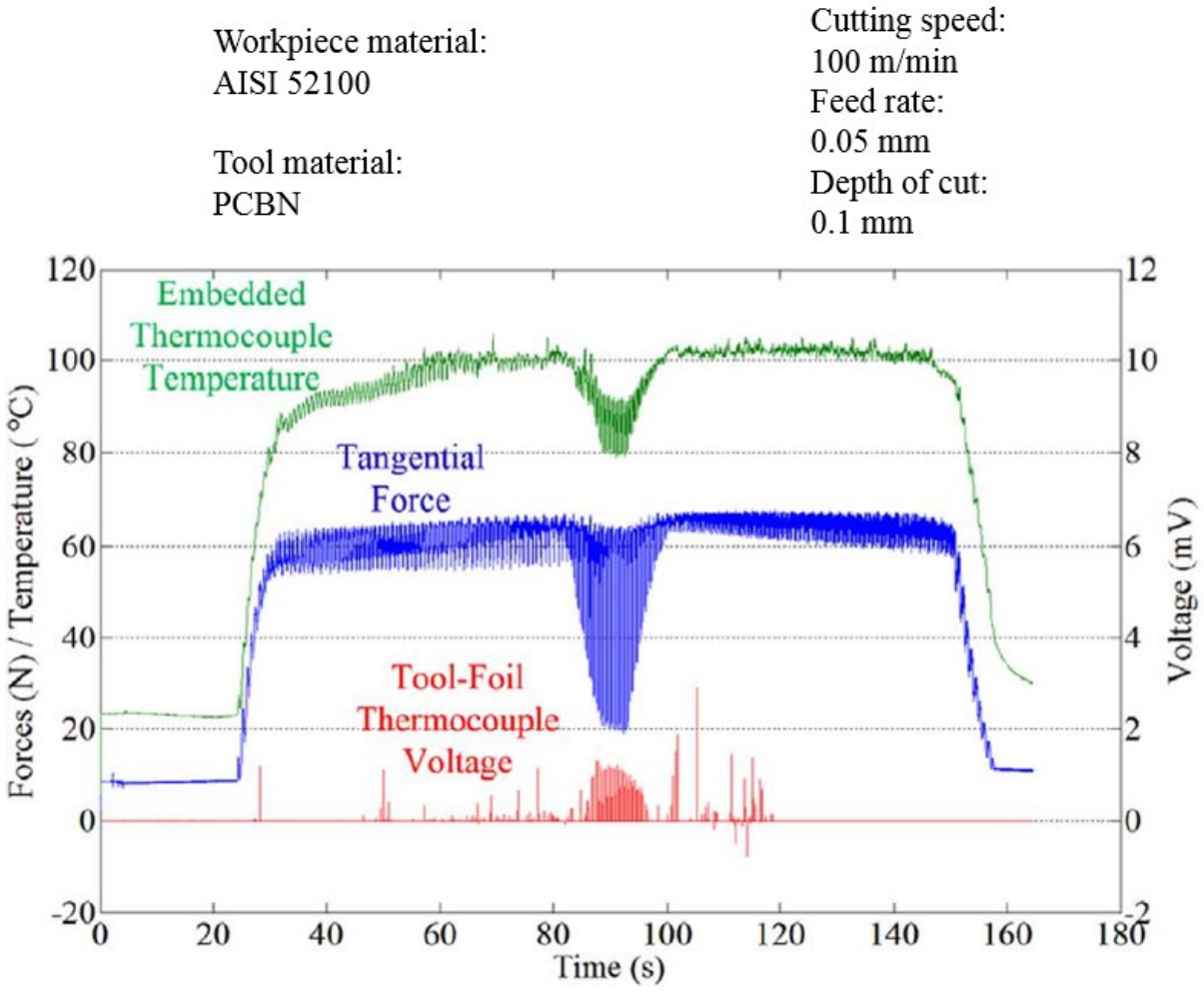

Source: Chen *et al.* [40].

Battaglia *et al.* [41] used 3 K type thermocouples embedded in a tubular workpiece at 2, 2.5, and 3.5 mm from the machined surface (Figure 23). The objective was to obtain the surface temperature during the machining of the XC48 steel. Each thermocouple was formed by two 10 mm wires. An AD595CQ amplifier was used for each thermocouple, this type of amplifier is specially designed for K type thermocouples. The thermocouple signals were transferred to an acquisition system using a slip ring. The temperature measurement from roughing and finishing processes can be seen in Figure 24.

Figure 23 – Assembly used to measure temperature.

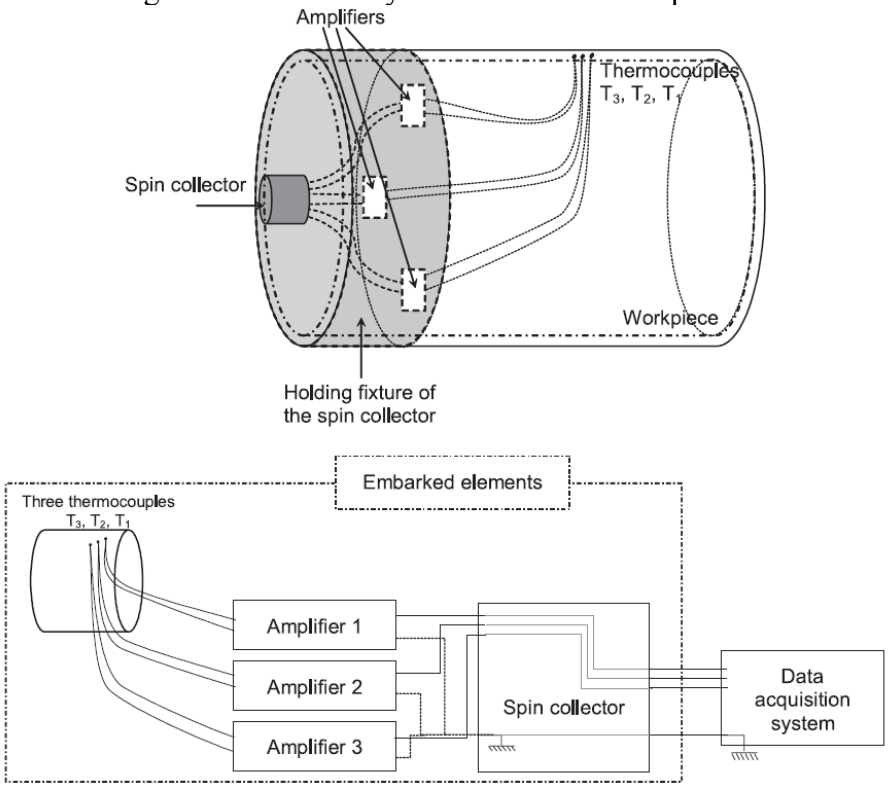

Source: Battaglia *et al.* [41].

Figure 24 – Measured temperature in roughing (left) and finishing (right) processes.

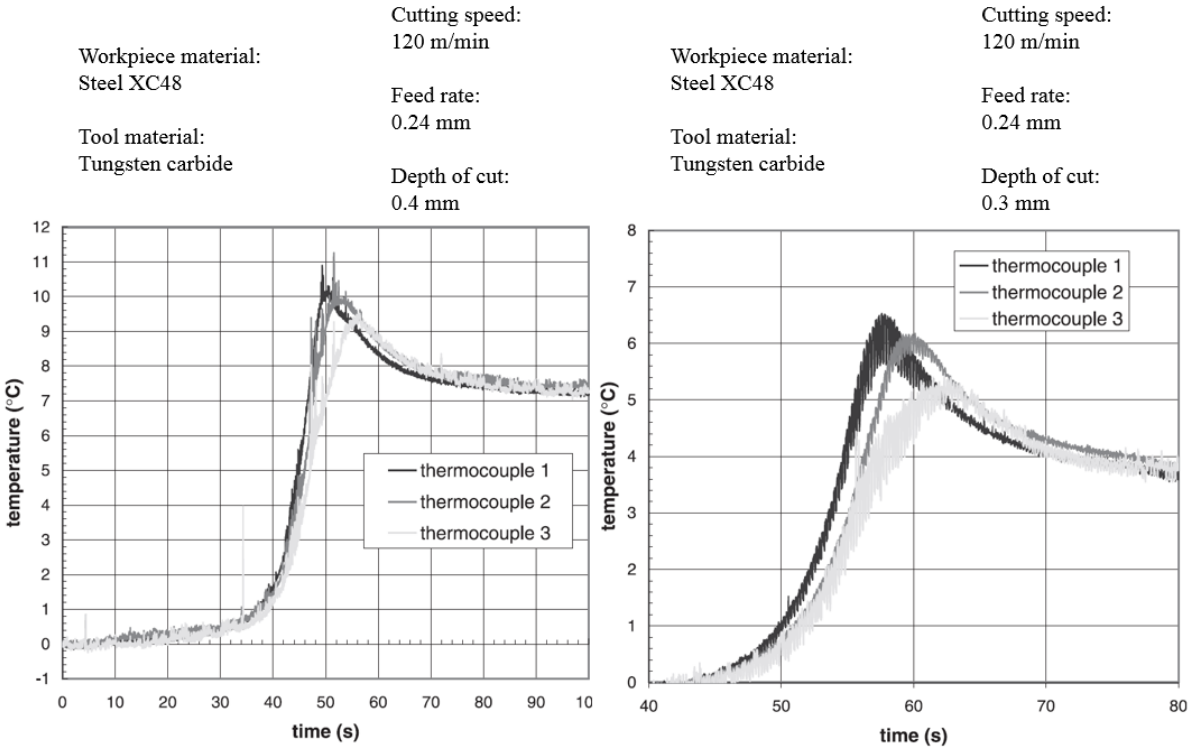

Source: Battaglia *et al.* [41].

These measurements were used to obtain the surface temperature using an inverse model, where temperature fields were estimated in a way that would fit with the data to determine the surface temperature. The results indicated temperature gradients of more than 100 ºC per 1/100 mm on the machined surface [41]. It must be noted that in the publication no compensation method was cited, and the cold junction or ambient temperature was not provided. As the measured temperatures start at 0 ºC for all thermocouples it is probable that no compensation was applied. This would mean that all measurements were in relation to the ambient temperature.

2.6.1 Temperature during the machining AISI 1040 and AISI 52100

AISI 1040 steel is widely used in the manufacturing sector, to fabricate studs, rods, springs, and crankshafts among other applications [42]. It has a composition, in mass, of 0.35 to 0.45% of carbon, 0.15 to 0.4% of silicon, 0.60 to 0.90% of manganese, and a maximum of 0.05% phosphorous [42].

Singh *et al.* [42] investigated the temperature during the turning of AISI 1040 steel with high speed steel tools. The parameters used were cutting speed of 70, 100, and 130 m/min, feed of 0.1, 0.3, and 0.5 mm, and depth of cut of 0.2, 0.4, and 0.6 mm. To measure the temperature the tool/chip thermocouple method was used.

The cutting speed had the greatest impact on the measured temperature. With the cutting speed of 70 m/min, the temperature varied between 141 up to 159 ºC. With the cutting speed of 100 m/min, the temperature varied from 150 to 174 ºC. With the cutting speed of 130 m/min, the temperature varied from 365 up to 410 ºC. This shows that the temperature is not linearly related to cutting speed.

In comparison, the AISI 52100 steel is used in the fabrication of bearings, and power transmission components among other applications [40]. It has a composition, in mass, of 0.95 to 1.05% carbon, 0.20 to 0.45% manganese, 1.30 to 1.65% of chromium, 0.20 to 0.35% silicon, a maximum of 0.015% sulfur, a maximum of 0.027% phosphorous, and a maximum of 0.30% nickel [43].

Chen et al. investigated the cutting temperature during the turning of AISI 52100 with PCBN tools. The parameter used were cutting speed of 100 m/min, feed of 0.05, 0.10, and 0.15 mm, and cutting depth of 0.1 mm. The temperature was measured using an embedded thermocouple on the tool and a tool/foil thermocouple.

With the feed of 0.05 mm the measured temperature began close to 500 ºC and after 24 min of cut reached close to 550 ºC with the embedded thermocouple and close to 650 ºC with the tool/foil thermocouple. With a feed of 0.10 mm the embedded thermocouple measured close to 690 ºC at the start and reached close to 720 ºC after 24 min while the tool/foil thermocouple started close to 660 ºC and reached 760 ºC after 24 min. With a feed of 0.15, the embedded thermocouple started close to 760 ºC and reached close to 840 ºC while the tool foil started close to 750 ºC and reached close to 875 ºC after 24 min.

Comparing both materials, the turning of AISI 52100 reaches temperatures much greater than the turning of AISI 1040. Comparing the temperature when both are turned with a cutting speed of 100 m/min and feed of 0.1 mm and AISI 1040 with a cutting depth of 0.2 mm and AISI 52100 with a cutting depth of 0.1 mm, the temperature of the AISI 1040 is 150 ºC while the AISI 52100 surpasses 650 ºC.

2.7 PROTOTYPING PLATFORMS

Prototyping platforms are tools used by hobbyists and professionals in electronics to test and develop concepts for new devices and systems. These platforms range from simple and inexpensive to very complex and expensive [44].

There are many brands of prototyping platforms, some built for teaching purposes while others focus on a more technical approach, some are licensed while others are open source. Among the most well-known prototyping platforms are the ones called Arduino®. The Arduinos boards are usually built around a microcontroller, with a port to interact with a computer to upload programs and to provide power, digital input and output pins, analog input pins, GND pins, voltage source pins (5 or 3.3V depending on the Arduino), PWM (power wave modulation) pins, a crystal oscillator, among other components [45].

Kondaveeti *et al.* [44] have shown that Arduino boards have been used for a great number of applications, from home automation and education to the prototyping of mining hazard detection devices. Arduino board's advantages are scalability, lack of need for deep knowledge of electronics, size, and compatibility with Windows, Linux, and MacOS, among others. However, the most important characteristic is that the Arduino® is open source and has an active community. As an example of applications, Gosai and Bhavsar [46] used an Arduino Uno to acquire tool temperature data in turning using a thermocouple. In Figure 25 an Arduino Uno can be seen; which is one of the most common Arduino boards used.

Figure 25 – Arduino Uno

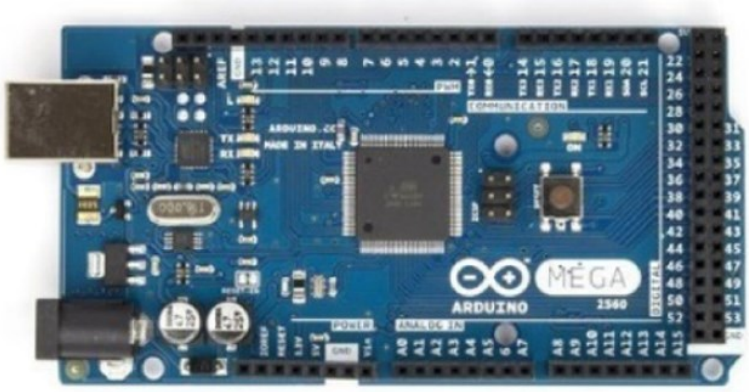

SOURCE: Kondaveeti *et al*. [44].

Another common Arduino model is the Arduino Nano, which uses the same microcontroller as the Arduino Uno and has a very similar configuration, but in a more compact form [45]. Due to this compact form, many pins share more than one function. In Figure 26 the Arduino Nano can be seen. The Arduino Nano also has a single Serial Peripheral Interface (SPI) connection used to control peripheral devices. More than one device can be controlled with the SPI connection, but only one can be active at a time meaning that using multiple peripherals in a single SPI shares the same total data transfer capacity.

Figure 26 – Arduino Nano.

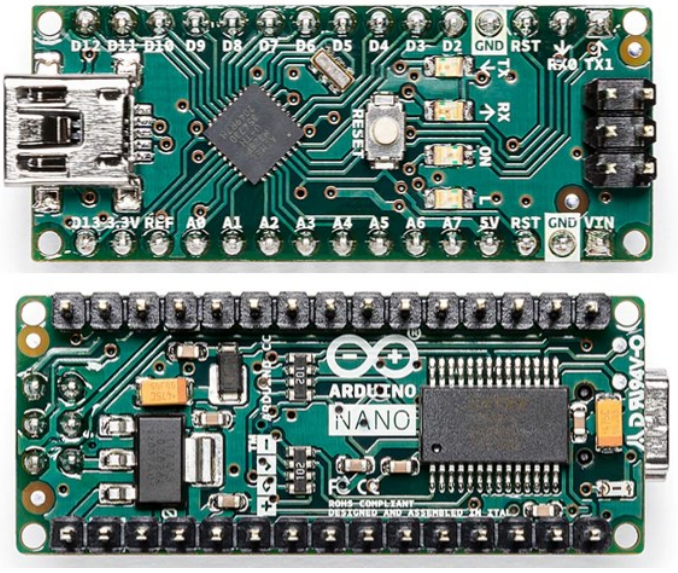

Source: Arduino web site [45].

There are peripheral devices compatible with Arduino used to acquire thermocouple signals like the MAX6675 [47] and the MAX31855 [48]. The MAX6675 has a limited

temperature range and thus is recommended for hobbyists while the MAX31855 has the full range of the thermocouple type used. One limitation of both is that they require an SPI connection.

2.8 INSTRUMENTATION AMPLIFIERS

An instrumentation amplifier (IA) is an electronic component commonly used to amplify the voltage difference between two inputs. It is particularly useful to amplify low voltage signals with high common mode voltage noise. The IA is used in combination with sensors in a wide range of applications from medical to automobilist industries [49].

An IA is usually an assembly of two or three operational amplifiers as can be seen in Figure 27. Like an operational amplifier, an IA usually has two inputs, two supplies, and an output. The IA can also have pins so to connect the gain resistor and a reference input to shift the output signal [49].

Figure 27 – Simplified schematics of an INA333 instrumentation amplifier.

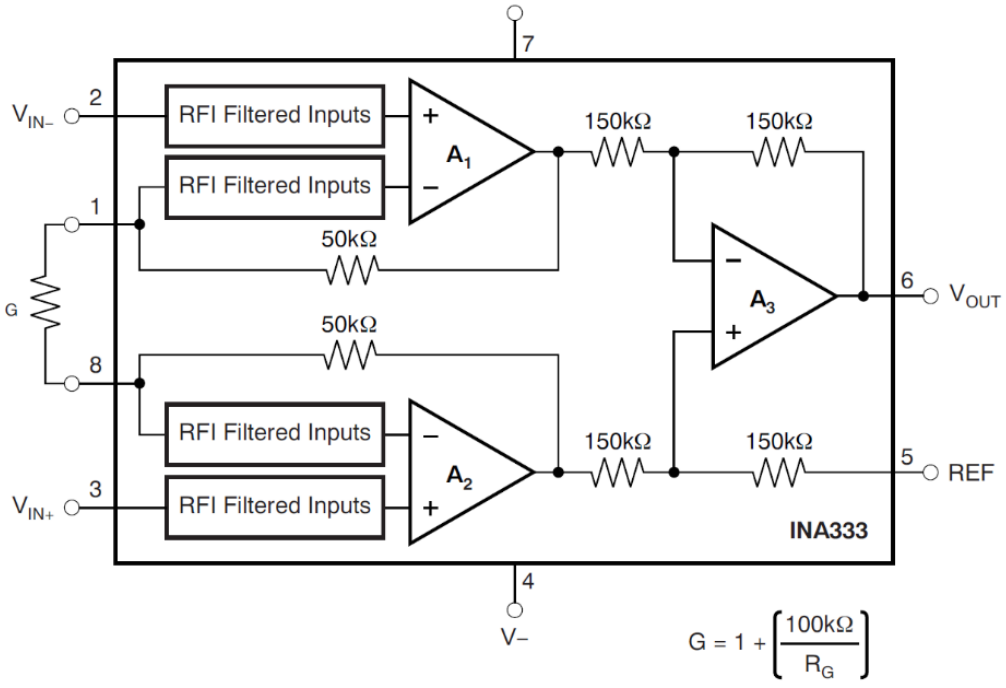

Source: INA333 datasheet [50].

Like an operational amplifier, an IA has many classifications. Among them, there are rail-to-rail amplifiers and single supply amplifiers. A rail-to-rail amplifier is one that can have an output very close to the supply voltages. A single supply amplifier is one that can be used with one only one voltage supply, being the other supply input grounded [49].

3 TEMPERATURE MEASURING DEVICE

This section aims to give an overview of the decision making of the development and the working of the temperature measuring device used in the present research project. Detail of the assembly of the device and drawings can be found in Appendix A and B respectively.

3.1 REQUIREMENTS AND SENSOR CHOICE

The first step of the development of the temperature measuring device was to determine the requirements for the application. The objective of the device was to verify if there was a difference in temperature in different radial positions, so the device should be able to measure temperature in more than one point. It would also help in the investigation of the possible causes for this increase if these temperatures were measured in the workpiece.

Due to this research being exploratory and the fact that the project has limited resources the cost of development and fabrication of the device should not be elevated. The errors in temperature measurement are usually above 10 ºC [34] and as a compromise between cost and precision an error up to 50 ºC can be accepted.

During previous studies the parameters used resulted in a maximum lathe spindle rotation close to 50 Hz. To acquire a signal it is recommended that the acquisition frequency be four times the filter cutoff frequency [51], this would mean that to acquire this signal the sampling frequency should be at of least 200 HZ. No analog filter would be used in the first prototype to prevent that any unpredicted signal be removed.

During the machining of AISI 52100 the temperature can reach close to 900 ºC [40] so the device should be able to acquire temperatures up to 1000 ºC so that it can measure the temperature without risks of signal saturation.

The main requirements for this device were:

a) Measure the temperature in the workpiece during its rotation on at least two points.
b) Low cost compared with commercially available measuring devices.
c) Measure temperature up to 1000 °C.
d) Maximum error below 50 °C.
e) Sample frequency of at least 200Hz.

The use of rotating electrical contacts was foregone due to costs while the use of tool-chip thermocouples was not considered due to lack of precision. Emission methods usually require that the measured object be stationary in relation to the measuring equipment. If this the

researcher process was longitudinal turning, this could be resolved by using the boring process that is very similar with longitudinal turning but with the tool being rotated. Unfortunately, a similar process with a stationary workpiece for radial turning would require that the tool move in the radial direction while it rotates and with both rotation and radial velocity varying.

Due to the technical and resource limitations it was decided that the temperature would be measured using a thermocouple and the signal acquisition would be done using an Arduino that would be rotated with the lathe spindle so that the device would be stationary with the workpiece.

Thermocouple can have a long time response that would make then not adequate for this measurement, but this is true only when they are used to measure fluid temperatures. When they are embedded in solids their time response can be considerably shorter [52].

3.2 ACQUISITION SYSTEM

The function of the acquisition system is to acquire and store signal data. The acquisition system used was an Arduino Nano® combined with a MicroSD® module. To create the programs to control the Arduino Nano® the free software Arduino Integrated Development Environment (IDE) was used with the standard libraries and the SdFat library [53]. To create the electronic diagrams and the Printed Circuit Boards (PCBs) footprints the free software KiCad® was used. Both the Arduino program used and the Matlab program for data translation can be found in Appendix C.

After testing a few configurations on a protoboard, it was decided that a configuration with four input signals and an acquisition frequency of 1 kHz was the best for this application. One input is necessary for the thermistor that would make the compensation for the thermocouples and at least two inputs were needed to the thermocouples, thus the temperature was measured at more than one point, and one extra input was so that there would be a redundancy in case of failure in one of them and to have an extra point of data. With these inputs, 1 kHz was a high enough frequency to completely capture the signal at the maximum rotation from the lathe and still not present buffer errors during the testing. Configurations with more inputs for thermocouples were tested but it was necessary to reduce the acquisition frequency to prevent buffer overflow. The device was powered by a 9 V battery since this was the readily available single battery to power the Arduino® Nano. This configuration uses interrupt functions to time the data acquisition.

As the analog digital converters (ADCs) use 10 bits as an output and the variables need to use entire bytes there was a need to use 2 bytes (16 bits) to store each acquired point of data for each sensor. This would mean a waste of 6 bits per channel per data point for each sensor. To diminish this waste and enable the use of a higher acquisition rate, three of the four signals were concatenated in a 4 bytes variable (32 bits). As the timekeeping function of the Arduino does not work in parallel with the interrupt function used, the last signal was concatenated with a 6 bits counter in a 2 bytes variable (16 bits). This is shown in Figure 28. This concatenation reduced the use of bytes per data point from 8 (64 bits) to 6 (48 bits) and added a counter to help identify buffer errors.

Figure 28 – Concatenation of signals in each data point.

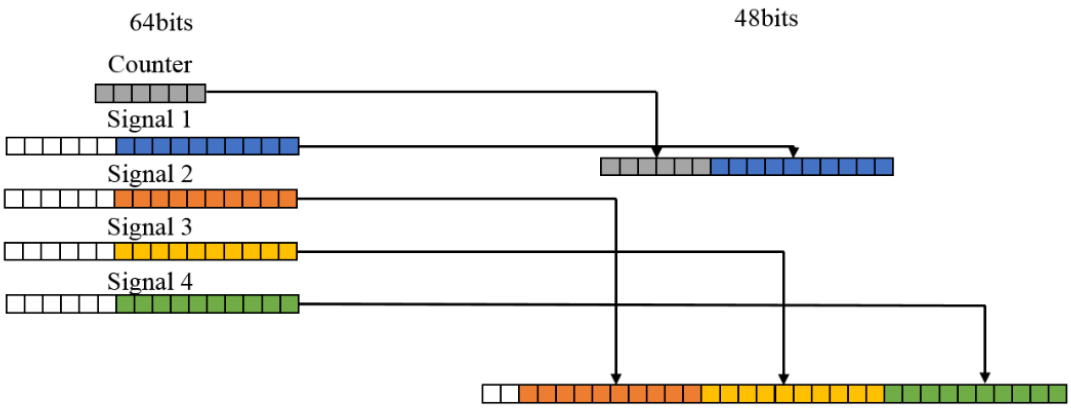

Source: Author

The counter and the buffer size are non-multiple so a data skip could be detected. The counter would begin at zero and would go up to 63 and then return to zero. Two buffers with 85 lines were used. This size was chosen to be close to the microSD card cache memory size and to not be a multiple of 64, the number of digits on the counter.

In Figure 29 a schematic of the acquisition system can be seen. Of the four signals, 3 would be used by type K thermocouples and one would be used by a thermistor for compensation for the thermocouple reference junction temperature.

Figure 29 - Acquisition system schematic.

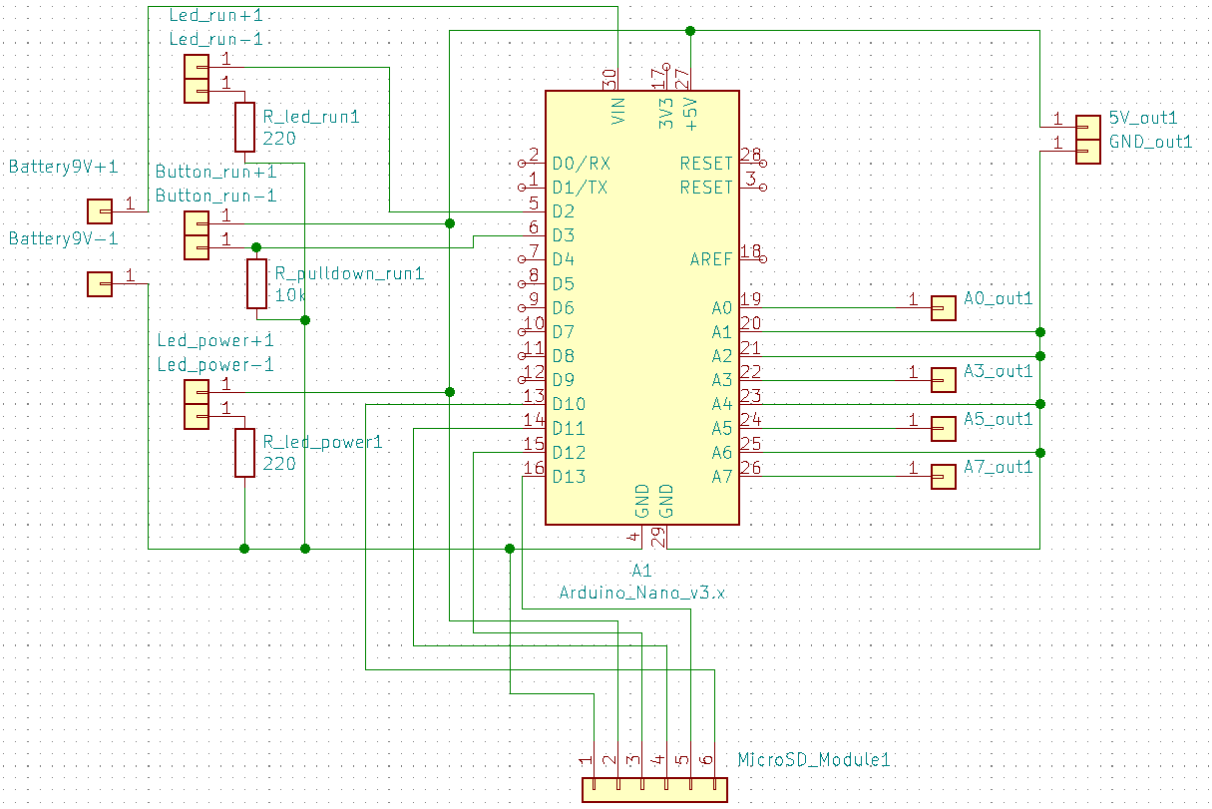

Source: Author.

Then, two buttons and two Light Emitting Diodes (LEDs) were added for signaling and control. One button is an on/off button connected to the 9 V battery and the other button is a run/stop button, that starts/stops the data acquisition. The LEDs indicate if the device was powered with a red LED and if the device was running with a green LED. The Arduino Nano was also responsible to provide a 5 V voltage and grounding for the amplification system.

3.3 AMPLIFICATION SYSTEM

As the chosen sensors were type K thermocouples that in the range from 0 °C to 1000 °C output voltages between 0 V and 42 mV (considering the cold junction at 0 °C) in a nonlinear relation, and the Arduino Nano has 10 bits ADCs with 5 V as the higher value, it was necessary to amplify the signals of the thermocouples. For the thermistor, a simple voltage divisor was used.

To do this amplification, the amplifier INA333 from Texas TI was chosen. This instrumentation amplifier has many characteristics that make it compatible with the Arduino Nano and have a very low power use. It is also a rail-to-rail amplifier (the outputs saturate very

close to the supply voltages) and can work as a single-supply amplifier, enabling the use of a 0-5 V output range.

Before creating the amplification circuit for the three thermocouples, software provided by Texas TI called Tina-TI was used to test the possible configurations. Recommendations presented in the datasheet [50] were used, like the use of a 100 nF capacitor connected to ground and power supply to prevent oscillations in the supply voltage and a 10 kΩ resistor between one input and ground to provide a path to input bias current [50]. A 1 kΩ resistor was used to set the gain close to one hundred. A common mode signal of 2.5 V was introduced in the input because when working with single supply the sum of the inputs needs to be close to 5 V for the output to be able to reach 5 V. The working assembly can be seen in Figure 30.

Figure 30 – Assembly of the INA333 in Tina-TI software.

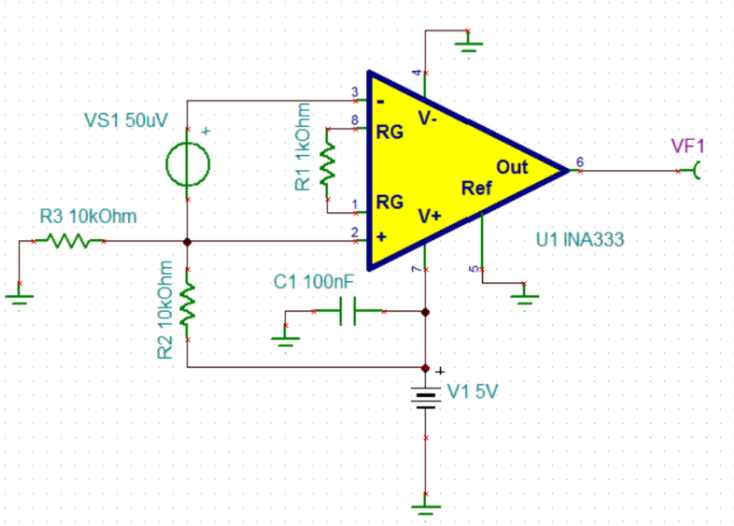

Source: Author

To test if this assembly truly worked, an INA333 was mounted in an adaptor so it could be used in a protoboard. A thermocouple heated with an uncontrolled heat source was used to provide a low enough signal and a multimeter was used to check the voltage amplification. In Figure 31 the schematic of the amplification system can be seen.

Figure 31 – Schematic of the amplification system.

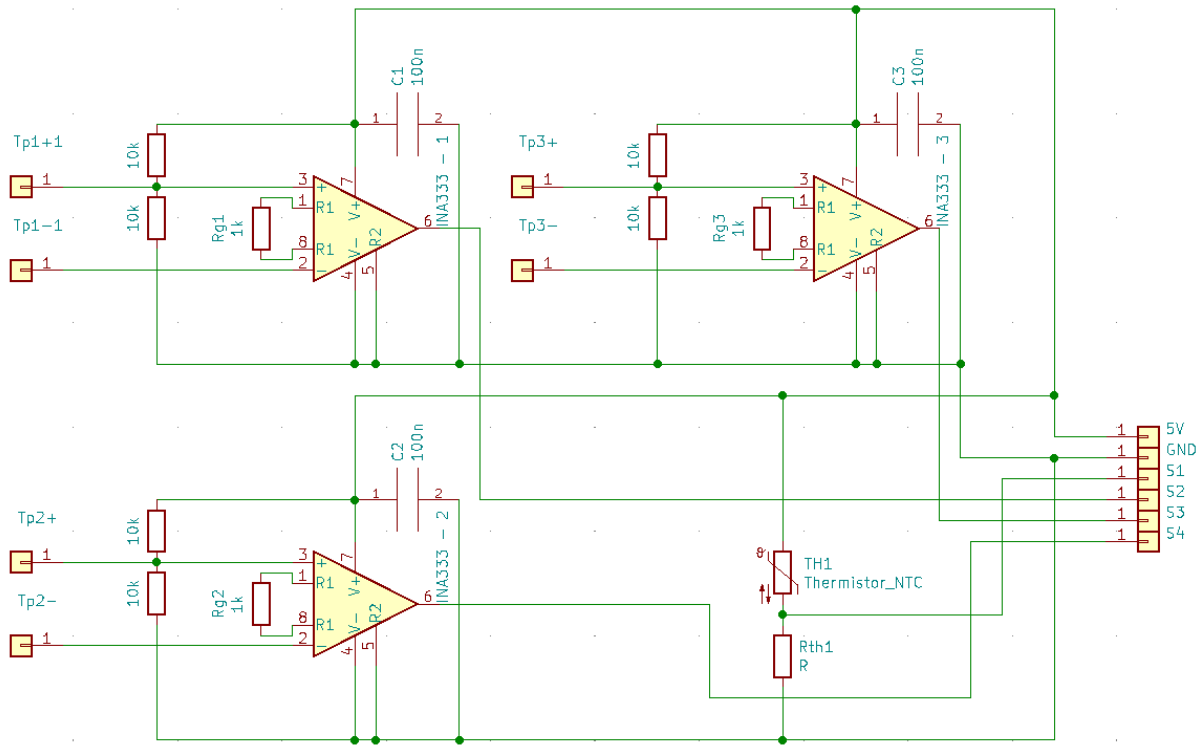

Source: Author.

The signals from the thermocouples are amplified and sent to the acquisition system. The thermistor measures the temperature on the thermocouple's cold junction, so the thermocouple's signal can be compensated. This amplification enables the ADCs to measure in a step of less than 2 °C, varying according to the measured temperature due to a nonlinear relation between voltage and temperature. Therefore, as a no analogical measuring device, the scale error of this device is close to 2 °C.

3.4 FASTENING SYSTEM

To fasten the device in a way that would facilitate the connection to the sensors in the workpiece and to reduce the strain that the device suffers during the rotation, it was decided to fasten it in the hole that begins in the chuck and continues through the shaft of the spindle. The lathe used was a Heiligenstadt and its chuck can be seen in Figure 32.

Figure 32 – Hole where the device was designed to be fastened in.

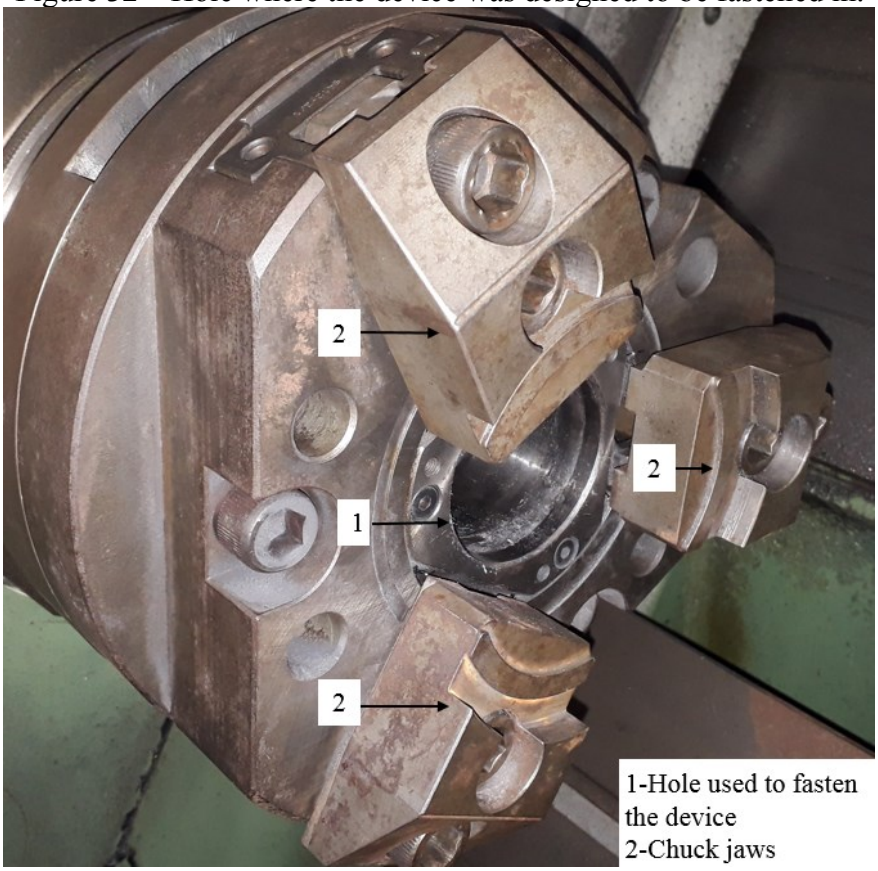

Source: Author.

The hole has a 65 mm diameter for its first 55 mm of depth and then the diameter decreases to 59 mm. It was decided to use an expansion clamp system due to its simplicity and low cost compared with other systems considered. The system was composed of a PVC tube of 60 mm of external diameter, with a rubber covering, and an aluminum 6061 cylinder. The cylinder was made with ramping protrusions and gaps were cut in the PVC tube to fit with the cylinder, allowing it to expand without breaking. The direction of the ramps was made so that the system would tend to tighten with the spindle rotation. Figure 33 shows these features that form the clamping system.

Figure 33 – Aluminum cylinder and PVC tube forming the expansion clamp.

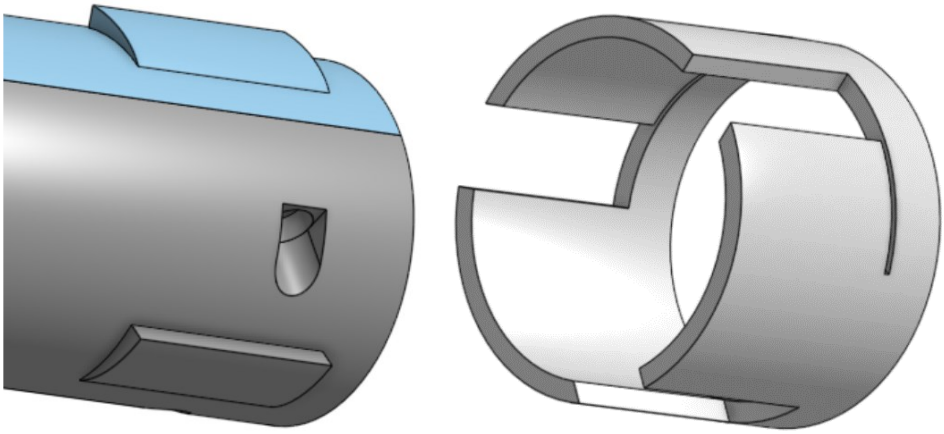

Source: Author.

The cylinder was built longitudinally sectioned and with enough length so that later cavities to contain the other subsystems could be made. The fastening system was tested on the lathe to confirm that there would be no need to alter it before the cavities were cut and the PCBs printed (see validation in the next subsection).

3.5 VALIDATION

Due to the lack of infrastructure to do a full calibration in the necessary temperature and conditions necessary, a simpler validation of the device prototype was made. The validation of the device was made in two steps and using equipment from LEPTEN (Laboratory of Conversion Processes Engineering and Energy Technology). A more detailed description and data from the validation can be found in Appendix D.

Firstly, the multicalibrator Omega CLD-II (Figure 34) was used to verify the voltage acquisition. The multicalibrator was used as a voltage source providing voltage from 0 V to 50 mV with a step of 5 mV. For each step, five thousand points were measured by each thermocouple channel, indicating the lower and upper saturation limits for each channel. After excluding the data outside the saturation, the least square method was used to find the gain for each channel (all curves resulted in R^2 above 0.99). Then, with the channel gain, the systematic and random errors for each channel at each voltage level were determined.

One channel presented a limited measuring zone due to amplifier saturation (200 to 800 °C), while the other two channels were able to measure from 5 to 1100 °C, both of these consider a cold junction of 0 ºC. The greater systematic error would result in an error of about

7 °C. One channel presented random errors between 0.5 to 0.6 mV and the other two presented random errors below 0.5 mV, and these errors would result in random errors below 15 °C. This error can be considered small for measuring temperature in machining processes.

Figure 34 – Omega CLD-II multicalibrator and the acquisition and amplification systems.

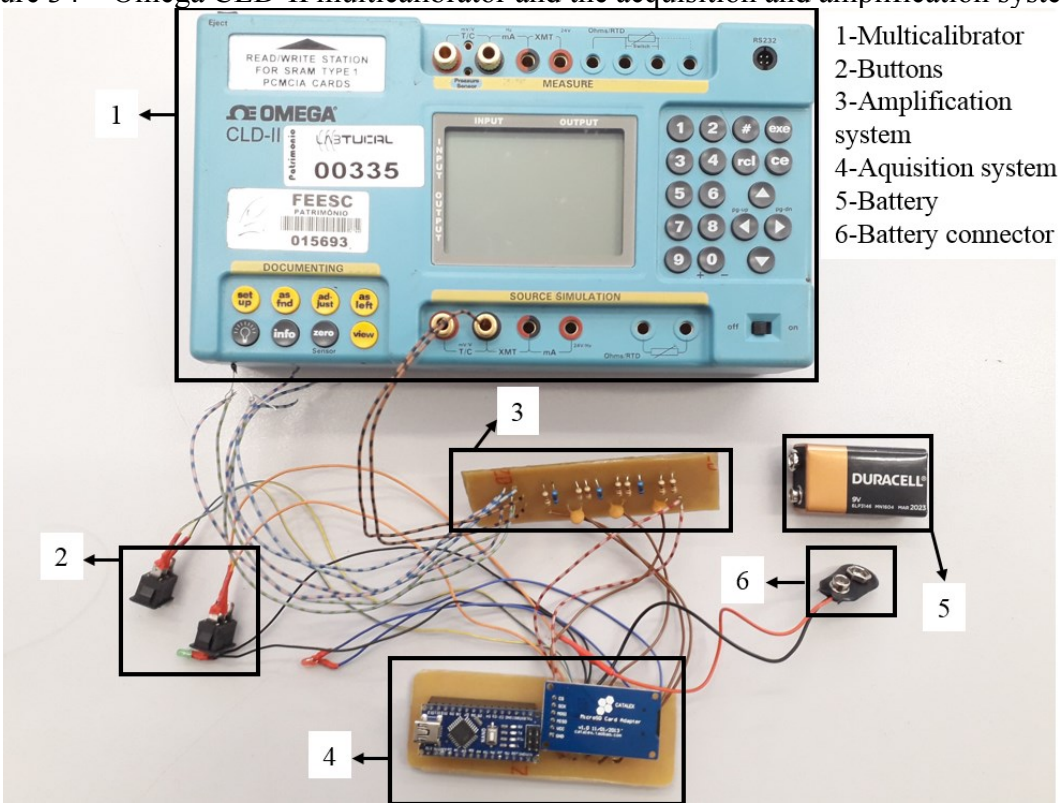

Source: Author.

In the second step of calibration (Appendix D), an oven Omega CL552 was used. The oven has a capacity to reach up to 1100 °C and is projected to be used with thermocouple probes, but also has its own internal thermocouple. The main objective of this step was to ascertain that the equations used to convert voltage to temperature were correct.

The errors increased with the increase in temperature, which was probably due to the thermocouple not being well positioned inside the oven, due to the use of bare wires instead of probes. Even so, the maximum error found was below 50 °C for all three thermocouples, which is not considered a high error for temperature measurement in machining processes.

Davies *et al.* [34], in a 2007 publication, reported that the most accurate method of measuring temperature had a random error above 10 ºC since most methods presented an error above 10 °C. However, the indication of the error in methods of measuring temperature usually is not presented, according to the publications analyzed for the elaboration of this project research. Generally, only their calibration or validation method is presented as in the work of

García-Martinez *et al.* [32]. Other studies only describe the device used for temperature measurement [38, 54]. Thus, an error between 15 and 50 ºC for the prototype developed in this research project was considered adequate.

The fastening system was tested before the cavities for the components were made on it, so that there would be less rework in case of a failure on this system. For the testing, the system was fastened in the lathe's chuck and a line was drawn passing through the system and the chuck. The lathe was activated for 5 minutes on a set rotation and then stopped to check the line, and if there is a misalignment it means that the device moved in relation to the chuck. The test was made up to 4500 rpm, which was the lathe maximum rotation, on the expected rotation direction and in reverse. The line kept its continuity and there was no visible movement of the fastening system.

4 MATERIALS AND METHODS

This section covers the details of the materials and methods used during the experiments. The experiments consisted of measuring the workpiece temperature and the cutting forces applied in the cutting tool during radial turning. The temperature and force measuring systems were not synchronized, consequently, the comparisons made between the behavior of the forces and temperature data for each machining test are global and not in specific moments.

The main objective of these experiments was to evaluate the temperature changes in the workpiece due to the variation of radial position in radial turning. Moreover, the experiments were done to test the developed device's prototype for temperature measurement, especially the thermocouples embedment method and their connection to the device.

4.1 EQUIPMENT

The lathe used for the tests was a Heyligenstaedt model 10U (Figure 35) with a spindle power of 70 kW, maximum rotation of 4500 rpm, and retrofitted with a numeric command Siemens 802D. The lathe has a three-jaw hydraulic chuck with an enclosed cutting zone.

Figure 35 – Lathe Heyligenstaedt model 10U.

Source: Author.

To measure the cutting forces a piezoelectric dynamometer Kistler type 9257A was used. The tool holder was held against the dynamometer using a block made for this purpose. The block was bolted to the dynamometer and all force applied to it by the tool holder is transferred to the dynamometer. The dynamometer can be seen in Figure 36.

Figure 36 – Dynamometer with the holding block.

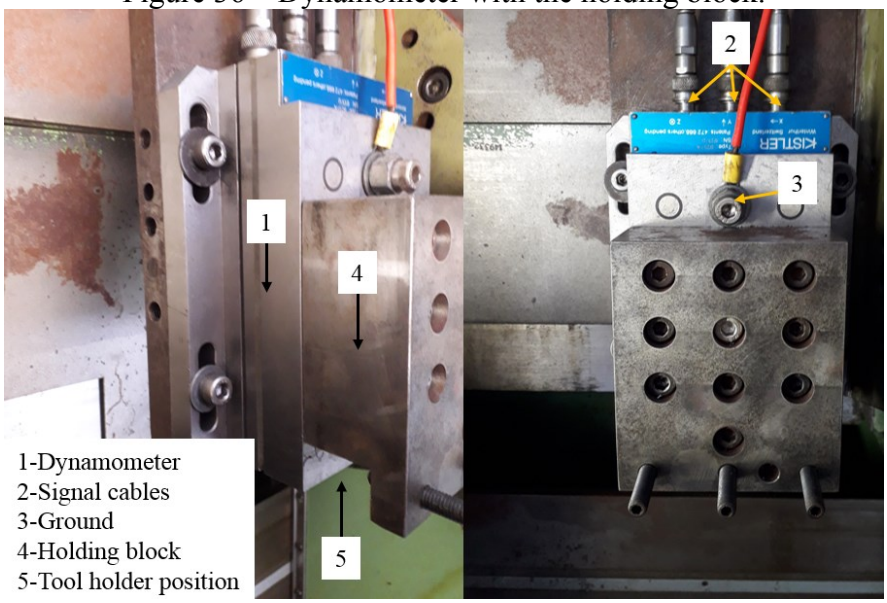

Source: Author.

To amplify the signals two Kistler model 5011 amplifiers and a Kistler model 5006 amplifier were used. To make the data acquisition, a NI-USB-6218 Multifunction I/O device was used for the analogical to digital conversion, and a laptop was used to store the signal with the aid of the software Labview®. The acquisition was made with a 10 kHz frequency and using a 300 Hz analog lowpass filter. This configuration was used in previous studies like the work of Camargo [6]. The amplifiers and the acquisition device can be seen in Figure 37.

Figure 37 – Force acquisition amplifiers and acquisition device.

Source: Author.

To measure the temperature on the workpiece the prototype of the device described in the previous chapter was used. The device was fastened in the lathe chuck as seen in Figure 38, thus it was not possible to download the data without removing the device, so the data could only be analyzed after the removal of the workpiece and the device from the lathe.

Figure 38 – Device fastened in the lathe chuck.

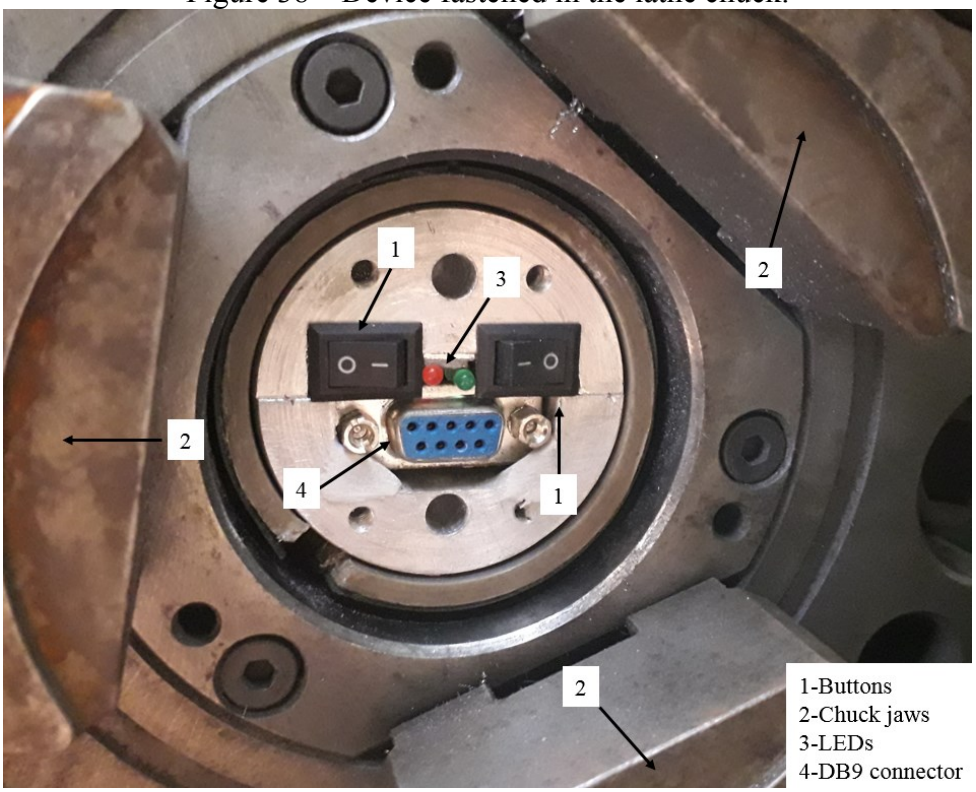

Source: Author.

4.2 WORKPIECES AND TOOLS

The workpieces used in the machining experiments were made from AISI 1040 steel and were all taken from the same billet. The workpieces were 100 mm discs with a 24 mm hole in their center, all edges of the workpiece were chamfered. The disc form was chosen to maximize the volume of removable material during radial turning and the hole limits the maximum rotation that the lathe requires to maintain the cutting parameters. The dimensions of the workpiece can be seen in Figure 39.

Figure 39 – Dimensions of the workpieces used.

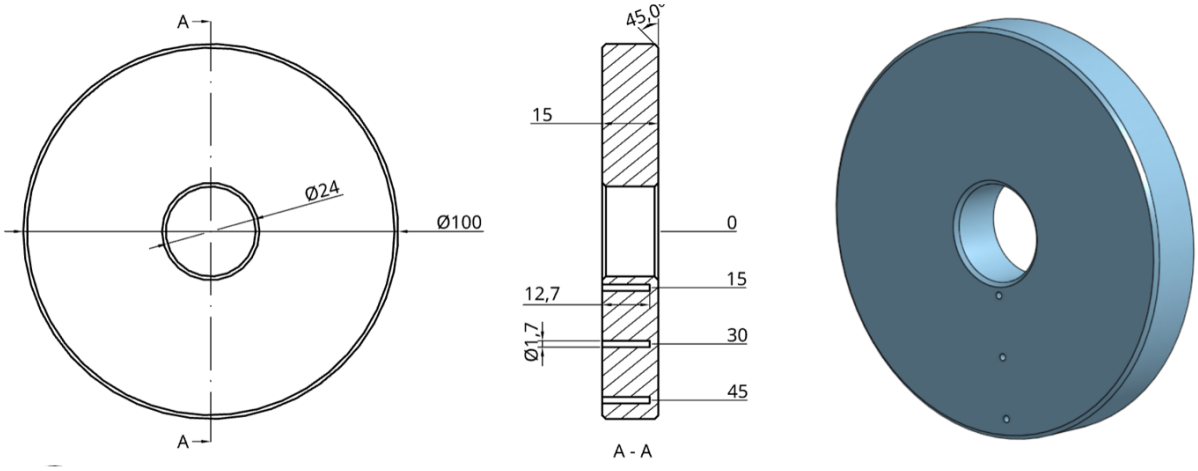

Source: Author.

In the back of each workpiece, 3 holes were made using EDM. These holes were made with a 1.6 mm diameter copper electrode and were radially positioned 15 mm, 30 mm, and 45 mm from the workpiece center and were made with 12.5 mm of depth. In each hole, a type K thermocouple made with 0.51 mm wires and with its points welded with capacitor discharge welding (CD Welding), equipment developed in the work of Silveira [55]. The thermocouple´s bare wires were then isolated using Kapton® tape. The thermocouples can be seen in Figure 40.

The use of EDM machining means that there will be white layer formation around the hole. As the white layer have different phase composition as the bulk material, it's thermal properties, like heat conductivity and diffusivity, will be different [56]. Although it is possible that this could affect the measurement, other possible sources of errors were given priority in this stage of development.

Figure 40 – Thermocouple used in the tests.

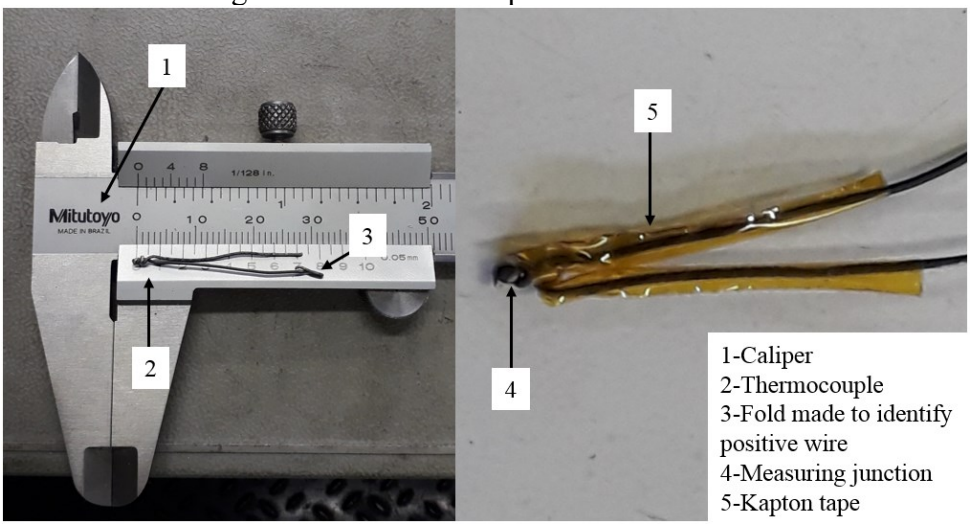

Source: Author.

The thermocouples were fixed in the workpiece using cyanoacrylate glue. This can be seen in Figure 41. The distance between each thermocouple is 15 mm and the distance between the first thermocouple and the workpiece center is also 15 mm.

Figure 41 – Thermocouples inserted and fixed in the workpiece.

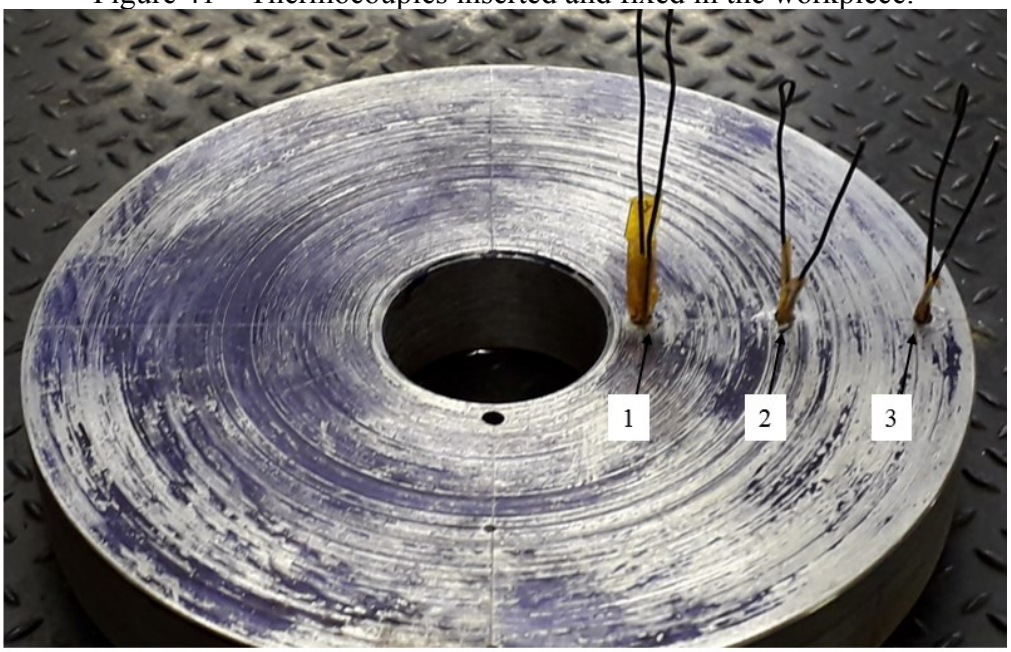

Source: Author.

These thermocouples were connected to a DB9 connector using thermocouple grade wire and a thermistor was added besides the cold junctions for compensation. (Figure 42).

Figure 42 – Workpiece with mounted thermocouple.

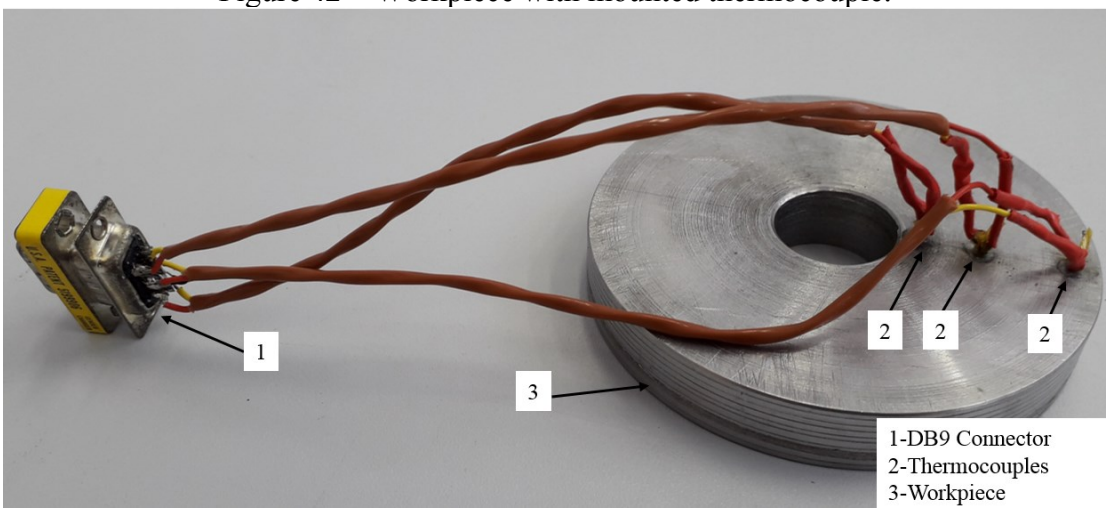

Source: Author.

In the first experiments, the thermocouple wires were connected using tin solder to mechanically connect them to the connector. This method was considered unreliable after a few experiments, but due to a lack of resources and shortage of components on the market, it was used in the first experiments as there was no better method available at the time. A cover for the DB9 was also not initially used due to a limitation of space between the device and the workpiece. This can be seen in Figure 43.

Figure 43 – First connector assembly.

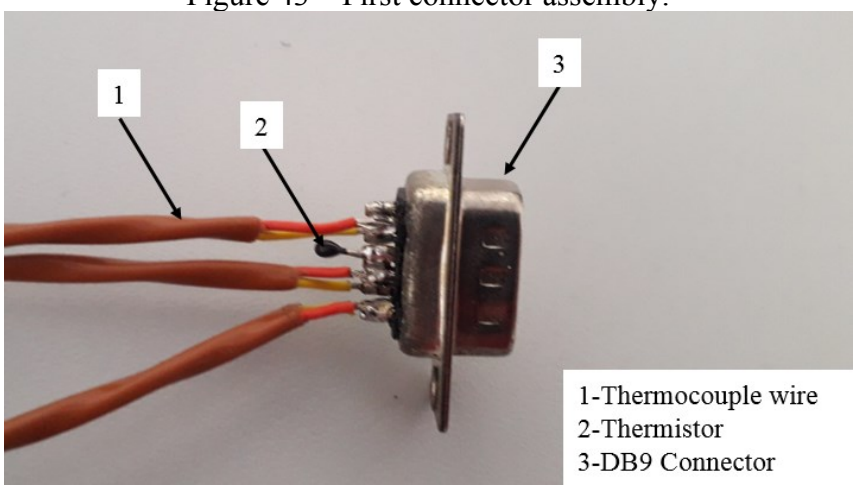

Source: Author.

In later experiments, an electric wire was added between the thermocouple and connector, and this wire was soldered to the connector and CD welded to the thermocouple wire. A cover was also added, it was necessary to remove part of the cover so it would fit in the

available space. This new assembly can be seen in Figure 44. In the first two workpieces, the thermocouple wires were reused from the device testing with the oven.

Figure 44 – New connector assembly. Left: addition of a wire between connector and thermocouple. Right: shortened cover.

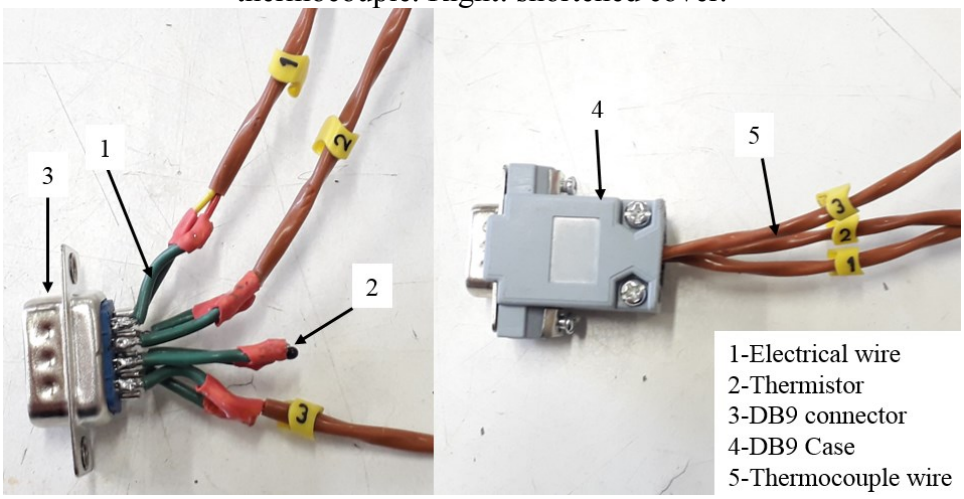

Source: Author.

The cutting tools used were the Sandvik SNMG 12-04 08-QM 525 with the tool holder DSBNR 2020K 12. The tool an uncoated carbide tool with corner radius of 0.794 mm and a clearance angle of zero degree. The tool holder has a tool cutting edge angle of 75 degree and an inclination angle of -6 degree.

Both new and worn cutting edges were used to see if there was a difference in temperature between them. The worn edges were obtained by turning a cylinder of AISI 1040 with a cutting depth of 0.5 mm and a feed of 0.3 mm, beginning with the removal of 270 000 mm^3 of material at a cutting speed of 100 m/min followed by the removal of 410 000 mm^3 of material at a cutting speed of 150 m/min.

In Figure 45 SEM images from the tools used for the first two tests. (a) and (b) are from the cutting edges before the tests and (c) and (d) are from after the tests. Due to technical problems, it was not possible to obtain SEM images from the other tools.

Figure 45 - SEM images from the tool used in the first tests. (a) New edge before testing. (b) Worn edge before testing. (c) New edge after testing. (d) Worn edge after testing.

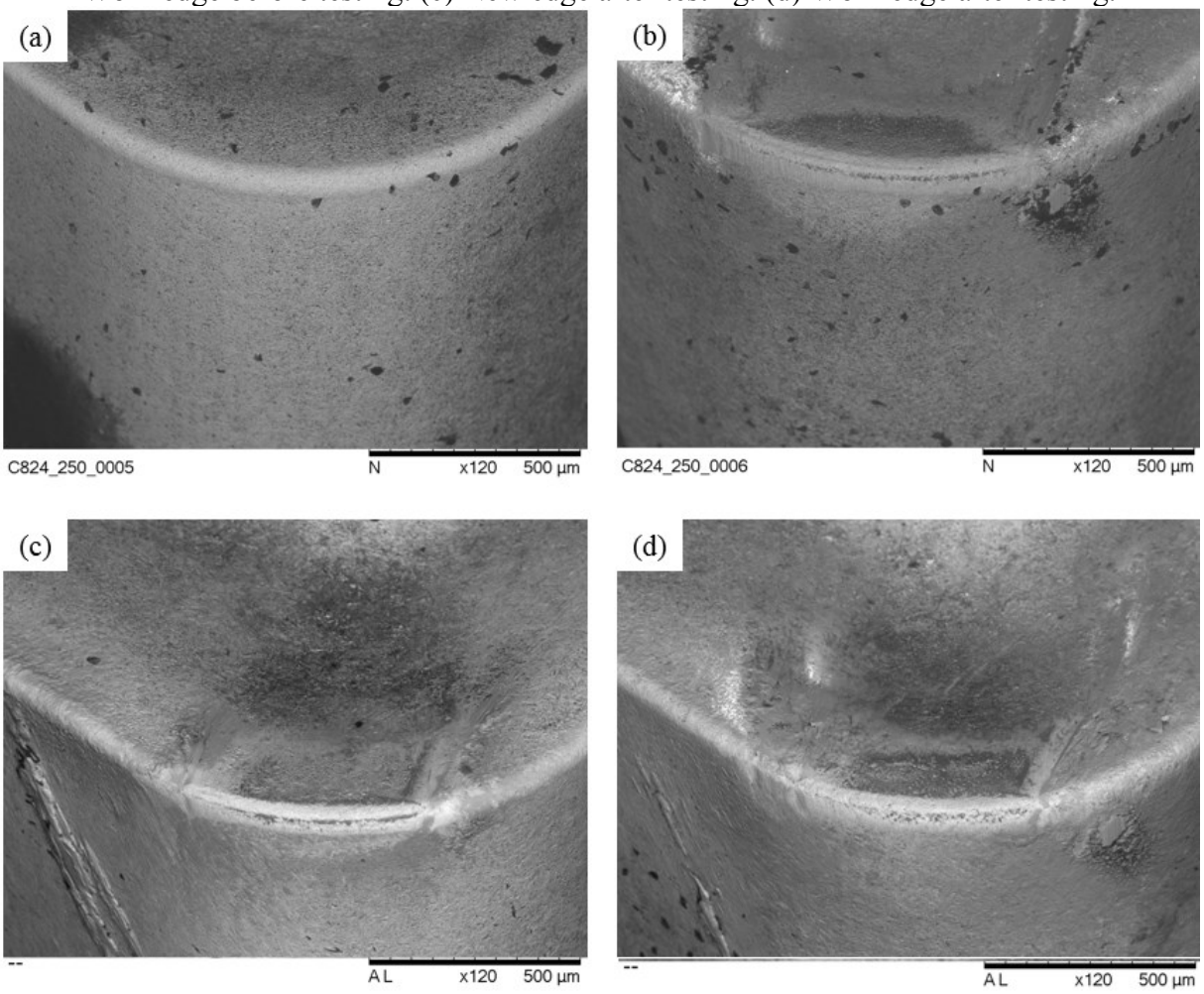

Source: Author

4.3 TESTING PARAMETERS

The cutting parameters chosen were the same used by Camargo [6]. Although the material and tools in this research project are very different from Camargo experiments [6], it is believed that the investigated phenomena are closely linked with the cutting parameters creating a heat wave superposition as described by Astakhov and Shvets [8].

An elevated cutting speed results in higher temperatures and smaller intervals between each tool passage close to a region. A low feed means that the tool will pass more time through the same area. An increase in cutting depth would increase the heat generated, but most of this extra heat would be eliminated by the chip instead of staying in the workpiece.

Besides magnifying the desired phenomenon, using the parameters for hardened steel will permit the device prototype to be better tested for its later intended application in hardened

steels. The cutting parameters used are cutting speed of 150 m/min, feed of 0.08 mm, and cutting depth of 0.2 mm.

At the beginning of each set of experiments, first, the workpiece was fastened in the lathe, and the material was removed with a specific tool at a rate of 0.1 mm to guarantee the alignment of the workpiece face. Then, the official machining experiments were carried out. The forces and temperature measured would be separately recorded in each pass. The number of passes until the thermocouples were revealed in the workpiece was also recorded. At the beginning of each pass, there was always a period where the signals were acquired without cutting, making a region empty of active signals and with only the background noise. This sequence can be seen in Figure 46.

Figure 46 – Sequence of preparation and testing.

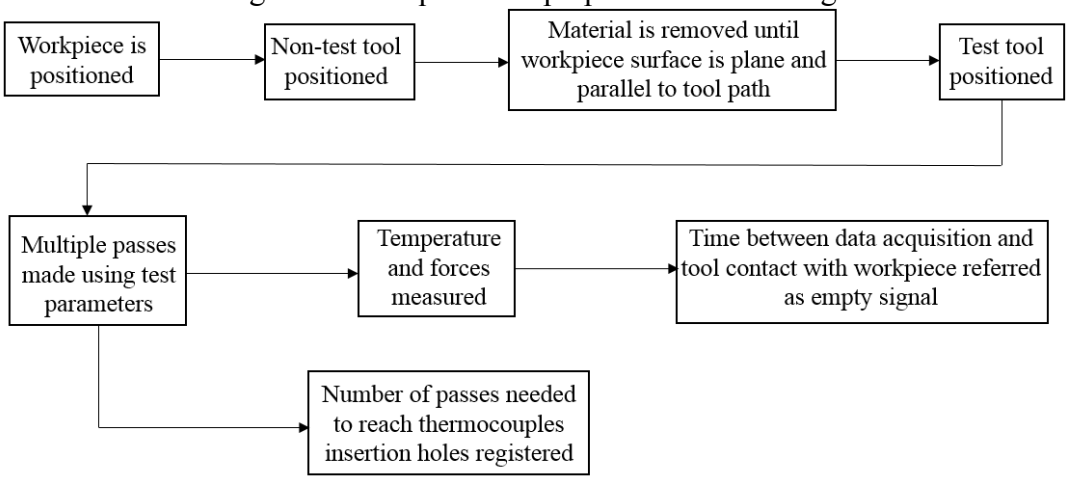

Source: Author.

The fastened workpiece in the lathe can be seen in Figure 47 (a). In Figure 47 (b) a front view of the workpiece and the fastened device power LED can be seen.

Figure 47 – a) Fastened workpiece. b) Front view of the fastened workpiece. The red light coming from the device indicates that it is powered but the absence of a green light indicates that it is not acquiring data.

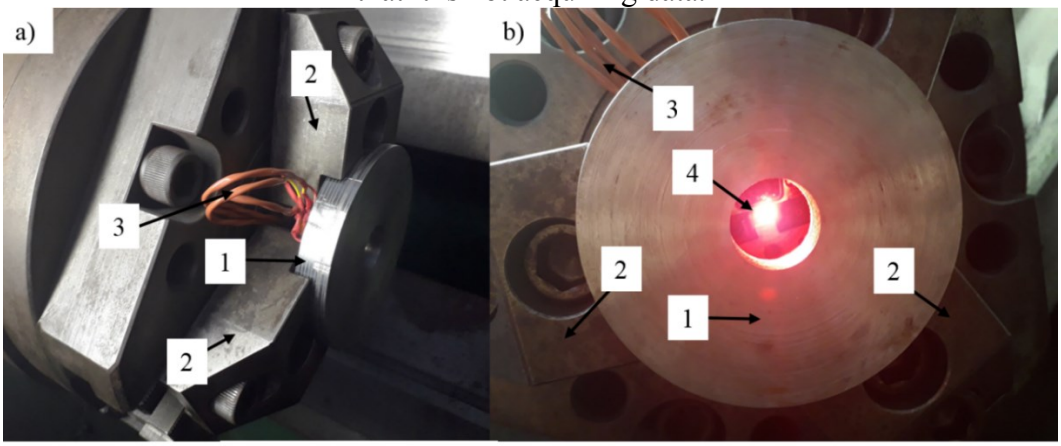

Source: Author.

At first, two series of tests with two experiments per series were planned. However, due to problems with the connectors, more tests were made, a total of six. The tests were first made paired, with a machining experiment with a new edge followed by a machining experiment with a worn edge. After the first two pairs, totaling four tests, they were made only with new tools and one at a time.

During the sixth machining experiment, a failure in the fastening system occurred, so a new prototype (which needs to be redesigned from a diagnostic of the failure cause) will need to be done for further tests. This research project encompasses the experiments made up to this point, indicating the diagnosis and suggestion of solutions for the failures found in the temperature measurement device.

Table 2 shows the combination of workpieces, cutting tools, and series of tests.

Table 2 – Division of series and tests.

Serie	Workpiece	Cutting edge
Series 1	Workpiece A	New edge
	Workpiece B	Worn edge
Series 2	Workpiece C	New edge
	Workpiece D	Worn edge
Series 3	Workpiece E	New edge
Series 4	Workpiece F	New edge

Source: Author.

4.4 DIGITAL SIGNAL PROCESSING

The raw temperature data was composed of two columns, the first with the 16 bits variables containing the 10 bits thermistor signal and 6 bits counter and the second with the 32 bits variables containing the three thermocouples 10 bits signals. To process the data an algorithm was made using the software Matlab® (Appendix C). First, the variables were separated, and the 10 bits signals of the thermistor and thermocouples were converted to a voltage value. Then the thermistor temperature was calculated, and the appropriate compensation was applied to the thermocouples.

With the thermocouples signals already compensated, the voltage signal was converted to a temperature signal using the K thermocouple table [39]. A new time variable was created starting at zero and increasing 0.001 each line and the counter was used to identify any skips that may have been caused by buffer overflow. In Figure 48 a schema of how the data is translated from raw data to temperature signals can be seen.

Figure 48 – Simplified data conversion process.

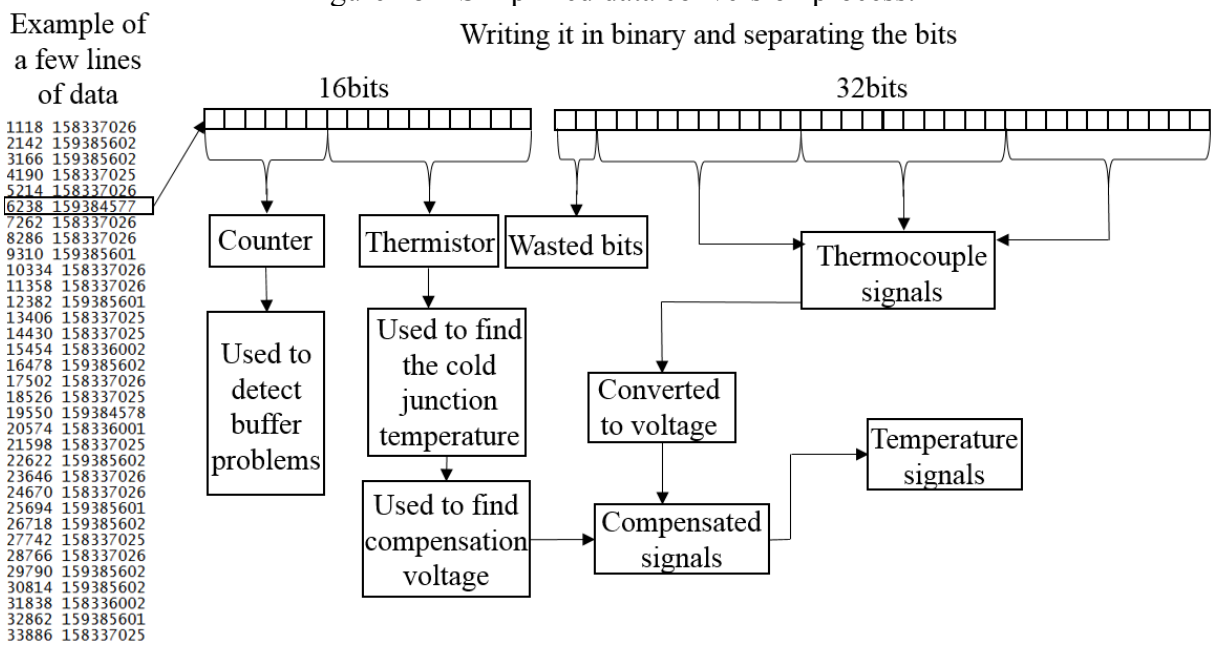

Source: Author.

After these conversions, a graphic of time versus temperature for each thermocouple was plotted. These graphics were critically analyzed to determine if the device worked correctly. The valid signals would then be used to compare the difference in the temperatures in different thermocouples in the same passes and of the same thermocouples in different

passes. As the device was considered a prototype and was only validated but not calibrated, most analyses were only qualitative.

Sequential temperature pulses were identified in the signals of some of the last passes. To analyze them, the Fast Fourier Transform (FFT) algorithm was used. First, the FFT of a section of empty signal was done for comparison and then an FFT of the region with the pulses was made to identify their frequency. This frequency was compared with the rotation frequency of the lathe spindle when the tool was cutting the region belonging to the specific thermocouple. The sequence of analysis of the temperature signals can be seen in Figure 49.

Figure 49 – Temperature signals analysis flowchart.

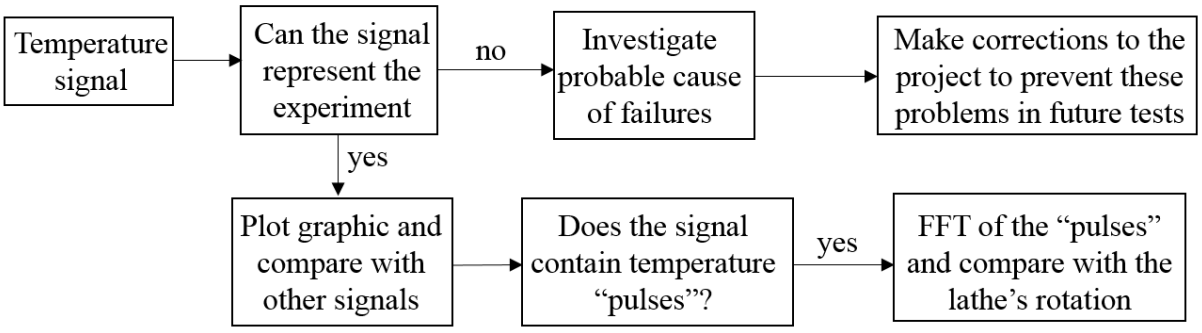

Source: Author.

The lathe spindle rotation will depend on the cutting speed and the tool radial position as described by Equation (1):

$$F = 25.v_c/3.\pi.R \quad (1)$$

Where "f" is the spindle rotation in Hz, "v_c" is the cutting speed in m/min and "R" is the tool radial position in mm. This equation was obtained using the basic circular movement equations and adapted to the desired units of the inputs and output.

Many electronic systems have imperfections that can cause signal drift. These drifts are a variation of the original signal caused by the system used to amplify and acquire the signal. One common drift is caused by a bias voltage that is added to the signal and changes its value. Another common type of drift is a voltage change over time. Usually, most devices have very low drift, but age and wear can cause an increase in drift.

To analyze the forces signals, a linear regression of empty signals was made to determine the drifts. For each point of the signal, the value of the drift on that point was subtracted. After the drift was subtracted, graphics of these signals over time were plotted.

Figure 50 – Force signals analysis flowchart.

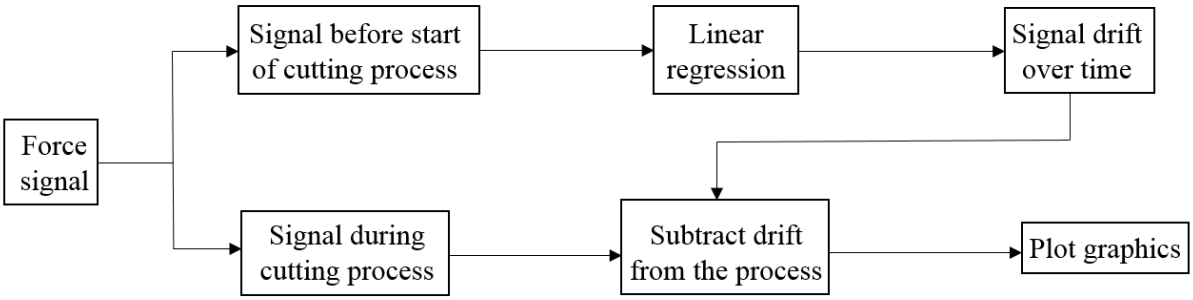

Source: Author.

After the graphics were plotted, the moment where the tool passed by each thermocouple was estimated, and two methods were considered for this. The first was to calculate the tool speed in the direction of the feed, this resulted in a complex equation as this speed depended on the spindle rotation that depended on the tool position. The second method considered that the tool would remove a constant area of material per second, this area can be obtained using Equation (2):

$$v_A = 100.v_c.v_f/6 \quad (2)$$

Where "v_A" is the removed area in mm²/s, "v_c" is the cutting speed in m/min and "v_f" is the feed in mm. "v_A" does not depend of time or the tool position. With the parameters used in the experiments ("v_c" = 150 m/min and f = 0.08 mm) "v_A" is equal to 200 mm²/s. With this information, calculating the time the tool needs to cross a certain radial distance can be done by calculating the surface area that the tool must cut between the two points divided by v_A. This area can be obtained by the area difference between two circles centered in the workpiece center and passing by each point. This can be seen in Equation (3):

$$t_i = \pi.(R_0^2 - R^2)/v_A \quad (3)$$

Where "t_i" is the time interval between two radial positions in s and "R_0" is the initial radial position in mm. Using Equation (3), the most relevant times were calculated and can be seen in Table 3.

Table 3 – Most relevant approximated time intervals.

	Process start to outermost thermocouple	**Outermost thermocouple to middle thermocouple**	**Middle thermocouple to centermost thermocouple**	**Centermost thermocouple to process end**	**Process start to process end**
Time interval	7.4 s	17.7 s	10.6 s	1.3 s	37 s

Source: Author.

Another detail that must be considered is that with the cutting speed used, between each data point the tool would move 2.5mm. This means that when the thermocouple is very close to the surface and the temperature variation becomes faster, the thermocouples will not be able to capture the full peak temperature consistently.

It is important to highlight that the temperature measuring device used is a not fully calibrated prototype, so the experiments in this research project were exploratory, and the number of successful tests was small. Therefore, statistical analysis or any attempt at modeling at this point would not be reliable.

5 RESULTS AND DISCUSSION

In this section, the data obtained in the machining experiments will be presented, analyzed, and discussed. Beginning with an analysis of the failures detected with the prototype, followed by the cutting forces and temperature data analysis. As the amount of the data is not extensive, the conclusions drawn in this work should be statistically revised when more data is available. This section will also discuss possible enhancements to the project initiated by this work.

There are still many failures to be addressed in the temperature measurement device developed, from the six tests made only two presented useful temperature data and only for two of the three thermocouples. For simplification, when analyzing the force and temperature the two successful tests will be referred to as worn tool test (Workpiece B) and new tool test (Workpiece E). Even with failures, its performance was still considered acceptable for the first prototype, and it shows promise that in a few iterations a reliable and more accurate device may be produced.

5.1 DEVICE FAILURES ANALISYS

Although four tests failed to acquire temperature, they are important to identify failures in the temperature measurement system. Starting from the failures that were considered most serious, each will be analyzed, and possible diagnostics and solutions will be proposed for further development.

The failures detected during the use of the temperature measurement device in the turning experiments are shown in Table 4, as well as their causes and proposed solutions.

Table 4 – Failures detected during device prototype testing.

Failure	Failure mode	Cause	Proposed solution	Frequency of occurrence
Lack of signal from thermocouples	No data collected in the test	Failure of the solder between thermocouples and the connector plug	Addition of intermediary wire to be soldered to the plug and welded to the thermocouples	Occurred in 3 tests (Workpieces A, C and D)
Lack of signal from thermocouples	No data collected in the test	Loose plug	Addition of a case with screws to hold the connector in place	Occurred in one test (Workpiece D)
Phantom signals	Data collected does not represent process	High lower limit for amplifier saturation caused compensation signal to generate a phantom signal	Add a voltage to dislocate signal so that it is always above lower saturation or adding a negative supply so the saturation would be lower	Occurred in most tests
Device not properly fastened	May damage device and lathe	Degradation of the fastening system	Redesigning fastening system or determine a frequency of parts substitution	Occurred in one test (Workpiece F)
Buffer overflow	Sections of the data lost	Fluctuation of the speed that data is saved to microSD card	Reducing acquisition rate or number of sensors or changing the used Arduino to one with native microSD	Occurred in all 6 tests but only small sections of data lost

Source: Author.

The failure that causes the greater number of experiments not to be able to capture the desirable temperature data was the lack of signal from the thermocouples due to the failure of the solder made between the thermocouple and the DB9 connector. This failure caused problems in three of the first four tests, workpieces A, C, and D.

In these tests, tin was used to solder the thermocouples wires to the connector, but due to chemical incompatibility between the materials, the connection was only mechanical, as seen in Figure 43 in the previous section. This resulted in some thermocouple wires getting loose from the connector. This method was used due to a lack of access to silver solder (which is more compatible with the thermocouple's material) and difficulty in acquiring parts for other solutions caused by the higher prices and shortages of parts promoted by the COVID-19 Pandemic.

In the tests with workpieces E and F, a possible solution was used: an intermediate wire soldered in the connector and welded to the thermocouple wire (as seen in Figure 44 in the

previous section). As this solution was used in only two tests, and one failed due to other failure causes, it is recommended that further tests with this method be made to test its reliability.

Other alternatives were considered, such as the use of DB9 connectors with screws or crimping, but there was a shortage of parts due to the COVID-19 pandemic, so this solution was not implemented. Moreover, connectors using terminal blocks were investigated but they were too big to fit in the available space.

Another failure with the DB9 connection was that the connection came loose in the last pass of Workpiece D. Due to the lack of space for a case, tight fit between the connectors, and the absence of strong forces that could pull the connection was held only by friction on the first four tests. When the assembly for the connectors was changed, a case was added to it (Figure 44). The case has built-in screws to fasten the connector. Due to a lack of space, the case was cut to shorten it. In the last two tests, this failure did not occur.

Another failure was the appearance of a phantom signal from the compensation due to the high lower saturation of the amplifiers. As the amplifiers saturated above 0 mV, and this voltage represent a signal when the workpiece was at the same temperature as the thermistor, the device could not measure temperatures below the temperature of the thermistor added to the saturation. With the thermocouple signal saturated and the thermistor being heated by conduction or cooled by convection, a false signal would be generated. This signal would appear when the constant saturated signal was compensated by the varying thermistor signal. An example of this can be seen in Figure 51.

Figure 51 – Temperature signal from the first pass from workpiece C with compensation. (a) Middle thermocouple. (b) Centermost thermocouple.

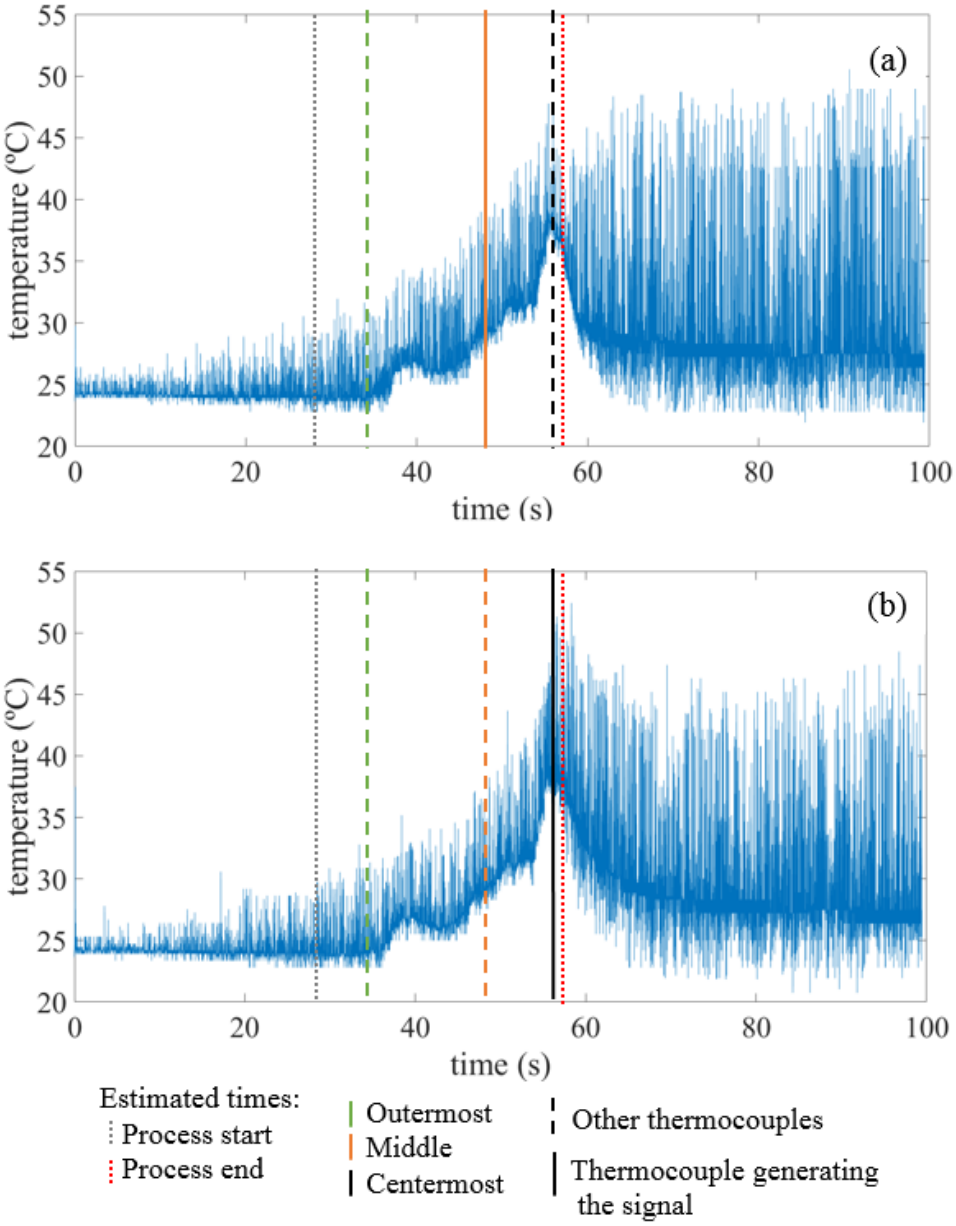

Source: Author.

This failure was detected since all three thermocouples signals of some passes of experiments presented similar curves. After confirming that there was no signal crossing, when one signal influences another, the data was plotted using a constant compensation and the signals became constant on their saturation. The same signal from Figure 51 with a constant compensation can be seen in Figure 52. After that, all data was plotted both with a fixed compensation and the thermistor compensation to check if the compensation was not generating a false signal by being applied in a saturated signal. This was not a solution, just a method to identify signals affected by this failure.

Figure 52 - Temperature signal from the first pass from Workpiece C without compensation. (a) Middle thermocouple. (b) Centermost thermocouple.

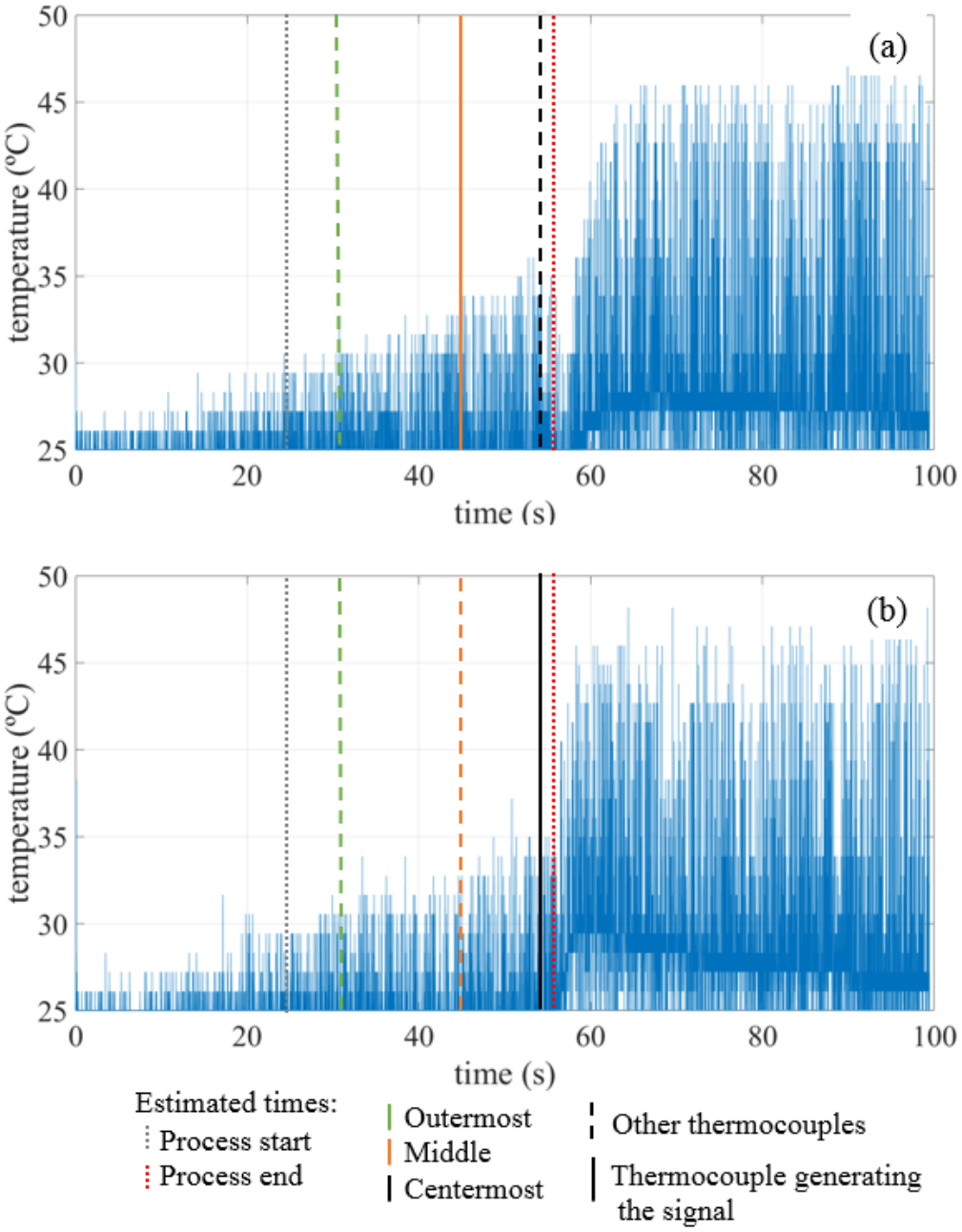

Source: Author.

One possible solution to this failure is to add a voltage to dislocate the signal away from the saturation and later subtract the amplified voltage from the signal. Depending if the subtraction was made before the ADC or on the data processing care would need to be taken because the Arduino Nano's ADC only accepts signals between 0 V and 5 V [45]. Another solution may be to use an amplifier in dual supply, making the lower saturation negative [50]. This second can require the use of ADCs capable of handling negative signals.

The last of the failures that hindered the data acquisition was the degradation of the fastening system. More specifically the degradation of the PVC tube and the rubber covering it. This failure was identified in Workpiece F and caused vibrations in the whole system, affecting the signals from the device but also from the dynamometer, as seen in Figure 53.

Figure 53 – Signal anomaly. First pass after battery exchange of Workpiece F.

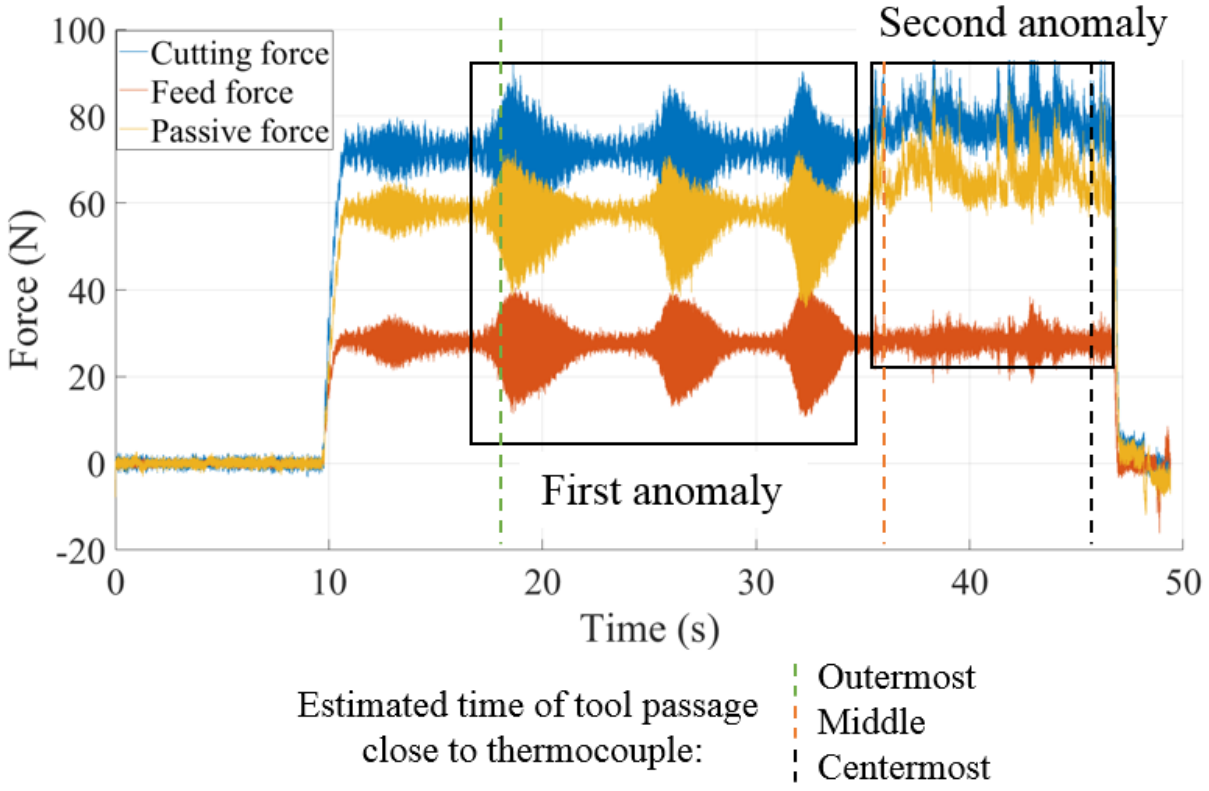

Source: Author.

Using FFT in both anomalies, as seen in Figure 54, peaks close to 71 and 81 Hz were identified. As the local electrical grid runs at 60 Hz and these anomalies were not seen in any other test it was concluded that they were generated by the device case vibration.

Figure 54 – FFTs of the signal in Figure 53. Top: FFT of the first part of the anomaly. Bottom: FFT of the second part of the anomaly.

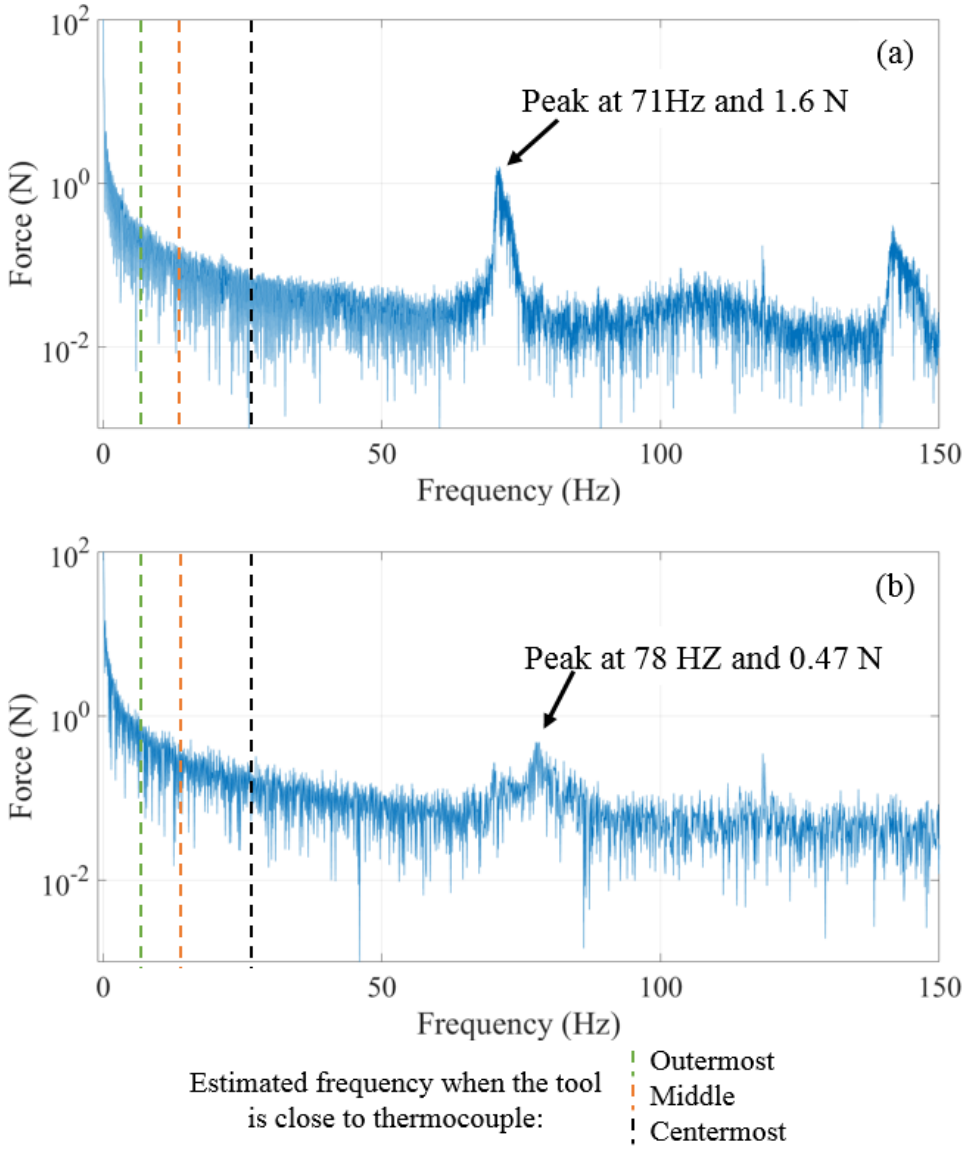

Source: Author.

There are two paths that can be taken to solve this failure. The first path is to redesign the fastening system, changing how it works or using more durable materials. The second is to make the PVC and rubber piece replaceable and change it every time it becomes worn. Moreover, a method that can be used to attenuate this failure is to make it possible to download the data without removing the device from the lathe, reducing the wear on the fastening system.

Another failure detected was buffer overflow, which was detected during data processing. One of the tests made during the processing of the data is checking the counter for data skips. The counter should begin at zero, increase by one for each line and return to zero

after reaching sixty-three. If the counter behaves differently, it indicates that a portion of the data was lost before it was saved.

As seen during the development of the temperature measurement device, there were fluctuations in the speed at which the data would be saved in the microSD that resulted in some data being overwritten before it was saved. In the validation, this only occurred in higher acquisition rates. The buffer overflow for the device is illustrated in Figure 55. Because of the way that the program identifies when a buffer is ready to be saved when there is an overflow both current buffers are lost.

Figure 55 – Difference between normal acquisition and buffer overflow in the device.

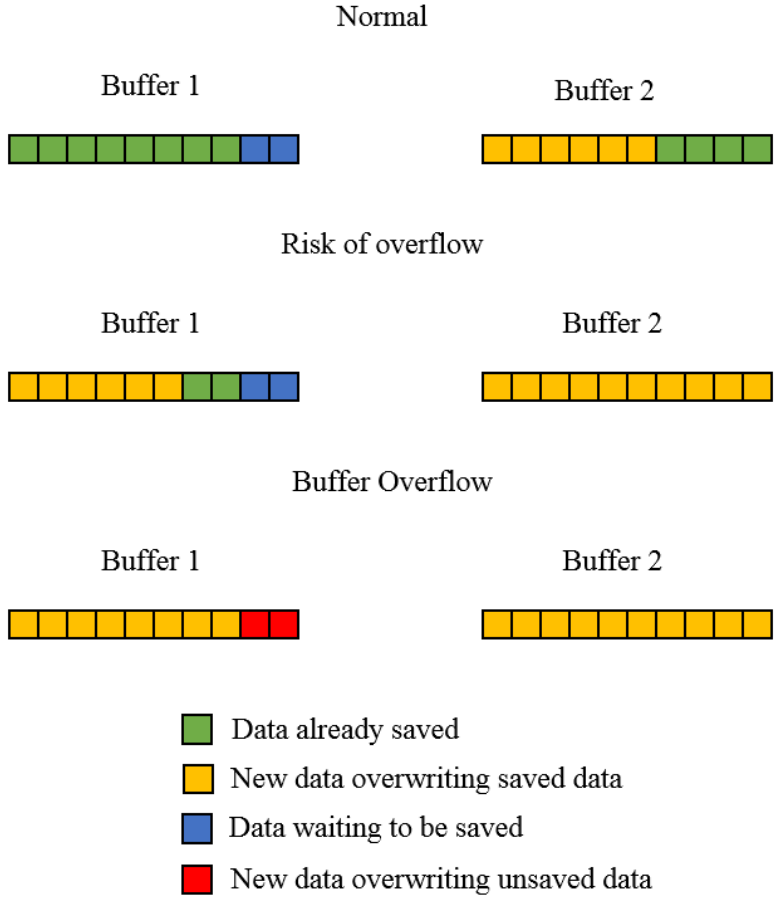

Source: Author.

Comparing the counter number skips it was identified that when the overflow occurred the overwriting of the data jumped a single cycle, jumping two buffers, or it jumped 1 cycle plus a number multiple of 32 cycles. This is because the buffer size for both buffers is 85 lines and the counter return to zero after each 64 data points. As 85 and 64 are prime to each other, it takes 5440 data points, 64 buffers, or 32 cycles to return to the same condition.

The fact that those buffer overflows did not occur in the validation and the number skip always being the same, points out that there was only a simple cycle of buffers skipped. This was considered a failure but did not happen enough to cause great problems in this stage, so it was decided that making alterations in the algorithm in the testing stage could bring other unforeseen problems.

There were three options considered to resolve this failure. The first is to reduce the acquisition rate or the number of thermocouples. The second is to use a prototyping platform with native microSD which have greater bandwidth than the module used. The third is to use a prototyping platform with a more random-access memory (RAM), enabling the use of additional buffers to reduce the speed fluctuation effect.

5.2 MACHINING FORCES MEASUREMENT ANALIZYS

One of the objectives of the measurement of machining forces in this research project is to check the existence of the phenomena of a decrease in all machining forces components values as the tool approaches the center of the workpiece, phenomena previously described by Camargo [6]. As the cutting parameters were chosen to try to replicate the phenomena previously observed and not to be adequate for the workpiece material, there is no reason to present a rigorous statistical analysis of the force's variations between tests. The data presented in this section will be only the data pertinent to this research project.

The forces magnitudes had some variations between tests, but this is usual in machining processes. This force variation and the failure of most temperature measurements resulted in a lack of enough data to try to associate the temperature variation with the variation of forces in a statistical way.

Furthermore, in some tests the variation between the forces of the new and worn tool is small (Figure 56). This could have been caused by the worn tool not presenting enough wear to create a significant difference in forces or the type of tool wear did not result in an increase in forces [7]. As there was difference in temperature behavior between the new and worn tool, as will be seen in the temperature measurement analysis, it is most probable that there was significant wear, but the wear type did not influence the forces significantly. At the end of some tests occurred a sharp increase of passive and cutting forces and a decrease of feed forces, probably due to the internal chamfer of the workpiece.

A small decrease of cutting and passive forces along the machining time was noted in some tests, although this decrease was always smaller than 10% of the initial value for cutting

and passive forces. In the feed forces, the decrease was more pronounced and present in all tests. It must be noted that this signal used the Kystler 5006 amplifier, that is older and more prone to interference, although similar behavior was not noticed in previous tests with longitudinal turning. Due to the drift correction done, this variation is not due to any drift that is linear time dependent and present in empty signal. Piezoelectric sensors can have signal decay due to lost charge with static signals [57], but during calibration and use in other tests, this was only noted on longer tests.

Figure 56 – Cutting forces on the first passes. (a) New tool test. (b) Worn tool test.

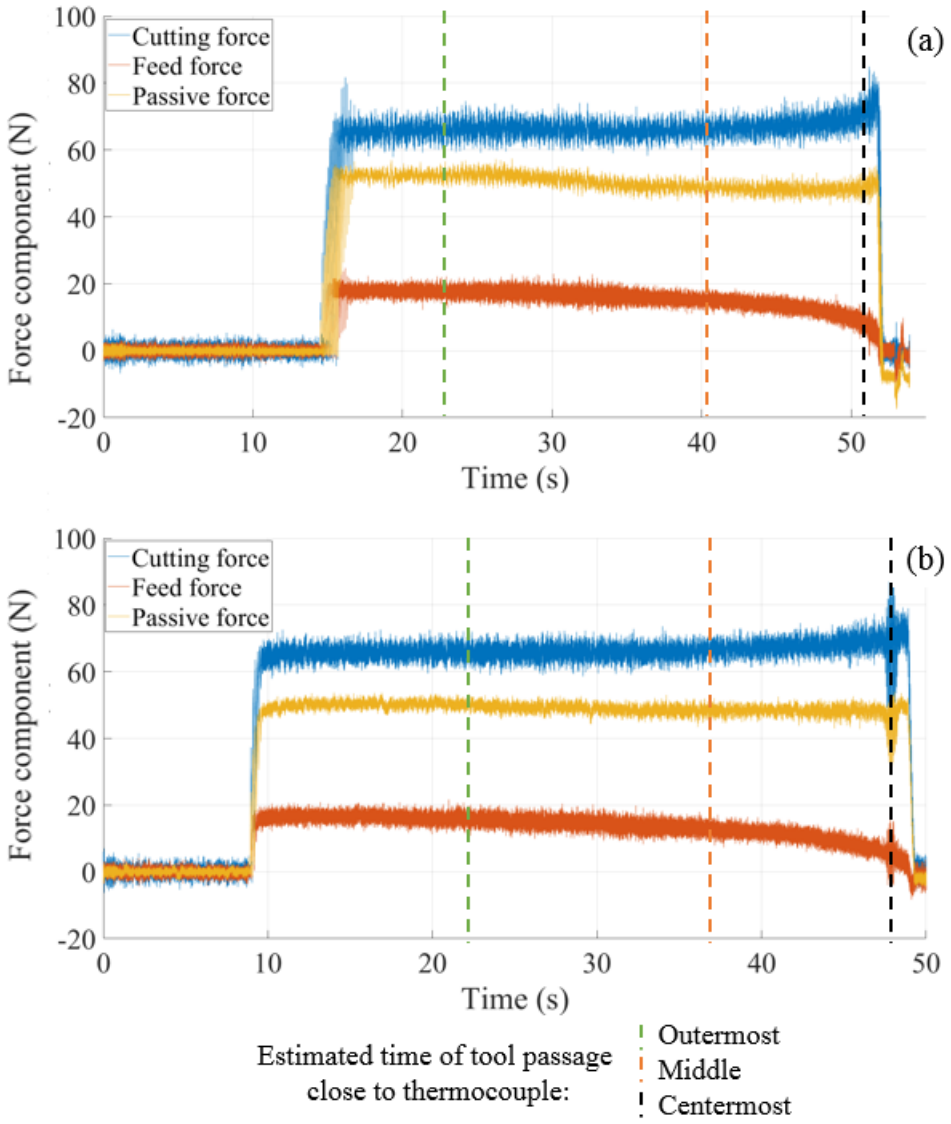

Source: Author.

The force diminishing effect was much subtler than the effect reported by Camargo [6], meaning that the temperatures involved in turning AISI 1040 are much lower. Although

the same parameter was used, the tools and material used in these tests would generate a much lower temperature than seen in Camargo's [6] study, reducing its effect on the forces. In hard turning (Camargo's [6] experiments) the formed chips are incandescent and present an orange color [11] while the tests made in this research did not present that, indicating that the temperature in these tests was lower. The lower amount of heat should also mean that the temperature increase phenomena should also be lower, and its effect in the forces also lower.

There were three anomalies in the force data that were considered pertinent to the study. The first anomaly was detected in a few signals and appears to occur at random. An example can be seen in Figure 57.

Figure 57 – Signal anomaly. Pass 5 of Workpiece C.

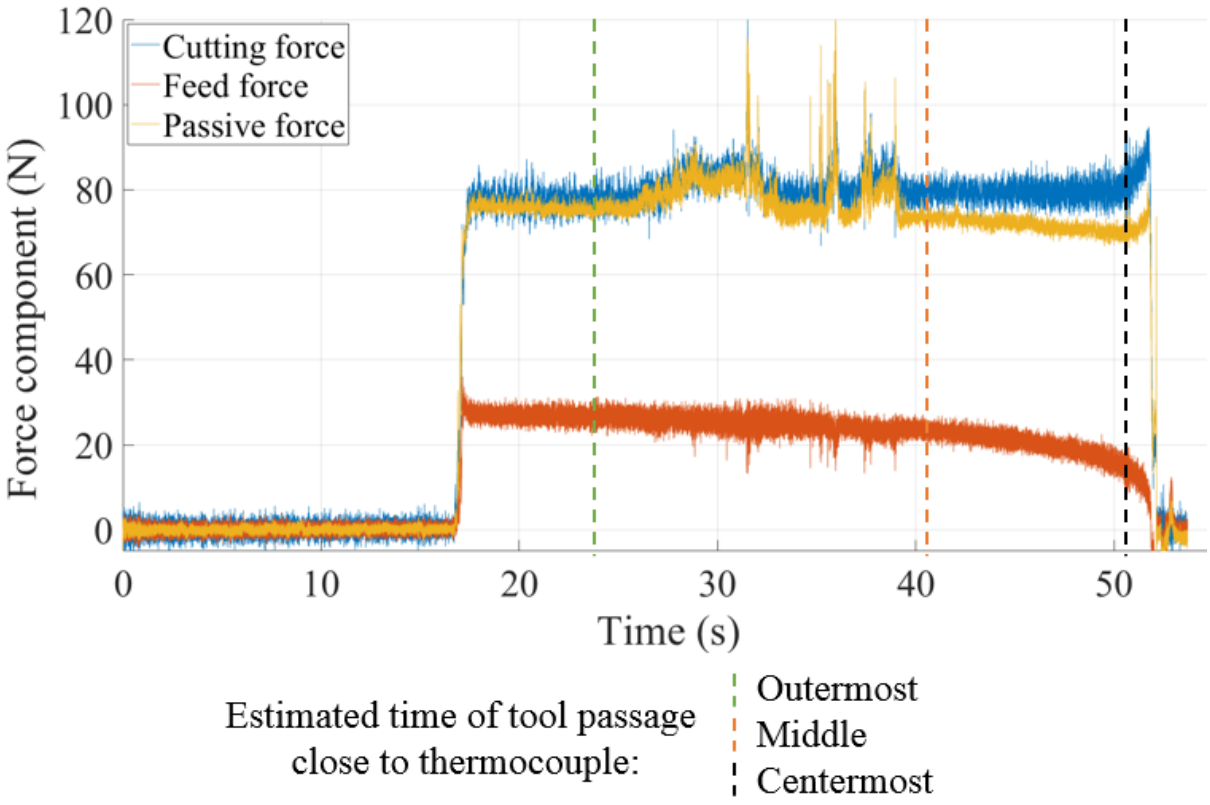

Source: Author

An FFT was applied to the section of a signal with the anomaly and Figure 58 was obtained. It can be observed that there are peaks in 120, 300, and 360 Hz. In some signals, a peak at 60 Hz could also be observed, although smaller than the one at 120 Hz. It is possible that there is a peak at 60 Hz in this signal, but due to other signals with a frequency close to it, it can be masked. The presence of a peak in 60 Hz and its multiples may indicate that this

anomaly was created due to interference of the local power grid, that runs at 60 Hz. If the system was rectified the grid interference would appear as peaks at 120 Hz intervals.

Figure 58 – FFT of the cutting force signal in the section with the anomaly detected on the signal of Figure 57.

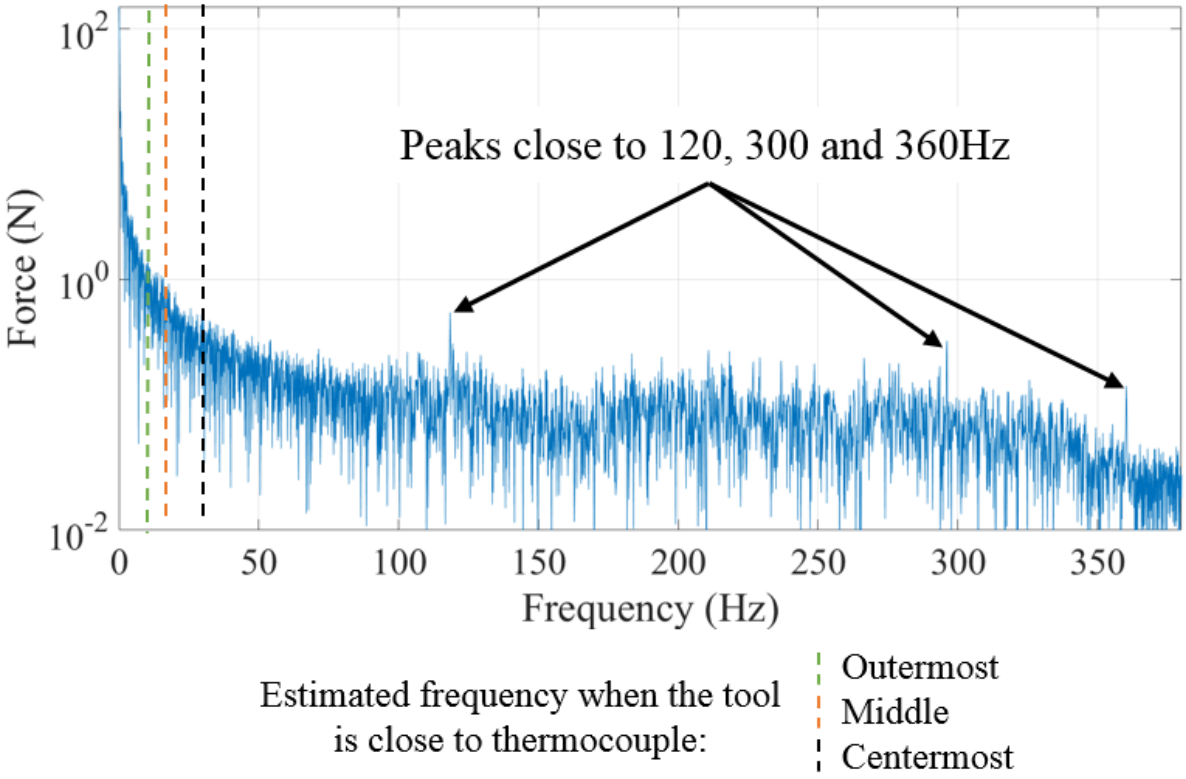

Source: Author.

The second anomaly detected was present in all signals of later passes, when the thermocouples were closer to the machined surface. Only on the first passes of the tests, it was not present, and after it appeared its intensity increased each subsequent pass.

The anomaly consists of the presence of interference at three distinct times. The time interval between the first to second and the second to the third interference are constant and corresponds to the time it takes for the tool to move between the thermocouples, approximately 17.6 s to move between the outermost and middle thermocouple and 10.6 s to move between the middle and centermost thermocouple. This anomaly is similar to the forces anomaly seen in Figure 22 in the work of Chen *et al.* [40] where there was a decrease in force and vibration when the tool passed by the region of the foil. An example of a signal with this anomaly can be seen in Figure 59.

Figure 59 – Signal anomaly. Pass 12 of Workpiece B.

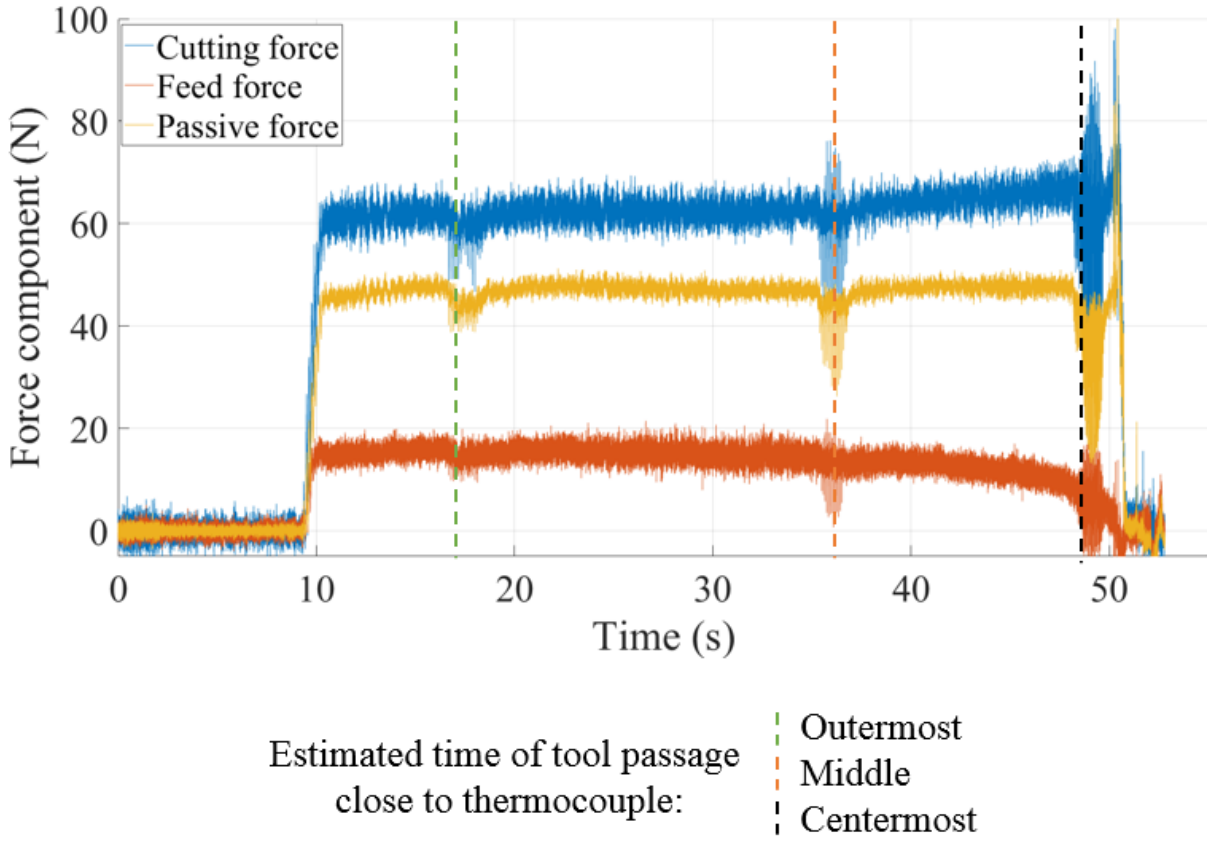

Source: Author.

After applying an FFT in the third anomaly of the cutting force of the signal it was noted that there were peaks in frequencies very close to the spindle rotation frequency in those points. Analyzing the anomalies from this and other signals presented similar results, peaks in frequencies that correspond to the rotation of the workpiece when the tool is passing close to the respective thermocouple and its multiples.

Figure 60 – FFT of the third anomaly on the cutting force of Figure 59.

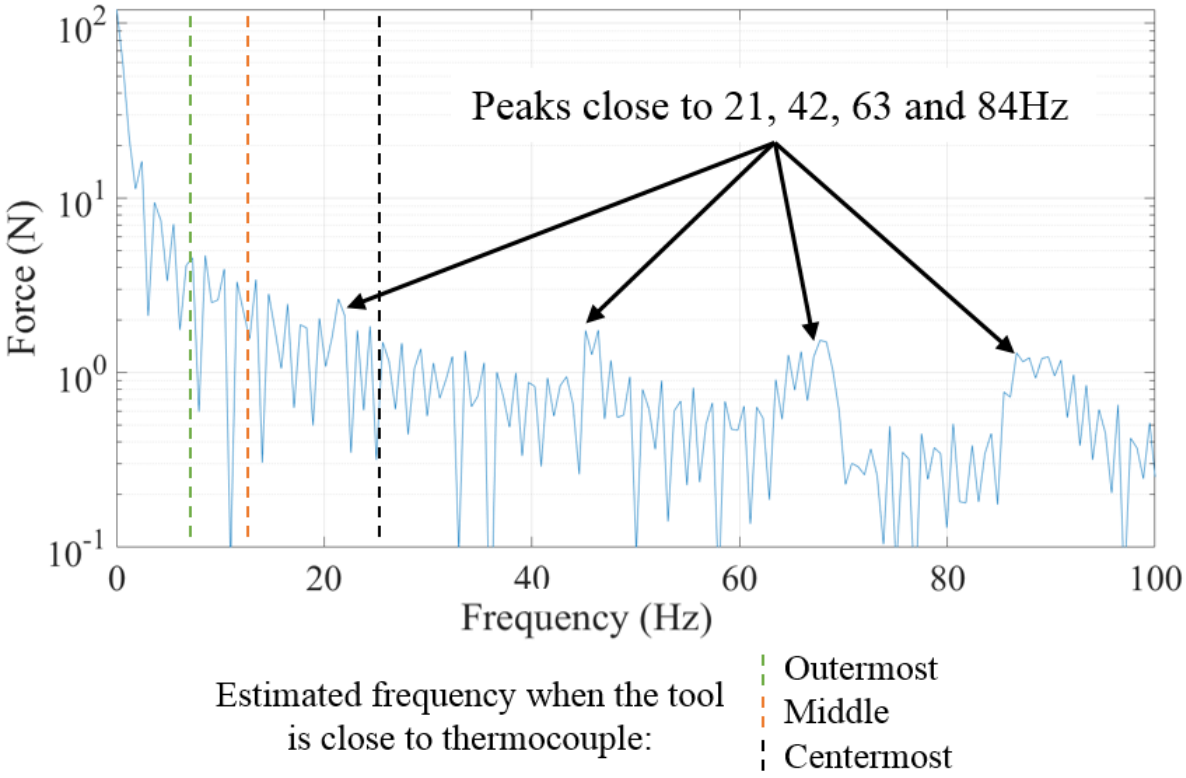

Source: Author.

As the only possible electrical interference between the dynamometer system and the temperature measuring device is through the dynamometer ground, which is also the lathe ground, this anomaly was probably not caused by electrical interference with the thermocouples. A possible cause for these interferences is the workpiece holes made to embed the thermocouples. These holes change the bulk material rigidity and after being revealed (Figure 61) would make the cut interrupted. This also can explain why this effect increases with further passes.

Figure 61 – Revealed thermocouple insertion holes.

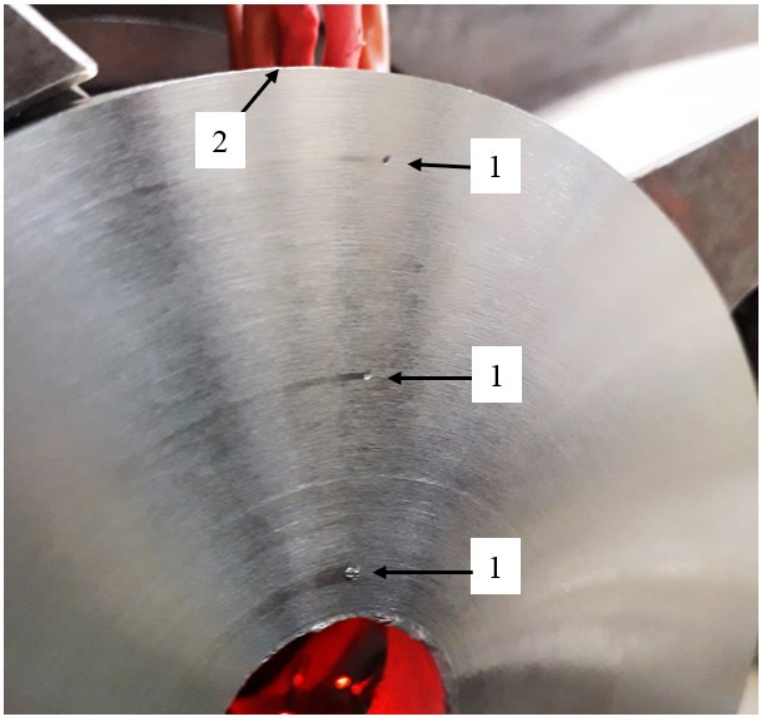

1-Revealed thermocouples holes
2-Thermocouples wires

Source: Author

Analyzing Figure 61, marks darker than the rest of the workpiece can be seen after the insertion holes. Compared with Figure 59, there is force variation during the tool passage on these regions, meaning that the darker marks indicate an area with a different level of conformation than the rest of the workpiece. Burr can be seen in the inner diameter of the workpiece; its presence explains a sudden increase of forces detected at the end of some tests. The burr can have been formed due to the low cutting depth that can cause the increase of conformation during the process.

5.3 TEMPERATURE MEASUREMENT ANALIZYS

There were two machining experiments where the temperature was successfully measured. The first was the Workpiece B test, using a worn edge, from the first test group. The second was the Workpiece E test, using a new edge, from the third test group. In both cases, the outermost thermocouples presented a high lower saturation and little data was usable from it. The Workpieces A, C, and D failed due to failures with the DB9 connectors. Workpiece F from the fourth test group failed due to failures with the fastening system.

During the experiments, in each subsequent pass the machined surface would be closer to the inserted thermocouples. For this reason, it was expected that in each subsequent pass the measured temperature would become higher.

Considering the errors measured during the device calibration it is possible to determine a minimum temperature difference between the middle and centermost thermocouple measurement so that a hypothesis test would determine that one has a higher temperature that the other. As the temperature signal is very dynamic it is not possible to use multiple data points for the hypothesis test. During validation, the standard deviation of the measured temperatures from the channels used for the middle and centermost thermocouples was always below 1. Considering a conservative case where the standard deviation from the signals from both middle an centermost thermocouples is 1, and the number of samples for each signal as 1 and using 99% of certainty, one thermocouple signal would need to be approximately 3,5 ºC above the other for the hypothesis test to fail. To be more conservative, the temperature of one thermocouple will be considered above another if the temperature difference is of at least 5 ºC above the other after applying the systematic error.

In the test with the worn edge (Workpiece B), there was a clear temperature signal since the first pass. In the test with the new edge (Workpiece E), a signal clearly above the amplifier's lower saturation was only seen after pass 13. By that point, the thermocouple was already revealed and was being cut and the edge was worn. This difference was expected as a worn tool usually generates more heat during the cutting [7].

In the first passes of the worn tool test, there was already a clear difference between the signal of the middle thermocouple and the centermost thermocouple. As seen in Figure 62 the middle thermocouple barely shows any temperature increase in the first pass and at the third pass (Figure 63) the temperature increases only a little. On the other hand, the centermost thermocouple shows a clear peak since the first pass, and this peak increases in the third pass. This tendency continues in subsequent passes, with the middle thermocouple always showing a lower temperature and a less clear peak than the centermost thermocouple. In both Figure 62 and Figure 63, there is an appearance of the phantom signal. In the signals plotted without compensation (to check for phantom signals) the middle thermocouple signal was constant in the first pass.

Figure 62 – Temperature signals of the first pass of Workpiece B (worn tool). (a) Middle thermocouple. (b) Centermost thermocouple.

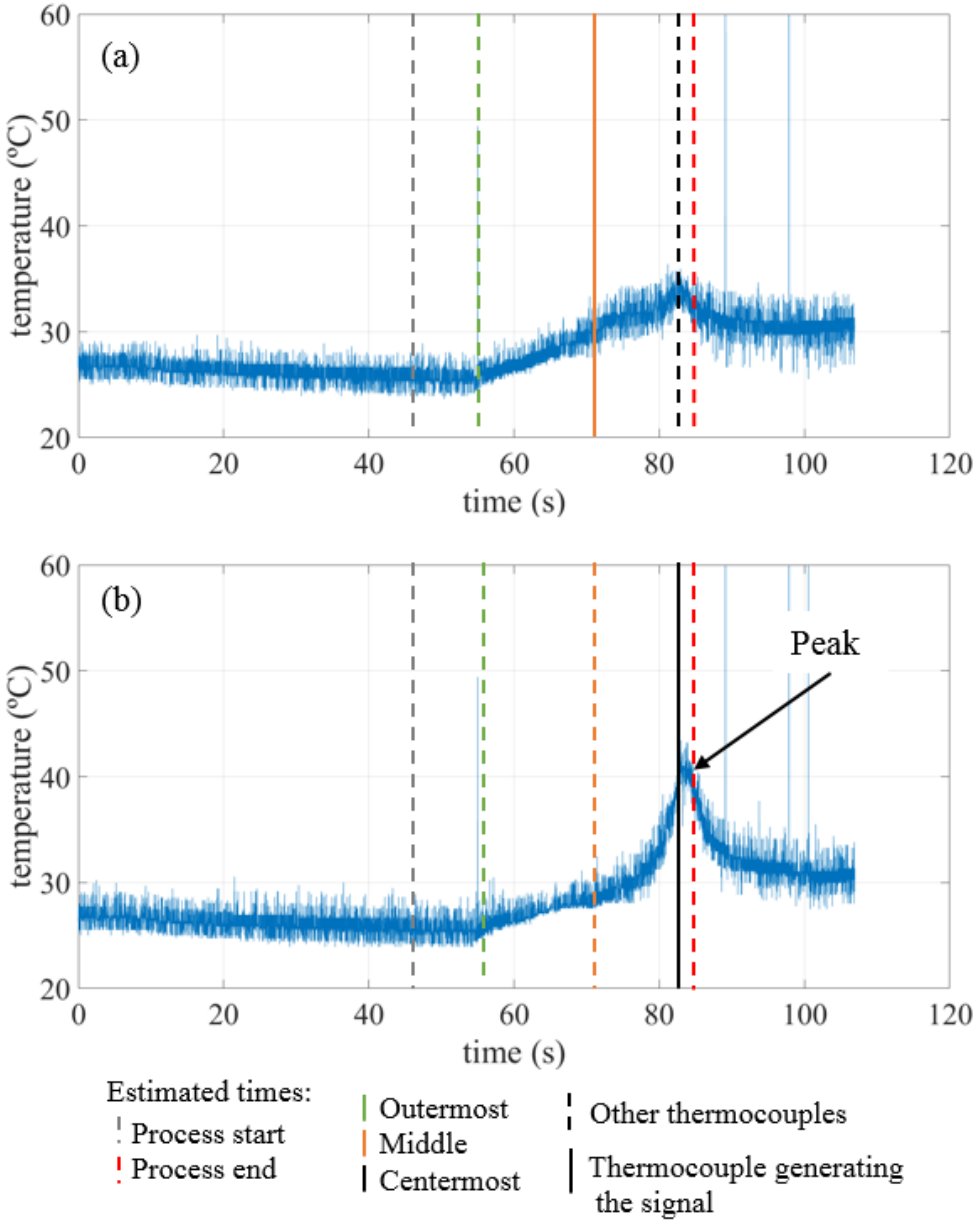

Source: Author

Comparing these results to those obtained by Battaglia *et al.* [41] (Figure 24), there are some similarities. Due to the saturation of the amplifiers, the beginning of the signal cannot be considered a measurement of the real temperature. The increase of temperature seen after 50 s is a phantom signal. The peak followed by the stabilization of the temperature above the previous temperature is very similar to the results from Battaglia *et al.* [41]. It is possible that after reducing the lower saturation of the amplifier and the whole signal is captured, the signal will become even closer.

Figure 63 - Temperature signals of the third pass of the Workpiece B (worn tool). (a) Middle thermocouple. (b) Centermost thermocouple.

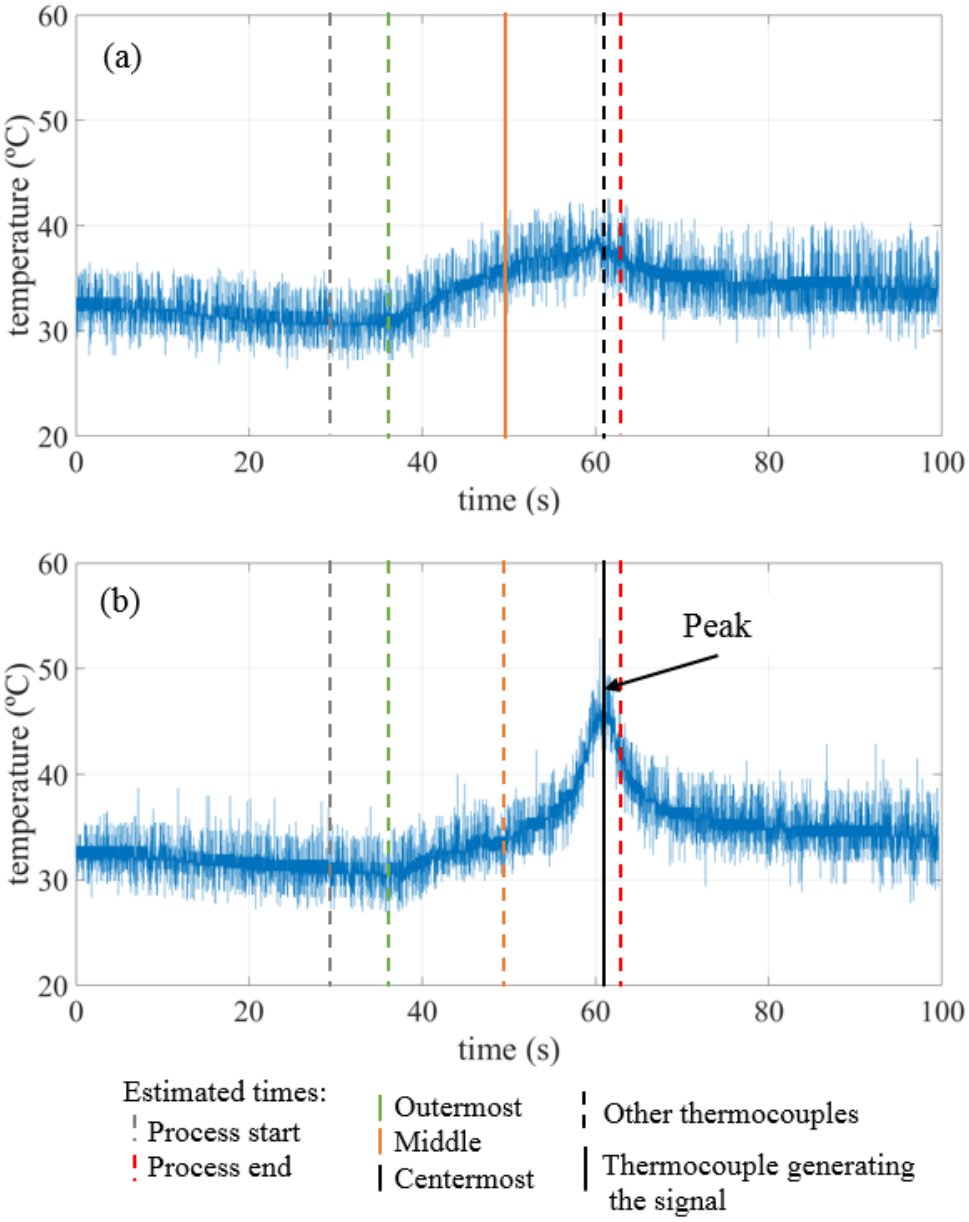

Source: Author

This behavior also happens in the new edge test. The centermost thermocouple starts to show a clear signal and until the last test the middle thermocouple barely shows a temperature increase. This corroborates with Bortoli's [5] and Camargo's [6] conclusions when they assumed that there was an increase in temperature as the tool approached the center of the workpiece. The lack of clear signal occurs due to the temperature not being high enough to generate a voltage that would surpass the saturation of the amplifiers.

Beginning at pass eight of the worn tool test a new type of signal, seen in Figure 64, started appearing together with the temperature peaks. This signal was a series of pulses that

would suddenly increase the temperature followed by a drop in temperature that started with a high derivate that decreased as the temperature decreased, as seen in Figure 65.

Figure 64 - Temperature signals of pass 16 of Workpiece B (worn tool). (a) Signal from the middle thermocouple. (b) Signal from the centermost thermocouple.

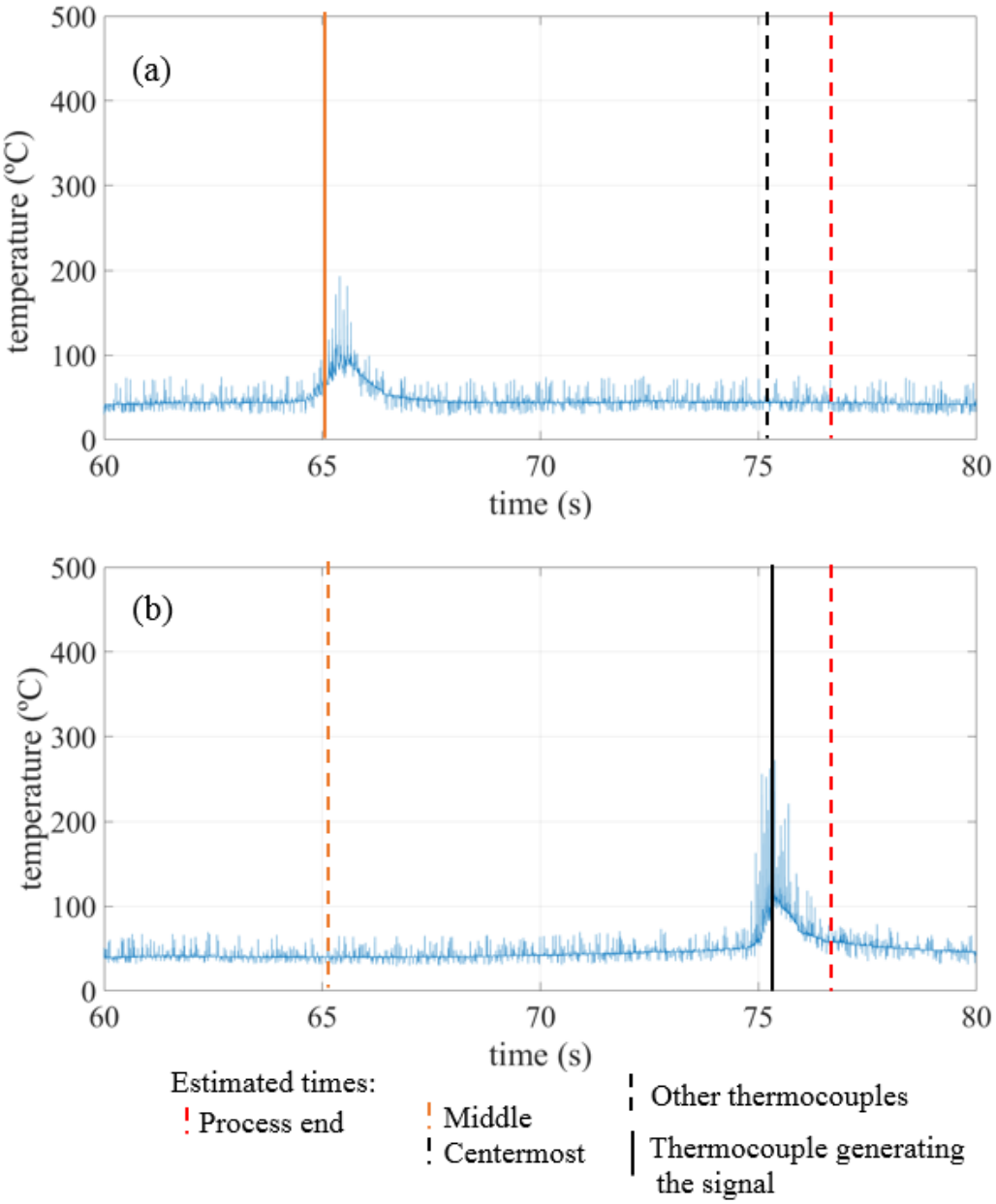

Source: Author.

This pulsed signal would indicate contact with a very concentrated heat source followed by a cooling period. The same type of signal started appearing in the middle thermocouple after pass thirteen. In the new edge test, this type of signal was detected only in

the centermost thermocouple at pass fifteen. In Figure 65 the zoomed-in sections of pass sixteen of the worn edge test can be seen.

Figure 65 – Temperature signals of pass 16 of the Workpiece B (worn edge) zoomed-in the section with the temperature pulses. (a) Signal from the middle thermocouple. (b) Signal from the centermost thermocouple

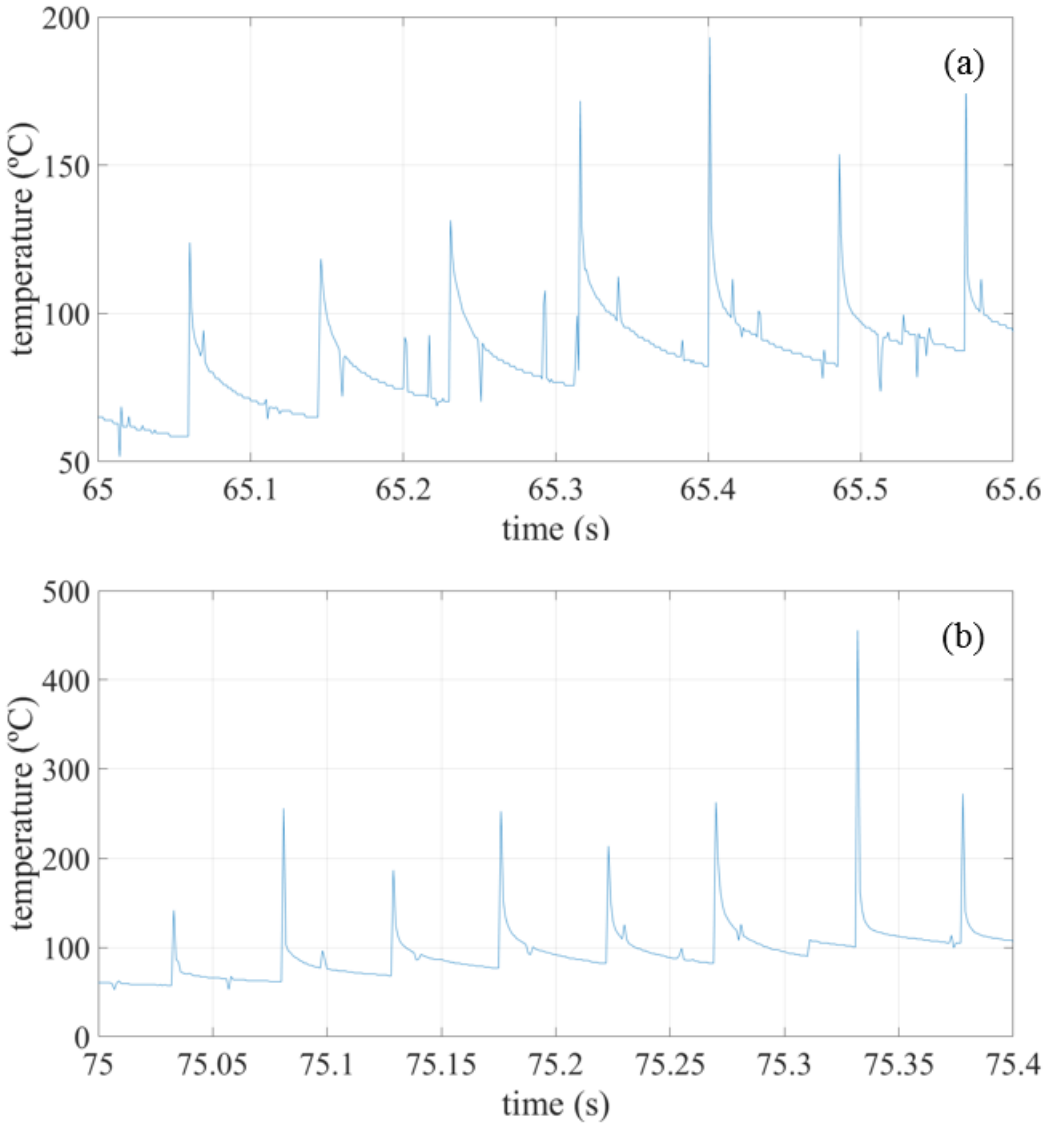

Source: Author

To determine a possible origin of the pulsed signal, FFTs were applied first to sections of empty signal to act as a control (Figure 66), and after in sections with the pulsed signals (Figure 67).

Figure 66 - FFTs of the empty signals. (a) FFT of empty signal from pass 16 of the middle thermocouple. (b) FFT of empty signal from pass 16 of the centermost thermocouple.

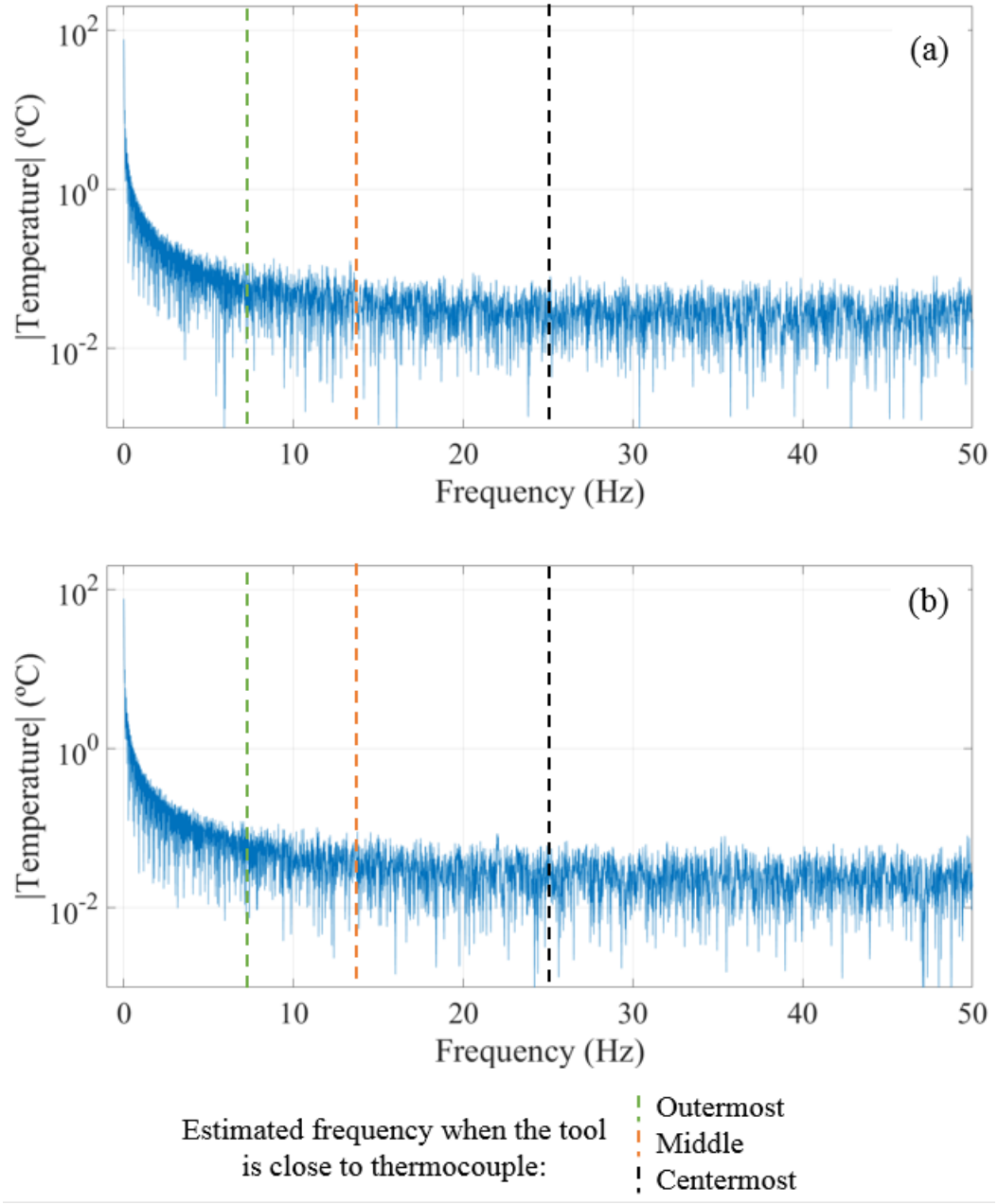

Source: Author.

Analyzing the FFTs of the empty signals, the amplitude of the signals above 10 Hz are all below 1 ºC. Therefore, there is no meaningful noise intrinsic to the device above 10 Hz up to the maximum frequency shown in Figure 66.

Figure 67 - FFTs of the pulsed signals. a) FFT from the pulse signal from pass 16 of the middle thermocouple. b) FFT from the pulse signal from the pass 16 of the centermost thermocouple.

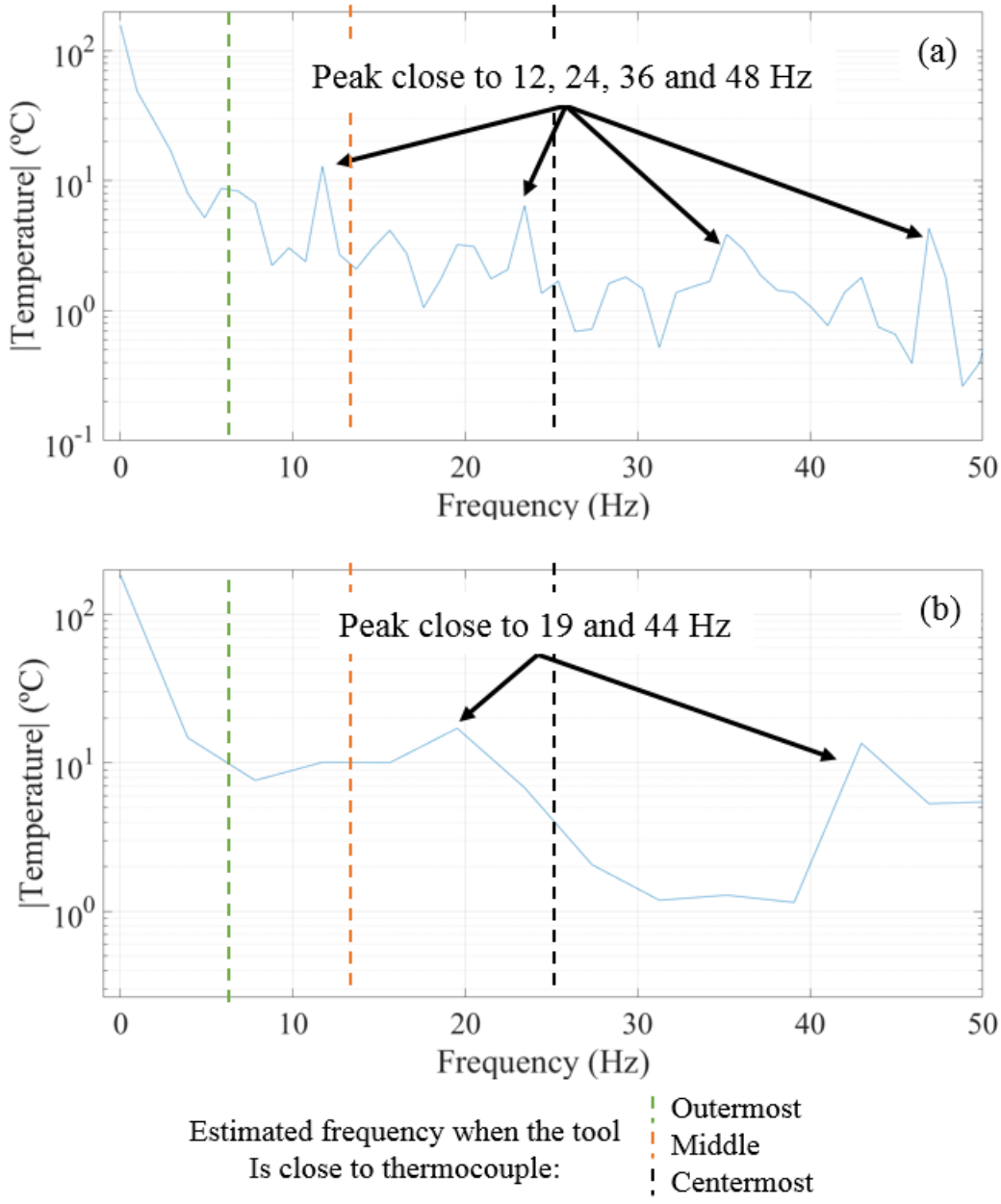

Source: Author.

The FFT from the pulse signal of the middle thermocouple show peaks in frequencies close to 12, 24 and 36, and 48 Hz. This means that the pulse frequency is close to 12 Hz in frequency. In the case of the FFT of the pulse signal for the centermost thermocouple these frequencies are close to 19 and 44 Hz, meaning the pulses probably have a frequency close to 21 Hz.

The cutting speed for all tests was 150 m/min and the centermost thermocouple was always 15 mm from the workpiece center point and the middle thermocouple was always

30 mm from the workpiece center point. Calculating the rotation of the lathe spindle for the position of the middle a frequency was 13,25 Hz was obtained and for the centermost thermocouple, the frequency was 26,50 Hz.

As the pulse signals have a close frequency to the theoretical spindle rotation when the tool is located above each thermocouple, so the pulses are most probably caused by the tool passage. As the pulsed signals appear only in later passes in the tests using a new edge there is a very low probability of it being generated by an electrical interaction between the tool and thermocouple.

Considering the pulses as a concentrated heat delivered by the cutting interface with the tool passage, the cooling time between pulses would be inversely proportional to the spindle rotation frequency. The cooling occurs by the diffusion of heat to nearby regions of the workpiece. This diffusion is faster the higher the temperature difference between the heated region and the cooler region. Therefore, the diffusion is much faster in the first moments when the heated region is at a higher temperature, but it becomes slower as the heated region temperature drops. This means that the shortening of cooling time can have little effect if it cuts a period of slower diffusion or a much greater effect if it cuts a period of faster diffusion. Thus, this effect should have a greater impact on material with low thermal conductivity, in situations with a greater amount of heat and with higher spindle rotation frequencies. As the machining of AISI 52100 generates more heat, confirmed by the difference in the incandescence of the chips, this effect should be more significant in it.

These findings corroborate what Camargo's [6] and Bortoli's [5] suspected, that there is an increase in temperature as the tool approaches the workpiece center. This also shows that the mechanism that causes this increase in temperature is very similar to the coherent heat waves described by Astakhov and Shvets [8]. It is expected that when these tests are repeated with hardened steels this effect will intensify due to greater heat generation.

5.4 PROPOSED ENHANCEMENTS FOR THE DEVICE

In addition to correcting the detected failures, there were many other enhancements that could be applied to make the temperature measurement device more practical and versatile. One of the first enhancements that was thought but its application was postponed was the addition of a way to download the data from the device without removing it from the lathe. This would diminish the degradation of the fastening system and permit the data to be transferred between tests. There were two ways proposed to do this.

The first way was to extend a Universal Serial Bus (USB) port from the Arduino to the front of the device. After checking the size of commercially available extensions and connectors it was determined that they were too big to fit inside the case without extending it and that assembling a smaller one could be difficult. This would also require access to the device front and the removal of the workpiece could be required.

The second way to do this was to use a prototyping board with wireless or Bluetooth capabilities. Both wireless and Bluetooth have a maximum baud rate (rate of data transference) of 115 200 bps while an SPI connection can reach up to half the clock frequency, 8 MHz in the Arduino Nano's case that would translate to 8 Mbps [45]. Then, wireless and Bluetooth were not considered for real time data transfer due to bandwidth and possible interferences that could occur during the tests, but it would be viable to transfer the data after the tests. This solution would be more expensive than the first, but it could also have more benefits. For instance, this could be used to synchronize the device with other data acquisition systems and permit to download of the data even if the device is physically inaccessible without the removal of the workpiece.

Another enhancement is modularity. This was the motive that in the first prototype there was a separation between the acquisition and amplification systems, and they were printed in separate PCBs. The objective of this is to enable the use of different sets of amplifiers, sensors, and filters, which would enable the device to be used in other processes and measure other types of signals. Moreover, limit the possibilities for miniaturization as there would be a need to keep the modules on separated boards and require that the acquisition system be compatible with all modules. There would be a need to develop specific fastening systems and cases for other applications.

An enhancement that would also help with modularity would be to fabricate the case for the electronics with additive manufacturing. The way that the fastening system is currently designed requires it to have a certain rigidity but with a few changes, it could be possible to make a fastening that could be fixed in a polymer case. This would simplify the manufacture of the fastening system and allow the use of different cases adapted for different modules.

An enhancement that will probably be applied to the finished device is the fabrication and assembly of the electronics board in a more specialized way. The lack of solder masks and more precise soldering means that the life expectancy of the device will be limited because of oxidation and other wear. This also affects the device's precision and reliability.

Another possible enhancement would be to remove the prototyping platforms and develop the device using the basic components. This associated with the use of Surface

Mounted Device (SMD) components could mean great miniaturization. As prototyping platforms are made for general use, they have many components that are not necessary for this device.

Although this path brings many advantages, it goes against the initial objectives of this project, which are the development of an inexpensive and simple temperature measurement device. The development and any future alteration or customization would require a much deeper knowledge of electronics compared to a device using a prototyping platform. It would also require a greater infrastructure to fabricate and assemble it. The path would be used if there was an objective to turn this device into a product to be produced and sold instead of being an open-source development.

The enhancements discussed previously were summarized in Table 5.

Table 5 – Proposed possible enhancements for the device.

Enhancement	**Advantage**	**Limitation**
In-loco data transfer via WIFI or blue-tooth.	Download data without need to disassemble test.	Requires WIFI or blue-tooth capable prototyping platform.
In-loco data transfer via USB.	Download data without the need to remove device from machine.	Requires the miniaturization of a USB connection or relocation of components.
Modularity.	More versatility of the device.	Limited miniaturization and need of different cases and fastening systems.
Fabrication of case with additive manufacture.	Simplification of the case manufacture process.	May require a separation between the case and fastening system.
Using better manufactory and assembly processes for the PCBs and Addition of solder mask.	Better precision and reliability form the device.	Require better infra-structure and/or require more resources.
Redesign the device without the use of prototyping platform.	Components would be better selected for the device application facilitating miniaturization and enabling better resolution and precision.	Requires much deeper knowledge of electronics and better infra-structure. This would make the device less accessible and less customizable.

Source: Author.

6 CONCLUSIONS

This research project began with the objective of investigating the assumptions made by in previous works that there is an increase in temperature during the radial turning of hardened steels as the tool approaches the workpiece center. The objective was both to develop a temperature measuring device and ascertain that there was a temperature increase as the tool approached the center of the workpiece in radial turning. The device was developed using an Arduino prototyping platform as a basis and after projecting and testing the individual systems of the device, a prototype for temperature measurement was fabricated.

The prototype was validated in two steps. First, using an Omega CLD-II multicalibrator to ascertain the gain from each channel and the errors in voltage acquisition. After that, an Omega CL552 oven was used to ascertain the temperature measuring errors using a type K thermocouple. During the validation, the total errors stayed always below 50 ºC.

The prototype was used to measure the temperature during radial turning experiments of the AISI 1040 steel. In addition to temperature measurement, the machining forces were measured using a dynamometer. During the machining experiments and subsequent data analysis, a few failures in the temperature measurement device were identified, and four of the six tests failed to produce reliable temperature data. The most pressing failures concerned the connection between the device and workpiece and wear on the fastening system, then a few solutions were attempted, and other solutions were proposed.

Analyzing the data from the successful tests has shown that the centermost thermocouple always presents a higher peak temperature than the thermocouple locater farther from the center of the workpiece. In the final passes of each test pulsed signals were detected that were associated with the tool passage due to their frequency matching the instant spindle rotation. The pulsed signal indicated a relation between the spindle rotation, tool passage frequency, and temperature difference. There was also vibration detected in the forces signals in later passes that were associated with the lack of material in the holes that contained the thermocouples, no other interaction between the dynamometer and the temperature measurement device was detected.

Although the development of the device was not finished and there was not enough data to make a reliable statistical analysis, this work was considered successful. This research developed a temperature measuring device that was used to confirm assumptions of previous studies about the temperature increase in radial turning. This research has also determined a

probable cause for the assumed effect. Thus, the objectives proposed by this work were fulfilled.

A temperature measurement prototype device was developed. The temperature was measured during radial turning and an increase in temperature was detected, corroborating the assumption made by Camargo [6] and Bortoli [5]. A clue of the mechanism for the temperature increase was detected in the form of pulsed signals that is similar to the phenomena described by Astakhov and Shvets [8]. Finally, with the results from this research project, both negative and positive, possible enhancements for the temperature measurement device were proposed.

However, the temperature measurement device is still in a prototype state and the tests were made with stand-in workpiece materials and tools. This research is the first step in a project intended in modeling and simulation of temperature in the radial turning of hardened steels and more studies are needed to reach that objective.

6.1 SUGESTIONS FOR FUTURE WORKS

The next step in this project is to review the failures, results, and proposed enhancements, besides revising the device project. This revision should eliminate the failures that prevent the device from working properly and eliminate or at least mitigate smaller failures. The revision should also balance the cost and benefit of the possible enhancements to judge which enhancements should be applied. It should also review the requirements for acquisition rate, the number of thermocouples, measurement resolution and measuring range, etc. to obtain better data.

After the project revision, the next step is to produce a new prototype and test it in machining with stand-in materials. If the results prove unsatisfactory, the review and revision step should be repeated until a satisfactory test is achieved.

The last step of the project should be to create a finished device, calibrate it, and use it to measure the temperature in radial turning of hardened steel using PCBN tools. This data should be used to develop and validate a temperature model for the process. It is expected that due to the higher process temperature, the temperature signals will be clearer. As the effect on the machining forces seen in Camargo's [6] work was much more pronounced, it is expected that the effect of rotation frequency in the pulsed signals will be much more pronounced and the temperature differences will be greater.

This research project has two main contributions that can be used as a basis for future works. The first is the identification of the increase in temperature during radial turning and a

probable mechanism for this temperature increase. The second is the developed device and the inclusion of drawing, schema, and algorithms necessary to replicate it in another work.

Based on the findings of this research project, the following suggestions for future works can be drawn:

a) Investigate the temperature during radial turning of hardened steels and other materials with high hardness.
b) Investigate the temperature during radial turning of polymers and other materials with low heat conductivity.
c) Adapt the device to measure temperature in other processes.
d) Adapt the device or part of the device for other applications.
e) Continue device development to increase reliability.
f) Develop a way to measure the distance between the thermocouple and the machined surface for each pass.
g) Develop a better procedure for workpiece preparation, both the thermocouple embedment method and connection to the device.

REFERENCES

[1] CITTI, P.; GIORGETTI, A.; MILLEFANTI, U. Current challenges in material choice for high-performance engine crankshaft. **Procedia Structural Integrity**, v. 8, p. 486–500, 2018.

[2] MOHRUNI, A. S.; YANIS, M.; KURNIAWAN, E. Development of surface roughness prediction model for hard turning on AISI D2 steel using cubic boron nitride insert. **Jurnal Teknologi**, v. 80, n. 1, p. 173–178, 2018.

[3] KLOCKE, F.; BRINKSMEIER, E.; WEINERT, K. Capability Profile of Hard Cutting and Grinding Processes. **CIRP Annals - Manufacturing Technology**, v. 54, n. 2, p. 22–45, 2005.

[4] GRIFFITHTS, B. J. **Manufacturing surface technology**. 1th. ed. London: Penton Press, 2001.

[5] BORTOLI, G. A. DE. **AVALIAÇÃO DA INTEGRIDADE DA SUPERFÍCIE USINADA EM FUNÇÃO DO DESGASTE DA FERRAMENTA DE PCBN NO TORNEAMENTO RADIAL DO AÇO AISI 52100 ENDURECIDO**. 2019. 73 f. Trabalho de conlusão de curso (Graduação em engenharia mecânica) - Universidade Federal de Santa Catarina. 2019.

[6] CAMARGO, F. J. DE. **INFLUÊNCIA DA DIREÇÃO DE CORTE NA PROGRESSÃO DO DESGASTE DE FERRAMENTAS DE PcBN APLICADAS NO TORNEAMENTO DO AÇO AISI 52100 TEMPERADO E REVENIDO**. 2019. 106 f. Dissertação (Mestrado em engenharia mecânica) - Universidade Federal de Santa Catarina. 2019.

[7] KLOCKE, F. **Manufacturing Processes 1**. 1th. ed. Berlin: Springer, 2011.

[8] ASTAKHOV, V. P.; SHVETS, S. V. A novel approach to operating force evaluation in high strain rate metal-deforming technological processes. **Journal of Materials Processing Technology**, v. 117, n. 1–2, p. 226–237, 2001.

[9] **Scopus**. Avaliable in: <https://www.scopus.com>. Access in: 7 jul. 2022.

[10] DEUTSCHES INSTITUT FÜR NORMUNG. **Din 8589-1: Fertigungsverfahren Spanen - Teil 1: Drehen; Einordnung, Unterteilung, Begriffe**. 2003. 15 f. 2003.

[11] ASTAKHOV, V. P. **Machining of Hard Metals**. Springer-Verlag London Limited, 2011.

[12] MACHADO, A. R.; ABRÃO, A. M.; COELHO, R. T.; SILVA, M. B. **Teoria da Usinagem dos Materiais**. 1. ed. [s.l.] São Paulo: Edgar Blucher, 2009.

[13] POULACHON, G.; MOISAN, A.; JAWAHIR, I. S. On modelling the influence of thermo-mechanical behavior in chip formation during hard turning of 100Cr6 bearing steel. **CIRP Annals - Manufacturing Technology**, v. 50, n. 1, p. 31–36, 2001.

[14] BYRNE, G.; DORNFELD, D.; DENKENA, B. Advancing cutting technology. **CIRP Annals - Manufacturing Technology**, v. 52, n. 2, p. 483–507, 2003.

[15] PAUCKSCH, E. **Zerspantechnik**. 1st. ed. [s.l.] Braunschweig; Wiesbaden: Vieweg, 1996.

[16] YALLESE, M. A.; CHAOUI, K.; ZEGHIB, N.; BOULANOUAR, L.; RIGAL, J. F. Hard machining of hardened bearing steel using cubic boron nitride tool. **Journal of Materials Processing Technology**, v. 209, n. 2, p. 1092–1104, 2009.

[17] KOMANDURI, R.; HOU, Z. B. Thermal modeling of the metal cutting process Part I - temperature rise distribution due to shear plane heat source. **International Journal of Mechanical Sciences**, v. 42, n. 9, p. 1715–1752, 2000.

[18] KOMANDURI, R.; HOU, Z. B. Thermal modeling of the metal cutting process - Part II: Temperature rise distribution due to frictional heat source at the tool-chip interface. **International Journal of Mechanical Sciences**, v. 43, n. 1, p. 57–88, 2001.

[19] KOMANDURI, R.; HOU, Z. B. Thermal modeling of the metal cutting process - Part III: Temperature rise distribution due to the combined effects of shear plane heat source and the tool-chip interface frictional heat source. **International Journal of Mechanical Sciences**, v. 43, n. 1, p. 89–107, 2001.

[20] COUNT OF RUMFORD, B. An Inquiry concerning the Source of the Heat Which is Excited by Friction. **Philosophical Transactions of the Royal Society of London**, v. 88, p. 80–102, jan. 1798.

[21] TAYLOR, F. W. On the Art of Cutting Metals. **Scientific American**, v. 63, n. 1619supp, p. 25942–25944, 1907.

[22] ARRAZOLA, P. J.; ÖZEL, T.; UMBRELLO, D.; DAVIES, M.; JAWAHIR, I. S. Recent advances in modelling of metal machining processes. **CIRP Annals - Manufacturing Technology**, v. 62, n. 2, p. 695–718, 2013.

[23] ROBINSON, S. **Simulation: the Practice of Model Development and Use**. 2nd. ed. West Sussex: MacMillan, 20014.

[24] SÖHNER, J. Beitrag zur Simulation zerspanungstechnologischer Vorgänge mit Hilfe der FEM. p. 162, 2003.

[25] RAO, R. V. **Advanced Modeling an Optimization of Manufacturing Processes**. Londom: Springer-Verlag London Limited, 2011.

[26] MERCHANT, M. E. Mechanics of the metal cutting process. I. Orthogonal cutting and a type 2 chip. **Journal of Applied Physics**, v. 16, n. 5, p. 267–275, 1945.

[27] MERCHANT, M. E. Mechanics of the metal cutting process. II. Plasticity conditions in orthogonal cutting. **Journal of Applied Physics**, v. 16, n. 6, p. 318–324, 1945.

[28] MOLINARI, A.; MOUFKI, A. The Merchant's model of orthogonal cutting revisited: A new insight into the modeling of chip formation. **International Journal of Mechanical Sciences**, v. 50, n. 2, p. 124–131, 2008.

[29] KLOCKE, F.; RAEDT, H. W.; HOPPE, S. 2D-FEM simulation of the orthogonal high speed cutting process. **Machining Science and Technology**, v. 5, n. 3, p. 323–340, 2001.

[30] TZOTZIS, A.; TAPOGLOU, N.; VERMA, R. K.; KYRATSIS, P. 3D-FEM Approach of AISI-52100 Hard Turning: Modelling of Cutting Forces and Cutting Condition Optimization. **Machines**, v. 10, n. 2, 2022.

[31] CARSLAW, H. S.; JAEGER, J. C. **Conduction of heat in solids**. second ed. London: Oxford University press, 1959.

[32] GARCÍA-MARTÍNEZ, E.; MARTÍNEZ-MARTÍNEZ, A.; MANJABACAS-TENDERO, M. C.; MIGUEL-EGUÍA, V. Proposal of a combined experimental-simulation methodology for the evaluation of machining temperature in turning processes. **Measurement: Journal of the International Measurement Confederation**, v. 189, n. August 2021, p. 110632, 2022.

[33] ZHOU, G.; XU, C.; WANG, X.; FENG, P.; ZHANG, M. Determination of tool tip steady-state temperature in dry turning process based on artificial neural network. **Journal of Manufacturing Processes**, v. 79, n. October 2021, p. 600–613, 2022.

[34] DAVIES, M. A.; UEDA, T.; M'SAOUBI, R.; MULLANY, B.; COOKE, A. L. On The Measurement of Temperature in Material Removal Processes. **CIRP Annals - Manufacturing Technology**, v. 56, n. 2, p. 581–604, 2007.

[35] PLOGMEYER, M.; GONZÁLEZ, G.; BIEHL, S.; SCHULZE, V.; BRÄUER, G. Wear-resistive thin-film sensors on cutting tools for in-process temperature measurement. **Procedia CIRP**, v. 101, p. 85–88, 2020.

[36] LEE, K. M.; HUANG, Y.; JI, J.; LIN, C. Y. An Online Tool Temperature Monitoring Method Based on Physics-Guided Infrared Image Features and Artificial Neural Network for Dry Cutting. **IEEE Transactions on Automation Science and Engineering**, v. 15, n. 4, p. 1665–1676, 2018.

[37] REZENDE, B. A.; MAGALHÃES, F. DE C.; CAMPOS RUBIO, J. C. Study of the measurement and mathematical modelling of temperature in turning by means equivalent thermal conductivity. **Measurement: Journal of the International Measurement Confederation**, v. 152, p. 107275, 2020.

[38] HAN, J.; TAN, X.; LI, T.; TANG, Z.; LIAO, G.; SHI, T. In-situ measurement of cutting edge temperature and its effect on tool wear in turning by a near-infrared fiber-optic two-color pyrometer. **Procedia CIRP**, v. 101, p. 89–92, 2020.

[39] GARRITY, K. **NIST ITS-90 Thermocouple Database - SRD 60**. Avaliable in: <https://doi.org/10.18434/T4S888>. Access in: 11 maio. 2022.

[40] CHEN, L.; TAI, B. L.; CHAUDHARI, R. G.; SONG, X.; SHIH, A. J. Machined surface temperature in hard turning. **International Journal of Machine Tools and Manufacture**, v. 121, n. November 2016, p. 10–21, 2017.

[41] BATTAGLIA, J. L.; PUIGSEGUR, L.; CAHUC, O. Estimated temperature on a machined surface using an inverse approach. **Experimental Heat Transfer**, v. 18, n. 1, p. 13–32, 2005.

[42] SINGH, V. K.; KUMAR, C.; BESRA, G.; MUKHOPADHYAY, A.; BARMAN, M. Measurement, modelling and optimization of the average temperature at the tool work interface for turning of AISI 1040 steel using ANN-GA methodology. **Engineering Research Express**, v. 3, n. 3, 2021.

[43] HOSSEINI, S. B.; BENO, T.; KLEMENT, U.; KAMINSKI, J.; RYTTBERG, K. Cutting temperatures during hard turning - Measurements and effects on white layer formation in AISI 52100. **Journal of Materials Processing Technology**, v. 214, n. 6, p. 1293–1300, 2014.

[44] KONDAVEETI, H. K.; KUMARAVELU, N. K.; VANAMBATHINA, S. D.; MATHE, S. E.; VAPPANGI, S. A systematic literature review on prototyping with Arduino: Applications, challenges, advantages, and limitations. **Computer Science Review**, v. 40, p. 100364, 2021.

[45] **Arduino**. Avaliable in: <https://store-usa.arduino.cc/>. Access in: 1 fev. 2022.

[46] GOSAI, M.; BHAVSAR, S. N. Experimental Study on Temperature Measurement in Turning Operation of Hardened Steel (EN36). **Procedia Technology**, v. 23, p. 311–318, 2016.

[47] INTEGRATED, M. Max6675. **Data sheet MAX6675**, p. 8, 2021.

[48] MAXIM INTEGRATED. MAX31855 Cold-Junction Compensated Thermocouple-to-Digital Converter. **Datasheet**, p. 1–13, 2016.

[49] TEXAS INSTRUMENTS. **TI training and videos**. Avaliable in: <https://training.ti.com/>. Access in: 8 nov. 2021.

[50] TEXAS INSTRUMENTS. INA333 INA333 Micro-Power (50μA), Zerø-Drift, Rail-to-Rail Out Instrumentation Amplifier. p. 33, 2008.

[51] SHIN, K.; HAMMOND, J. **Fundamentals of signal processing for sound and vibration engineers**. [s.l.] John Wiley & Sons, Ltd, 2008.

[52] RABIN, Y.; RITTEL, D. A Model for the Time Response of Solid-embedded Thermocouples. n. May 2014, 1999.

[53] GREIMAN, B. **SdFat library**. Avaliable in: <https://github.com/greiman/SdFat>. Access in: 11 maio. 2022.

[54] GHOSH, P. S.; CHAKRABORTY, S.; BISWAS, A. R.; MANDAL, N. K. Empirical Modelling and Optimization of Temperature and Machine Vibration in CNC Hard Turning. **Materials Today: Proceedings**, v. 5, n. 5, p. 12394–12402, 2018.

[55] SILVEIRA, C. A. DA. **Análise da movimentação síncrona e simultânea entre scanner galvanométrico e eixos lineares em aplicações laser**. 2020. 148 f. Tese (Doutorado

em engenharia mecânica) - Universidade Federal de Santa Catarina. 2020.

[56] GHRIB, T. Heat treatment effect on the microstructural , hardness and thermal properties of XC48 steel. **Journal of Thermal Analysis and Calorimetry**, v. 139, n. 3, p. 1829–1837, 2020.

[57] KARKI, J. **Signal conditioning piezoelectric sensors**. Texas Instruments. Avaliable in: <https://www.ti.com/lit/an/sloa033a/sloa033a.pdf>.

[58] JOINT COMMITTEE FOR GUIDES IN METROLOGY ISBN. Evaluation of measurement data — Guide to the expression of uncertainty in measurement. **International Organization for Standardization Geneva ISBN**, n. September, 2008.

APPENDIX A – ASSEMBLED DEVICE

After testing the individual systems, the cavities for the electronics were machined in the case, as seen in Figure 68. Each cavity was designed to carry specific components and their dimensions were according to the components' size.

Figure 68 – Machined cavities inside the case.

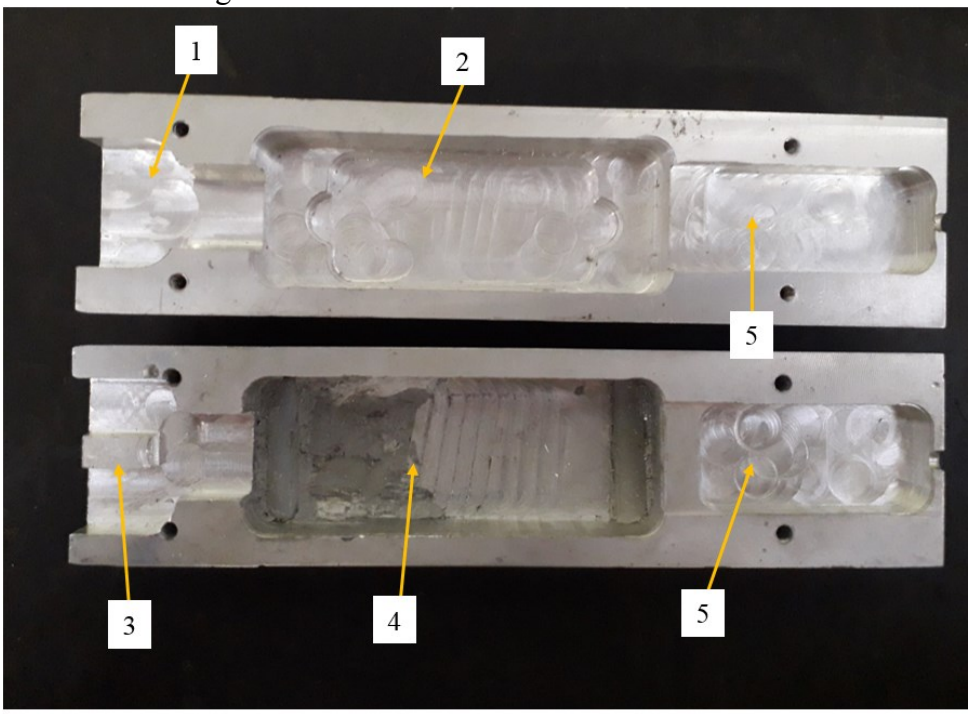

1-Connector cavity
2-Amplification system cavity
3-Buttons and LEDs cavity
4-Acquisition system cavity
5-Battery cavity

Source: Author.

Then, the components were arranged inside the case as seen in Figure 69. After the first tests, insulation was added between the PCB and the case. As it was still a prototype, the wires were left longer than necessary so that minor alterations could be made without needing to rewire the electronic system.

Figure 69 – Components arranged inside the case.

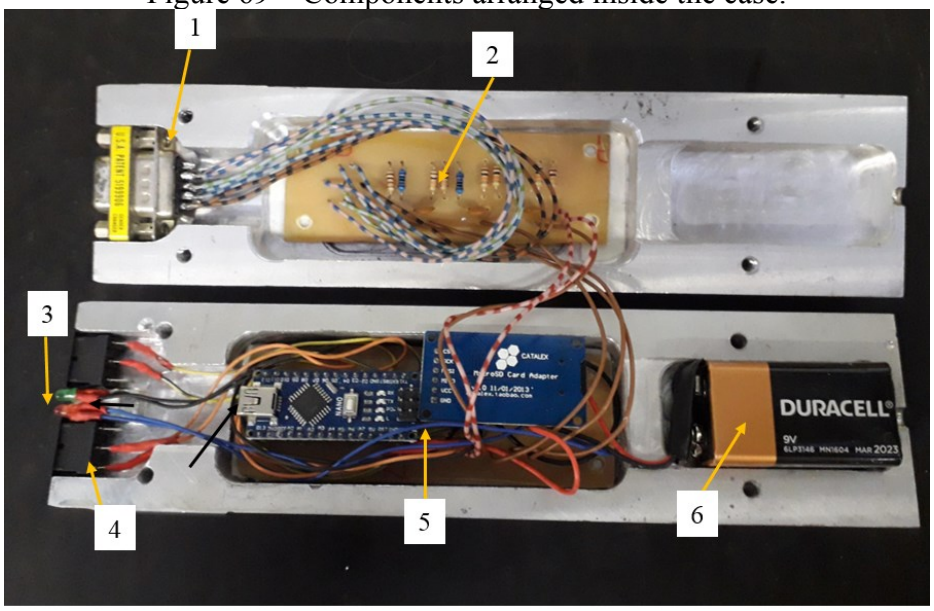

1-DB9 Connector
2-Amplification system
3-LEDs
4-Buttons
5-Acquisition system
6-Battery

Source: Author.

After all components were in place, the case was closed, and a few simple tests were made to ensure that the system was working properly inside the case. In Figure 70 the assembled device can be seen.

Figure 70 – Assembled device Top: without the complete fastening system. Bottom: with the complete fastening system. Right: front panel. Left: side view.

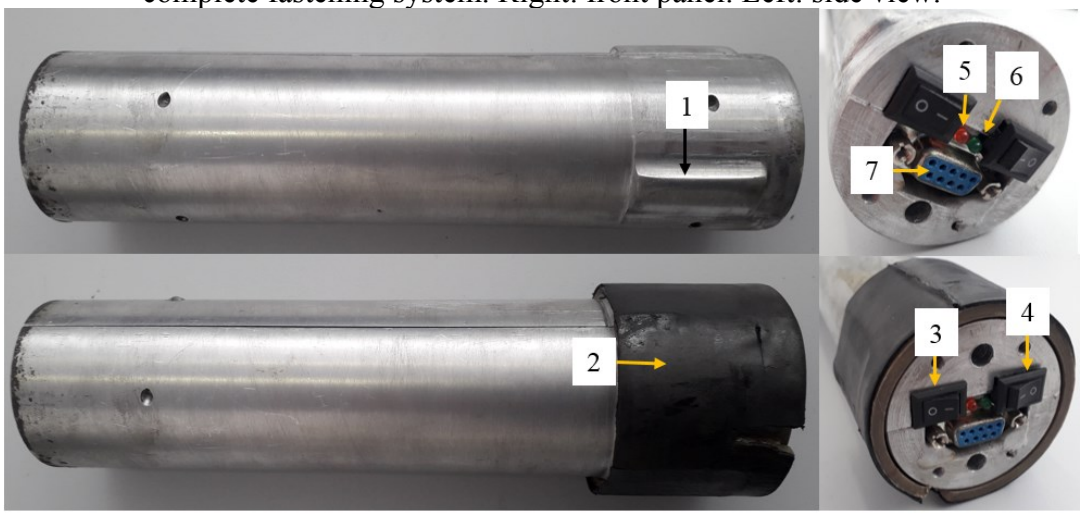

1-Protrusion
2-Rubber covered PVC tube
3-Power button
4-Run button
5-Power LED (red)
6-Run LED (green)
7-DB9 connector

Source: Author.

In the front of the device, the buttons and LEDs from the acquisition system can be seen. The DB9 connector where the thermocouples will be connected can also be seen. The length covered by PVC and rubber is the fastening system and the rest of the cylinder is the case.

APPENDIX B – DRAWINGS

In Figure 71 the case that holds the electronic systems can be seen. It was fabricated of aluminum 6061. The complexity of the machined cavities is due to the need to hold and bear different components, from the PCBs to the battery and buttons. Even so, both halves of the cylinder case were made as close to each other as possible to simplify fabrication. All internal curvatures were made with a 6 mm radius so a 12 mm diameter mill could be used to make all cavities.

The PCBs were not completely plane, due to solder and components, so there was a need to make depressions below where each circuit would stay. The battery was isolated, with a narrow passage between it and the other components for the wires, so that if the battery leaked the rest of the system would not be damaged.

Figure 71 – Case for the electronic systems. All measures are in mm.

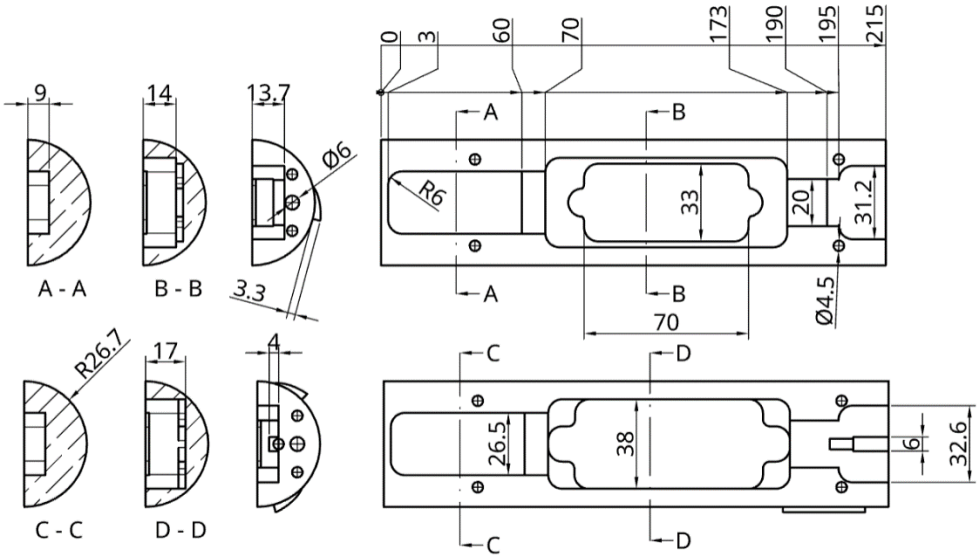

Source: Author.

In Figure 72 the PVC tube that was part of the fastening system can be seen. It was made to fit over the case when closed. The case protrusions fit in the three indentations on the tube. Rotating the case while the tube is held static, forces the protrusions to go under the tube walls and force them to expand. A single slot on the tube was made, then a hooked tool was used to hold the PVC tube static.

Figure 72 – PVC tube used for the fastening system. All measures in mm when not specified.

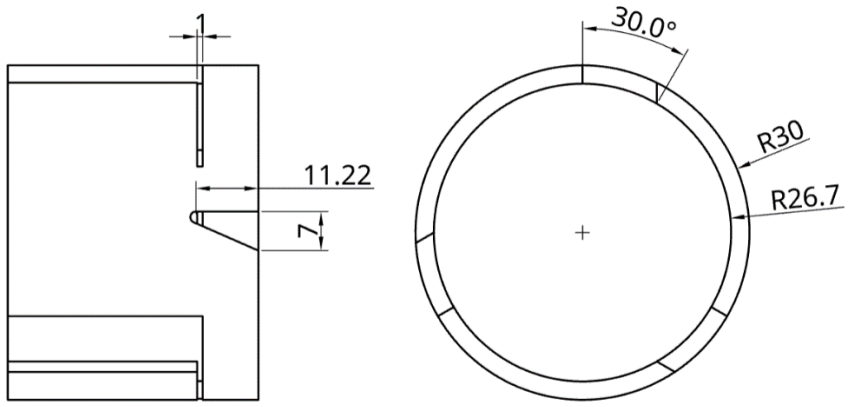

Source: Author.

In Figure 73 the method used to fasten the device is displayed. With the system in position inside the lathe chuck, the tool in yellow rotates counterclockwise while a hook holds the PVC tube.

Figure 73 – Method used to fasten the system in place.

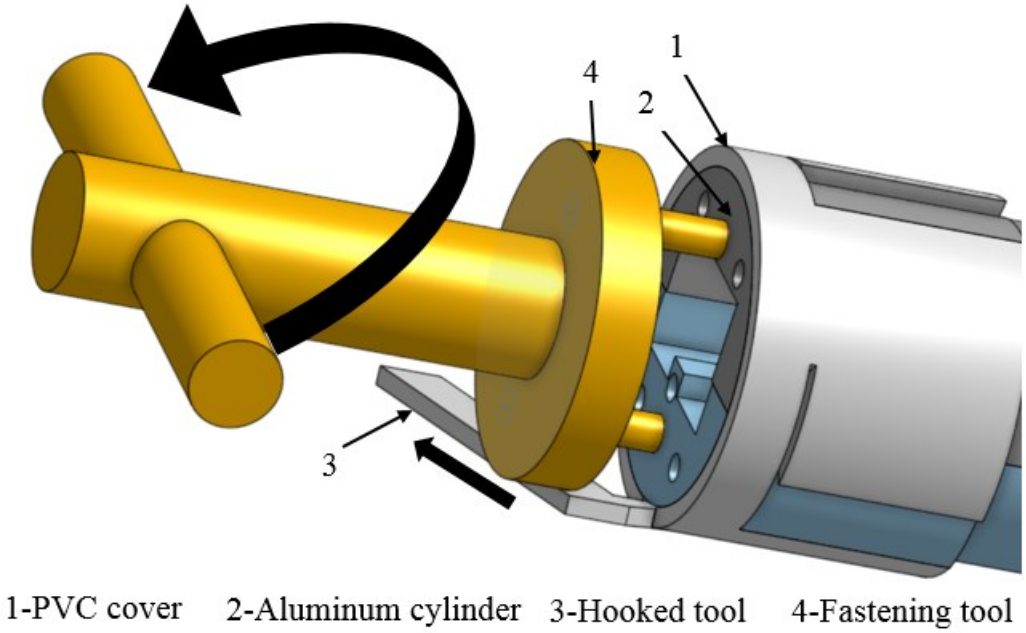

Source: Author.

In Figure 74 an image of the PCBs used for the acquisition and amplification system is shown. The space limitations and the intention to rotate them had a great impact on the format of the board and positioning of components. Bigger or more delicate components were positioned closer to the center of the board, so the centripetal force was applied more

perpendicular to the surface. Their fabrication was made in the Instituto SENAI de Inovação em Sistemas de Manufatura e Processamento a Laser.

Figure 74 – PCB for the acquisition system (top) and amplification system(bottom).

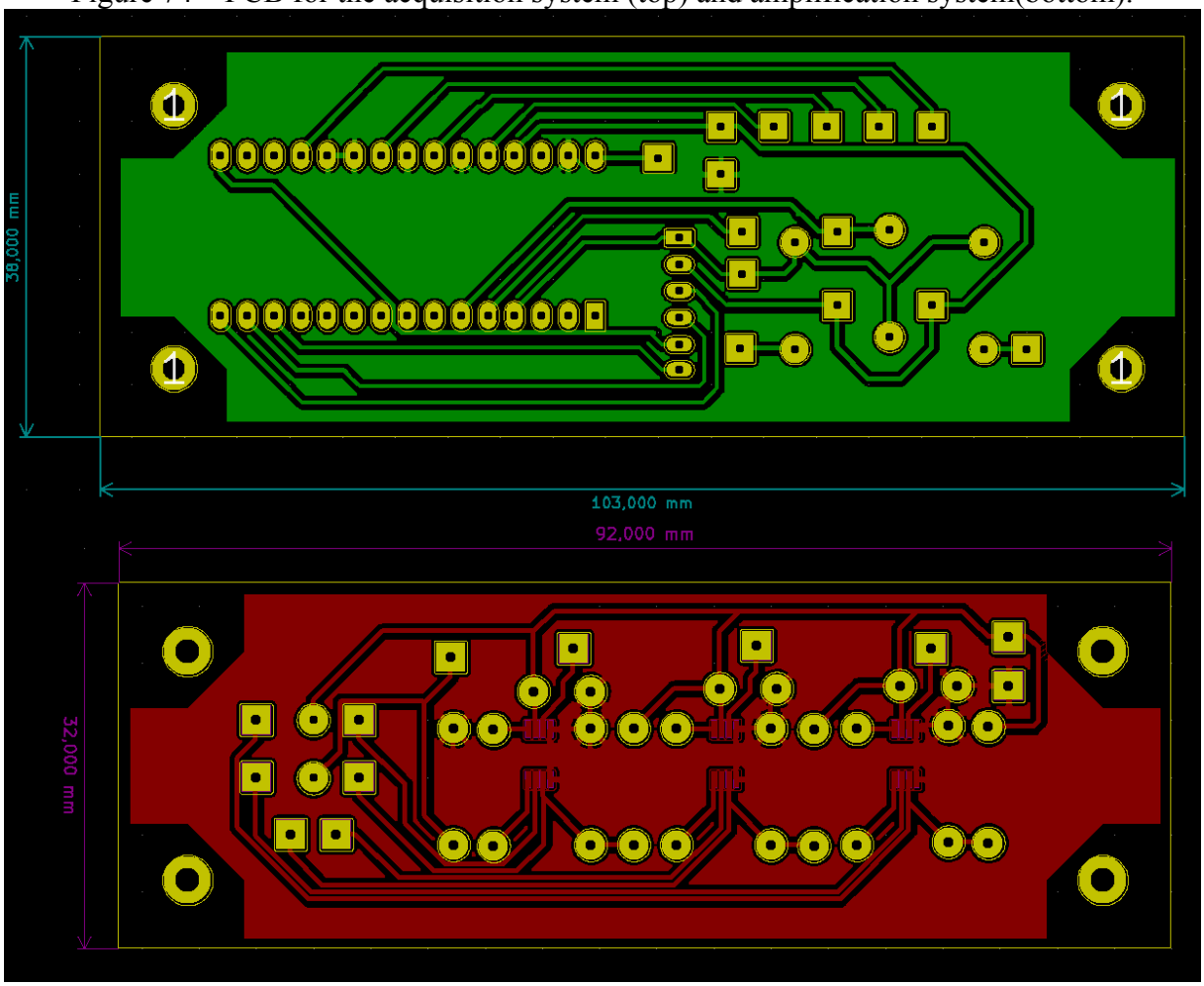

Source: Author.

APPENDIX C – ALGORITHMS

In this appendix, the algorithms developed for this work will be presented. This algorithm will be presented with commentaries, but their workings will not be further explained in this section. Knowledge of C++ and Matlab languages is necessary to fully understand their workings.

The first presented is the Datalogger used for the acquisition system. This algorithm was developed using elements from the datalogger example of the SdFat library that was heavily altered for this application. The Algorithm used to extract the data from the microSD card without removing it from the system is not presented for there were too few alterations from the original one contained in the library. The second Algorithm presented is the one used for the translation of the raw data to temperature data. For this, the software Matlab® was used for coding and running it.

Datalogger: Code for Arduino IDE.

```
/*
 * Datalogger using Arduino nano with 4 analog channels.
 * Based on example on SdFat library.
 * Interrupt code obtained at:
 * https://www.instructables.com/id/Arduino-Timer-Interrupts/
 */

#include <SdFat.h>

//Define the base name of the generated files.
#define FILE_BASE_NAME "Data"
//Define the number of buffers. Limited by available memory.
#define NUMBER_BUFFERS 2
//Define the size of the buffer. Limited by Micro SD cache.
#define BUFFER_SIZE 85

// SD chip select pin.
const uint8_t chipSelect = SS;
```

```
// File system object.
SdFat sd;

// Log file.
SdFile file;

//Variables to be recorded. And setting buffer coordinates.
uint16_t logvalue_a[NUMBER_BUFFERS][BUFFER_SIZE];
uint32_t logvalue_b[NUMBER_BUFFERS][BUFFER_SIZE];
uint8_t buffer_id = 0;
uint8_t buffer_item = 0;

//Intermediate variables.
uint16_t sensor1;
uint16_t sensor2;
uint16_t sensor3;
uint16_t sensor4;
uint8_t current_count = 0;


//Define inputs.
uint8_t Analog1 = A0;
uint8_t Analog2 = A3;
uint8_t Analog3 = A5;
uint8_t Analog4 = A7;

//Set button pin.
const uint8_t activation_button = 3;
const uint8_t led_button = 2;
// Set full buffer flag.
bool full_buffer_flag = false;

//Set the complete name of the first file with its number.
```

```
const uint8_t BASE_NAME_SIZE = sizeof(FILE_BASE_NAME) - 1;
char file_name[13] = FILE_BASE_NAME "00.txt";

//Initial settings of the system.
void setup() {


  // Initialize at the highest speed supported by the board that is
  // not over 50 MHz. Try a lower speed if SPI errors occur.
  sd.begin(chipSelect, SD_SCK_MHZ(50));

  pinMode(activation_button, INPUT);
  pinMode(led_button, OUTPUT);

  //Setting the interrupt.
  cli();//Stop interrupts

  //Set timer0 interrupt at 1kHz
  TCCR0A = 0;// set entire TCCR0A register to 0
  TCCR0B = 0;// same for TCCR0B
  TCNT0  = 0;//initialize counter value to 0
  // Set compare match register for 1khz increments
  OCR0A = 249;// = (16*10^6) / (1000*64) - 1 (must be <256)
  // Turn on CTC mode
  TCCR0A |= (1 << WGM01);
  // Set CS01 and CS00 bits for 64 prescaler
  TCCR0B |= (1 << CS01) | (1 << CS00);
  // eEnable timer compare interrupt
  TIMSK0 |= (1 << OCIE0A);

  sei();//Allow interrupts
}

//Code to be executed during interrupt. Where the data is acquired.
```

```
//Timer0 interrupt 1kHz
ISR(TIMER0_COMPA_vect){
  if(digitalRead(activation_button) == HIGH){
    //Read the input values
    sensor1 = analogRead(Analog1);
    sensor2 = analogRead(Analog2);
    sensor3 = analogRead(Analog3);
    sensor4 = analogRead(Analog4);
    //Concatenate input values in two variables
    logvalue_a[buffer_id][buffer_item] = 0;
    logvalue_a[buffer_id][buffer_item] += current_count;
    logvalue_a[buffer_id][buffer_item] *= 1024;
    logvalue_a[buffer_id][buffer_item] += sensor1;
    logvalue_b[buffer_id][buffer_item] = 0;
    logvalue_b[buffer_id][buffer_item] += sensor2;
    logvalue_b[buffer_id][buffer_item] *= 1024;
    logvalue_b[buffer_id][buffer_item] += sensor3;
    logvalue_b[buffer_id][buffer_item] *= 1024;
    logvalue_b[buffer_id][buffer_item] += sensor4;
    current_count++;

    //Circular buffer.
    buffer_item++;
    buffer_item = buffer_item % BUFFER_SIZE;
    if(buffer_item == 0){
      buffer_id++;
      buffer_id = buffer_id % NUMBER_BUFFERS;
      full_buffer_flag = true;
    }
  }
 }

//Main program. Runs in a loop while Arduino is powered.
void loop() {
```

```
//Returns to first buffer.
uint8_t active_buffer_id = 0;


//Starts the recording when the activation button is set to high.
if (digitalRead(activation_button) == HIGH) {
 //Returns to the first line of the buffer.
  active_buffer_id = 0;

  //Turns the green LED on to indicate data acquisition.
  digitalWrite(led_button, HIGH);

  // Finds an unused file name.
  while (sd.exists(file_name)) {
    if (file_name[BASE_NAME_SIZE + 1] != '9') {
      file_name[BASE_NAME_SIZE + 1]++;
    } else if (file_name[BASE_NAME_SIZE] != '9') {
      file_name[BASE_NAME_SIZE + 1] = '0';
      file_name[BASE_NAME_SIZE]++;
    }
  }

  //Create an open a file to be written.
  file.open(file_name, O_WRONLY | O_CREAT | O_EXCL);

  //Print buffer data to file.
  while (digitalRead(activation_button) == HIGH) {
    if (full_buffer_flag) {
      full_buffer_flag = false;
      for (uint8_t k = 0; k < BUFFER_SIZE; k++) {
        file.print(logvalue_a[active_buffer_id][k]);
        file.write(" ");
        file.print(logvalue_b[active_buffer_id][k]);
```

```
        file.write("\r\n");
      }
      active_buffer_id++;
      active_buffer_id = active_buffer_id % NUMBER_BUFFERS;
      file.sync();
    }
  }

  //Close the file.
  file.close();
  digitalWrite(led_button, LOW);
  //Reset buffers
  buffer_id = 0;
  buffer_item = 0;
  active_buffer_id = 0;
  current_count = 0;
 }
}
```

Data Translator: Code for Matlab®

```
%Data - Data table provided by the device
%data_temperature_thermocouple, data_voltage_thermocouple
%are tables provided by the thermocouple makers.
%These tables need to be preloaded.

%Constants.
reference_resistor=1000;
input_voltage=5;
thermistor_resistance_25C=10000;
temperatur_Kelvin_25C=298.15;
B=3950;

%Amplification of each channel.
```

```
amplificationA7=108.31;
amplificationA5=108.42;
amplificationA3=107.89;

%Import data from .txt
filename='C:\data00.txt' ;
fileID = fopen(filename , 'r');
Data = textscan(fileID, '%f%f');
fclose(fileID);

%Separates the concatenated signals.
A0 = (mod(Data{1,1}(:),2^10))*5/1023;
A3 = ((Data{1,2}(:)-mod(Data{1,2}(:),2^20))/2^20)*5/1023;
A5 = ((mod(Data{1,2}(:),2^20)-mod(Data{1,2}(:),2^10))/2^10)*5/1023;
A7 = (mod(Data{1,2}(:),2^10))*5/1023;
counter = ((Data{1,1}(:)-mod(Data{1,1}(:),2^10))/2^10);

%Verifies the counter condition
nPoint = length(counter);
verifier = counter;

%Analyzes the counter to see if there was a buffer problem, if a problem is
%detected it returs 1.
for index = 1:(nPoint-1)
        if (counter(index+1) == 0) && (counter(index) == 63)
       verifier(index) = 0;
   elseif counter(index+1) - counter(index) == 1
       verifier(index) = 0;
   else
       verifier(index) = 1;
   end
end

%counts the number of buffer overflows
```

```
        erros = nnz(verifier);

        %Calculate the thermistor temperature
        R_thermistor=reference_resistor*(input_voltage-A0)./A0;
        temperature_thermistor =
B./log((R_thermistor./thermistor_resistance_25C)*exp(B/temperatur_Kelvin_25C));
        temperature_thermistor = temperature_thermistor - 273.15;
        %temperature_thermistor = 25; %Activating this will fix the compensation
        %at 25 degree Celcius.

        %Interpolation with the thermocouple table
        voltage_compensation=interp1(data_temperature_thermocouple,
data_voltage_thermocouple, temperature_thermistor);

        %*1000 converts volts to milivolts
        voltage_thermocoupleA3=A3*1000/amplificationA3;
        Voltage_thermocoupleA5=A5*1000/amplificationA5;
        Voltage_thermocoupleA7=A7*1000/amplificationA7;

        %Apply the compensation.
        voltage_thermocouple_compensatedA3=voltage_thermocoupleA3 +
voltage_compensation;
        temperature_thermocoupleA3=interp1(data_voltage_thermocouple,
data_temperature_thermocouple, voltage_thermocouple_compensatedA3);
        voltage_thermocouple_compensatedA5=Voltage_thermocoupleA5 +
voltage_compensation;
        temperature_thermocoupleA5=interp1(data_voltage_thermocouple,
data_temperature_thermocouple, voltage_thermocouple_compensatedA5);
        Voltage_thermocouple_compensatedA7=Voltage_thermocoupleA7 +
voltage_compensation;
        temperature_thermocoupleA7=interp1(data_voltage_thermocouple,
data_temperature_thermocouple, Voltage_thermocouple_compensatedA7);

        %Creates a time axis for the data
```

```
%1khz is the aquisition rate
k = length(counter)*0.001;
time = 0.001:0.001:k;
time = time';

%plot the data.
f(1)=figure(1);
plot(time,temperature_thermocoupleA3);

title('thermocouple A3')
xlabel('time (s)')
ylabel('temperature (ºC)')

f(2)=figure(2);
plot(time,temperature_thermocoupleA5);

title('thermocouple A5')
xlabel('time (s)')
ylabel('temperature (ºC)')

f(3)=figure(3);
plot(time,temperature_thermocoupleA7);

title('thermocouple A7')
xlabel('time (s)')
ylabel('temperature (ºC)')
```

APPENDIX D – VALIDATION DATA

The validation of temperature measuring for the developed temperature measuring device was made in two steps. The first step used the Omega CLD-II muticalibrator and the second step used the Omega CL552 oven.

In the first step (Figure 34) the Omega CLD-II multicalibrator was used as a voltage source. Voltage was measured with each channel that would later be used to measure the thermocouple voltage, they were the Analog input 3 (A3), Analog input 5 (A5), and Analog input 7 (A7). For each channel the voltage from 0 to 50 mV was measured with steps of 5 mV, for each step 5000 points of data were acquired. In A3 the validation was stopped at 40 mV because the signal was already saturated.

For each channel, a graph of input voltage against measured tension was plotted. Each graph had a linear interval and at least one constant interval. The constant interval indicated that the amplifiers were saturated. The data for each channel can be seen in Figure 75, Figure 76, and Figure 77.

Figure 75 – Validation data from the A3 channel.

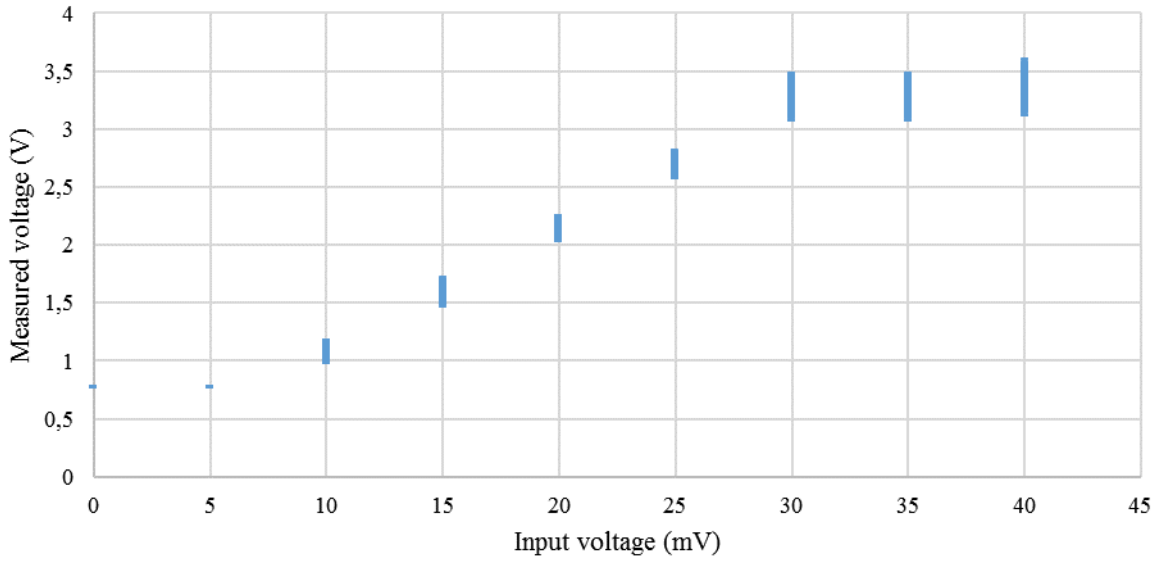

Source: Author

Figure 76 - Validation data from the A5 channel.

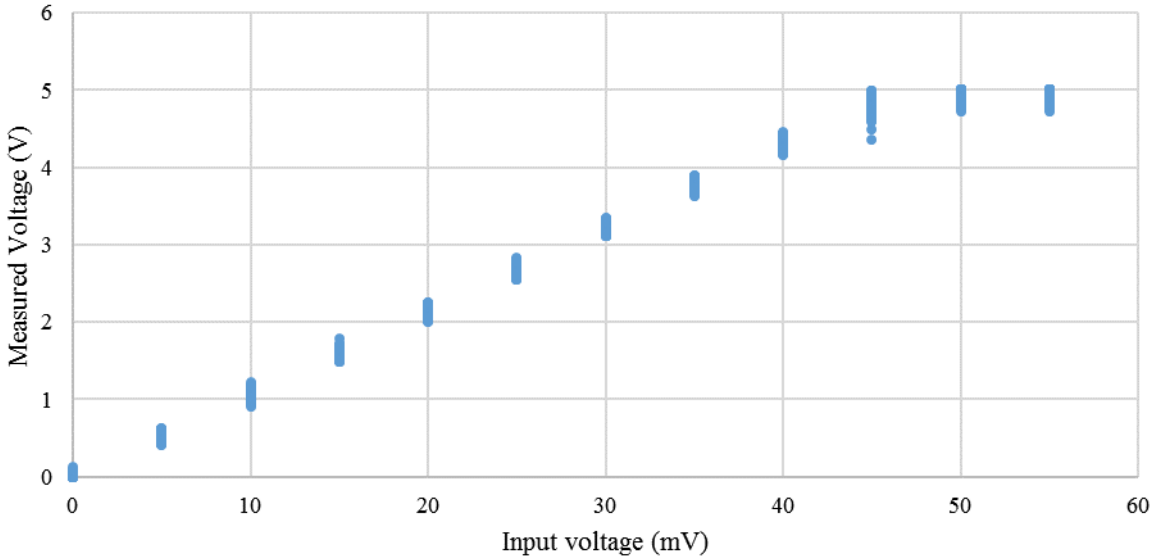

Source: Author

Figure 77 - Validation data from the A7 channel.

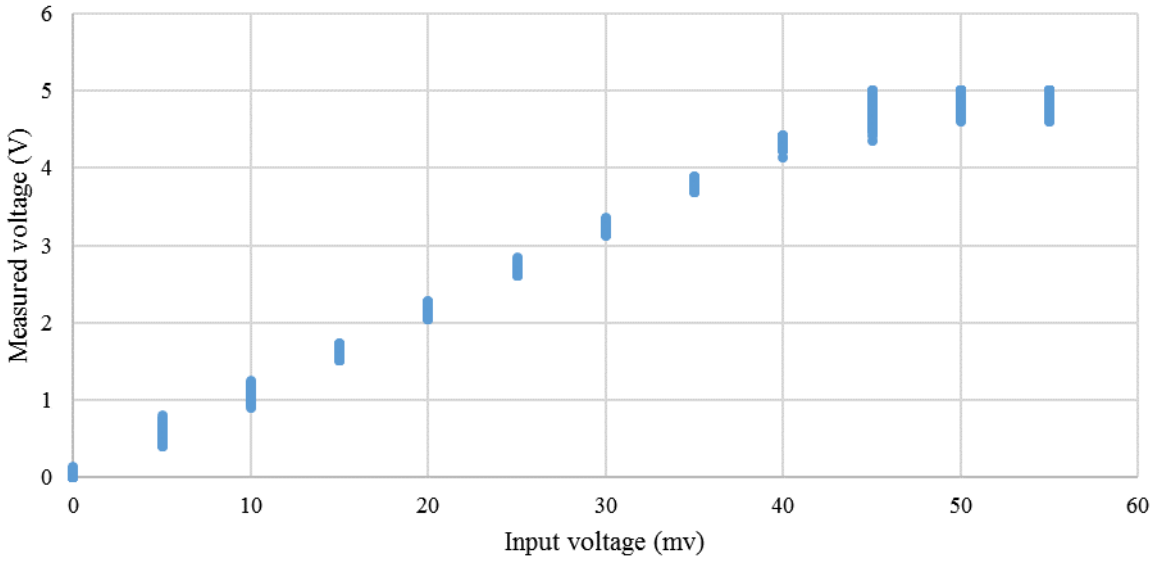

Source: Author.

After identifying the saturated intervals, all data considered saturated or close to saturation was separated from the unsaturated data. All data with 0 mV as input was considered saturated. Using only the unsaturated the least squares method was used to obtain the gain from each channel. This can be seen in Figure 78, Figure 79, and Figure 80.

Figure 78 – Least squares method applied to the unsaturated data of A3 channel.

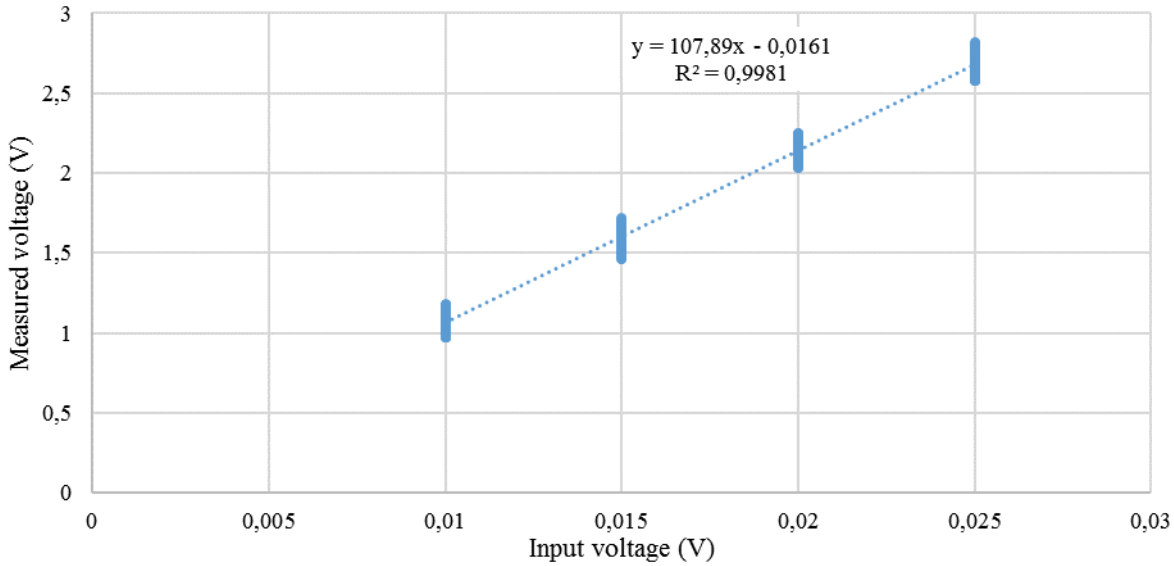

Source: Author.

Figure 79 - Least squares method applied to the unsaturated data of A5 channel.

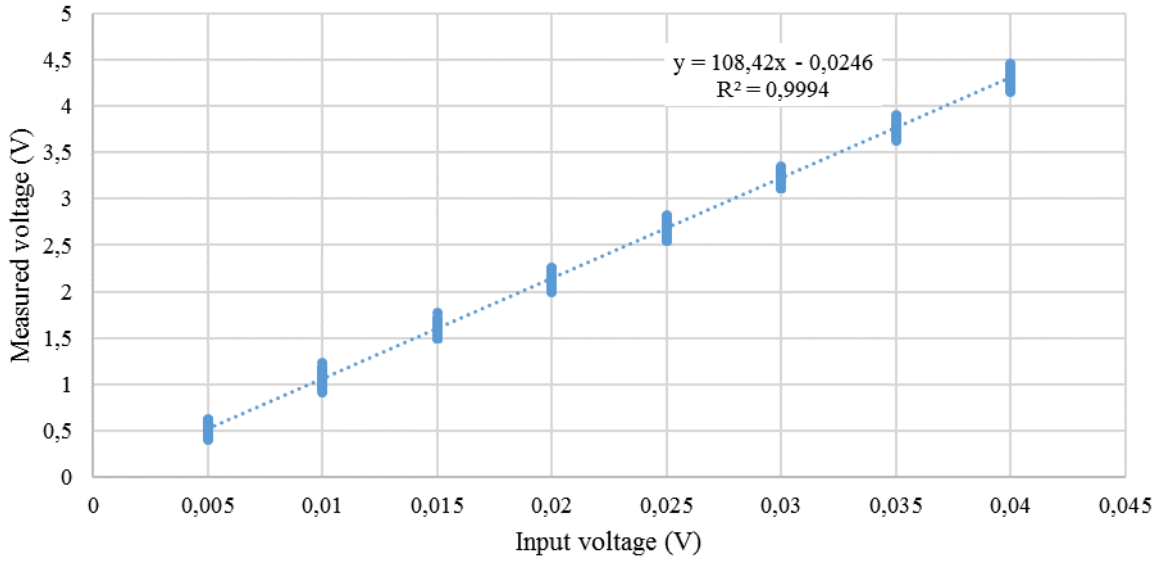

Source: Author.

Figure 80 - Least squares method applied to the unsaturated data of A7 channel.

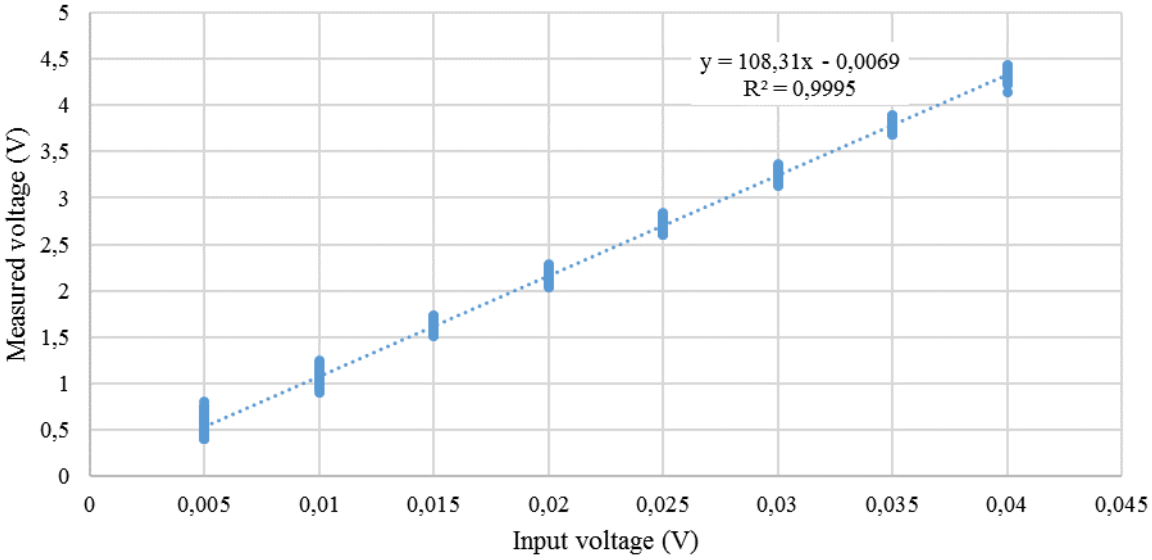

Source: Author.

Defining the measured voltage as the input multiplied by the gain for each channel, the GUM method [58] was used to determine the systematic and random errors. The errors for the whole unsaturated data for each channel were calculated. The saturated data was used to estimate the saturation limit by calculating the theoretical input that would generate the saturated signal and calculating the mean value of this input for data in the upper or lower saturation. The results of gain, saturation, and general errors can be seen in Table 6.

Table 6 – Gain, saturation systematic errors and random errors for each channel.

Channel	Gain	Lower saturation (mV)	Upper saturation (mV)	Systematic errors (mV)	Random error (mV)
A3	107.89	7.144	32.249	-0.149	0.485
A5	108.42	0.200	45.877	-0.228	0.533
A7	108.31	0.004	45.432	-0.048	0.0629

Source: Author.

All channels presented a gain close to 108, the greater random errors were 0.533 mV. Both A3 and A7 presented a lower saturation close to zero and an upper saturation close to 45 mV. Channel A3 presented a higher lower saturation limit and a lower upper saturation limit, which means that the measurement range of this channel will be limited. As the relation between voltage and temperature is not linear, the exact temperature errors will vary depending on the measured temperature. Considering the system at 0 ºC the greater random error would result in

an error close to 15 ºC. The A3 limited range would be able to measure temperatures between 176 ºC and 775 ºC. A5 and A7 would be able to measure temperatures from 6 ºC up to 1109 ºC. Although it would be safer to measure temperature farther from the saturation limits. These limits consider the cold junction at 0 ºC, if the cold junction has other temperature the limits will change.

The second step in the validation was made using an Omega CL552 oven. In this test temperature was acquired from all channels in several levels, beginning close to 200 ºC due to the oven limitations with each level around 100 ºC above the previous level up to 1100 ºC. At each level, the acquisition system was activated for at least 10 s, acquiring at least 10 000 points, and then deactivated. The temperature displayed on the oven dashboard, from the internal thermocouple, was recorded for each level.

The oven was projected to be used with probes, but bare wire thermocouples were used, this may have caused an increase in errors due to the thermocouples' positioning. The data was analyzed, and random and systemic errors were obtained for each level. Up to the 300 ºC level, all systematic errors remained below 20 ºC in module. The systematic error grew at each level reaching around 50 ºC in unsaturated signals.

All random errors were below 3 ºC on unsaturated signals. In Figure 81, the relation of the mean value measured in each thermocouple in relation to the oven temperature is shown. The A3 signal saturated close to 800 ºC while the A7 thermocouple saturated a little above 900 ºC.

Figure 81 – relation between measured temperature and oven temperature.

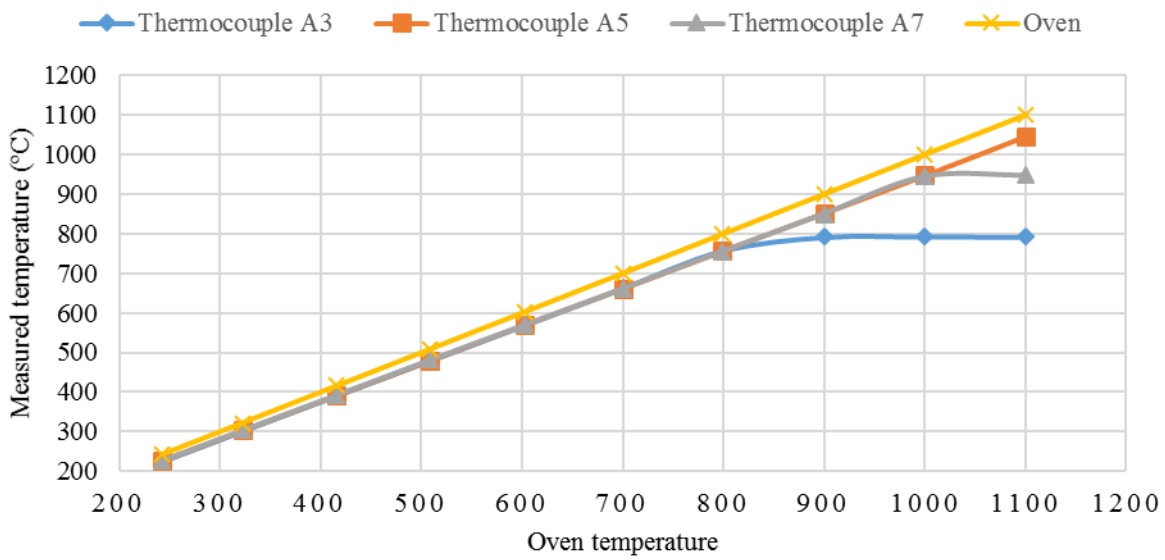

Source: Author